

การใช้เทคนิคเอกซัฟส์และการจำลองโมเลกุลเพื่อศึกษาโครงสร้างระดับ
อะตอมของเมมเบรนเซลล์เชื้อเพลิงชนิดไอโอโนเมอร์
ที่มีหมู่ซัลโฟเนต

นายคงวิทย์ ประสิทธิ์นอก

วิทยานิพนธ์นี้เป็นส่วนหนึ่งของการศึกษาตามหลักสูตรปริญญาวิทยาศาสตรมหาบัณฑิต
สาขาวิชาเคมี
มหาวิทยาลัยเทคโนโลยีสุรนารี
ปีการศึกษา 2551

**EXAFS AND MOLECULAR SIMULATION STUDIES
OF ATOMIC STRUCTURE OF FUEL CELL
MEMBRANE BASED ON SULFONATED IONOMERS**

Khongvit Prasitnok

A Thesis Submitted in Partial Fulfillment of the Requirements

for the Degree of Master of Science in Chemistry

Suranaree University of Technology

Academic Year 2008

**EXAFS AND MOLECULAR SIMULATION STUDIES OF
ATOMIC STRUCTURE OF FUEL CELL MEMBRANE BASED
ON SULFONATED IONOMERS**

Suranaree University of Technology has approved this thesis submitted in partial fulfillment of the requirements for a Master's Degree.

Thesis Examining Committee

Malee Tangsathikulchai

(Assoc. Prof. Dr. Malee Tangsathikulchai)

Chairperson

Visit Vao

(Asst. Prof. Dr. Visit Vao-soongnern)

Member (Thesis Advisor)

Jatuporn Wittayakun

(Assoc. Prof. Dr. Jatuporn Wittayakun)

Member

Wantana Klysubun

(Dr. Wantana Klysubun)

Member

P. Sattayatham

(Prof. Dr. Pairote Sattayatham)

Vice Rector for Academic Affairs

P. Manyum

(Assoc. Prof. Dr. Prapan Manyum)

Dean of Institute of Science

คงวิทย์ ประสิทธิ์นอก : การใช้เทคนิคเอ็กซาฟส์และการจำลองโมเลกุลเพื่อศึกษาโครงสร้างระดับอะตอมของเมมเบรนเซลล์เชื้อเพลิงชนิดไอโอโนเมอร์ที่มีหมู่ซัลโฟเนต (EXAFS AND MOLECULAR SIMULATION STUDIES OF ATOMIC STRUCTURE OF FUEL CELL MEMBRANE BASED ON SULFONATED IONOMERS) อาจารย์ที่ปรึกษา : ผู้ช่วยศาสตราจารย์ ดร.วิสิทธิ์ แวสูงเนิน, 193 หน้า.

ได้ศึกษาโครงสร้างระดับอะตอมของไอโอโนเมอร์ ซัลโฟเนต พอลิสไตรีน (SPS) และซัลโฟเนต พอลิอีเทอร์อีเทอร์คีโตน (SPEEK) โดยใช้เทคนิค EXAFS และ การจำลองโมเลกุล ทั้งนี้ได้เติมไอออนของโลหะโพแทสเซียมและแคลเซียมลงในไอโอโนเมอร์ที่สนใจ เพื่อศึกษาผลของไอออนดังกล่าวต่อโครงสร้างและสมบัติของไอโอโนเมอร์ งานวิจัยนี้ได้ใช้ SPS ที่มีหมู่ซัลโฟเนต 3.4 เปอร์เซ็นต์ต่อโมล และใช้ SPEEK จากการเตรียมผ่านปฏิกิริยาซัลโฟเนชันกับกรดซัลฟิวริกเข้มข้น โดยค่าเปอร์เซ็นต์ต่อโมลที่เตรียมได้เท่ากับ 25.0 เปอร์เซ็นต์ จากนั้นได้เติมเกลือโพแทสเซียมและแคลเซียมลงในไอโอโนเมอร์ทั้งสองชนิดโดยผ่านกระบวนการแลกเปลี่ยนไอออนกับไฮโดรเจนของหมู่ซัลโฟเนต จากการศึกษาโดย EXAFS พบว่าไอออนที่เติมลงไปทั้งสองชนิดจะเหนี่ยวนำให้หมู่ซัลโฟเนตของไอโอโนเมอร์เข้ามาล้อมและเกิดการเกาะกลุ่มของไอออน (Ionic aggregation) ขึ้น ทั้งนี้พบว่าอะตอมแคลเซียมใน Ca-SPS จะถูกล้อมรอบด้วยอะตอมออกซิเจน 6 อะตอมซึ่งมาจากน้ำ 2 โมเลกุล และหมู่ซัลโฟเนต 4 หมู่ สำหรับ Ca-SPEEK พบว่ามีออกซิเจนเข้ามาล้อม 5 อะตอม โดยมาจากน้ำ 1 และหมู่ซัลโฟเนต 4 หมู่ ส่วนระบบไอโอโนเมอร์ที่เติมเกลือโพแทสเซียม พบว่ามีจำนวนออกซิเจนเข้ามาล้อมน้อยกว่าระบบที่เติมเกลือแคลเซียม โดยทั้ง K-SPS และ K-SPEEK มีออกซิเจนเข้ามาล้อมโพแทสเซียมเท่ากันคือ 4 อะตอมซึ่งจากการวิเคราะห์พบว่าออกซิเจนดังกล่าวเป็นของน้ำ 2 โมเลกุล และหมู่ซัลโฟเนต 2 หมู่

ต่อจากนั้นจึงเป็นการศึกษาโดยการจำลองโมเลกุลด้วยคอมพิวเตอร์ โดยใช้เทคนิคพลวัตเชิงโมเลกุล (Molecular Dynamics) เพื่อศึกษาโครงสร้างและสมบัติของพอลิเมอร์ออสัญฐาน ทั้ง PS และ PEEK ซึ่งพบว่าการทำนายนิวตรอนและ X-ray structure factor พารามิเตอร์การละลายพลังงานพื้นผิว และสัมประสิทธิ์การแพร่ของน้ำในพอลิเมอร์สอดคล้องกับการทดลองเป็นอย่างดี ดังนั้นจึงใช้เทคนิคดังกล่าวจำลองโครงสร้างระดับอะตอมระบบซัลโฟเนตไอโอโนเมอร์เพื่อศึกษาการล้อมของไอออนโลหะเทียบกับผลที่ได้จากการทดลอง EXAFS ทั้งนี้จำนวนองค์ประกอบที่ใช้ในการจำลองแบบได้จากการวิเคราะห์โดยเทคนิคการวิเคราะห์เชิงความร้อนเทอร์โมกราวิเมตริก (TGA) จากฟังก์ชันการกระจายเชิงรัศมี (RDF) ของผลการจำลองแบบพบว่าระยะห่างระหว่างอะตอมโลหะกับออกซิเจนทั้งในไอโอโนเมอร์ที่เติมไอออนแคลเซียมและโพแทสเซียมได้ผลการคำนวณที่สอดคล้องกับผลการทดลอง โดยพบว่าในระบบไอโอโนเมอร์ที่เติมไอออนของ

แคลเซียมจะมีน้ำ 1 โมเลกุล และหมู่ซัลโฟเนต 3 โมเลกุลมาล้อมรอบไอออน ส่วนระบบที่เติมโพแทสเซียมนั้นจะมีโครงสร้างการล้อมรอบเหมือนที่พบในแคลเซียมคือ 1 โมเลกุลจากน้ำ และ 3 โมเลกุลจากหมู่ซัลโฟเนต จากการทดลองและการจำลองโมเลกุลแสดงให้เห็นสอดคล้องกันว่า ไอออนที่เติมลงไปไนโอโอโนเมอร์จะเหนี่ยวนำให้ไอออนลบของหมู่ซัลโฟเนตเข้ามาเกาะโดยมีน้ำเข้ามาแทรก 1 ถึง 2 โมเลกุลเพื่อจำกัดขอบเขตของการเกาะกลุ่มที่เกิดขึ้น งานวิจัยนี้ยังได้คำนวณสัมประสิทธิ์การแพร่ผ่านของโปรตอนไนโอโอโนเมอร์ โดยพบว่าค่าดังกล่าวในระบบที่เติมไอออนแคลเซียมและโพแทสเซียมมีค่าใกล้เคียงกับระบบไนโอโอโนเมอร์ที่ไม่มีการเติมไอออนโลหะ

สาขาวิชาเคมี

ปีการศึกษา 2551

ลายชื่อนักศึกษา ดวงวิทย์ ประสิทธิ์อันต

ลายชื่ออาจารย์ที่ปรึกษา ปิย คุ้มผล

KHONGVIT PRASITNOK : EXAFS AND MOLECULAR SIMULATION
STUDIES OF ATOMIC STRUCTURE OF FUEL CELL MEMBRANE
BASED ON SULFONATED IONOMERS. THESIS ADVISOR :
ASST. PROF. VISIT VAO-SOONGNERN, Ph.D., 193 PP.

SPS/SPEEK/SULFONATED IONOMERS/EXAFS/MOLECULAR DYNAMICS
SIMULATIONS

The local atomistic structure of sulfonated polystyrene (SPS) and sulfonated poly (ether-ether-ketone) (SPEEK) ionomers were investigated mainly by EXAFS and molecular modeling techniques. Calcium and potassium cations were chosen to dope the sulfonate ionomers and the change in structure and properties were studied. SPS and SPEEK with 3.4% and 25.0% sulfonate groups, respectively, were obtained by the sulfonation reaction of these polymers with concentrated sulfuric acid. Then, both SPS and SPEEK ionomers were neutralized with a stoichiometric amount of potassium and calcium ions via an ion-exchange process between the hydrogens of sulfonate groups and the cations of metal salts. EXAFS results revealed that sulfonated groups of ionomers were induced by cations to form an ionic aggregation structure. The first solvation shell of Ca-SPS consists of six oxygen atoms, while Ca-SPEEK was coordinated by five oxygen atoms. The best structures for both Ca-SPS and Ca-SPEEK in the EXAFS fittings contain four oxygens from the sulfonate groups surrounding calcium ion with the remaining two and one water of hydration, respectively. For the systems of monovalent cation, the best-fit structure for K-SPS and K-SPEEK was tetrahedrally rather than octahedrally coordinated. It was indicated

from EXAFS that potassium atoms in K-SPS and K-SPEEK were surrounded by two water molecules and two sulfonate anions.

Next, an atomistic morphous model of PS and PEEK were simulated via MD simulation technique. The predictions of neutron and X-ray structure factor, solubility parameters, surface energy and diffusion of water molecules were in good agreement with the experimental observations. Then, the atomistic models of sulfonated ionomers with estimated amount of molecular species obtained from TGA experiment were performed via MD simulation. It was evident from the RDFs of MD simulation that the first coordination shell distance between Ca-O and K-O agreed very well with the EXAFS fits. Coordination number obtained by an integration of the RDF peak revealed one water and three anions in the first coordination shell of the probed for both Ca and K-ionomer. Both experimental and simulation techniques revealed that sulfonate anions can be induced by cations to form an ionic aggregation and one or two water molecules must be present in order to satisfy the coordination needed by the metal cation at the aggregated boundaries where the repeat structure terminates. Moreover, the diffusion coefficients of proton through the ionomers were estimated by MD method. It was found that the diffusion coefficients of proton through Ca and K-ionomers were comparable to the one found in H-form ionomer.

School of Chemistry

Academic Year 2008

Student's Signature ကျော်စွာ မိုးလင်း

Advisor's Signature မိတ်ချီ

ACKNOWLEDGEMENTS

I am grateful to my thesis advisor, Asst. Prof. Dr. Visit Vao-Soongnern, for his valuable advices, comments for research work and for kindness and suggestions about positive thinking. I am also very thankful for thesis examining committee for reading and comments throughout the entire thesis. I wish to thank all the lecturers of school of Chemistry, Suranaree University of Technology for their good attitude and useful advice, all of the staff at the Center for Scientific and Technological Equipment for their assistance to use instruments. Special thanks for Dr. Wantana Klysubun, National Synchrotron Research Center for her valuable suggestions and EXAFS beam times. I would like to express my sincere thank to Prof. Bing-Joe Hwang and his students at National Taiwan University of Technology, Taipei, Taiwan, for valuable advices and software to analysis EXAFS data.

I am thankful to all graduate students especially, all members in Department of Chemistry for their patience, support, encouragement and made this a fun time.

I would like to thanks the National Synchrotron Research Center for financial support.

Last, but certainly not least, I would like to thank my beloved family who support, believe and encouragement.

Khongvit Prasitnok

CONTENTS

	Page
ABSTRACT IN THAI.....	I
ABSTRACT IN ENGLISH.....	III
ACKNOWLEDGEMENTS.....	V
CONTENTS.....	VI
LIST OF TABLES.....	XI
LIST OF FIGURES.....	XIII
LIST OF ABBREVIATIONS.....	XXI
CHAPTER	
I INTRODUCTION.....	1
II LITERATURE REVIEW.....	10
2.1 Polymer Electrolyte Membrane Fuel Cell (PEM-FC).....	10
2.2 Sulfonated poly (styrene) (SPS) and Sulfonated poly (ether-ether-ketone) (SPEEK).....	14
2.3 Ionic aggregation and Proton transport pathway in PEM-FCs.....	16
2.4 Ionomer crosslinking by cationic donors.....	22
2.4.1 Ionic conductivity in cationic doped-ionomers.....	23
2.4.2 Improving of PEM properties by cationic crosslinking.....	31

CONTENTS (Continued)

		Page
2.5	Extended X-ray Absorption Fine Structure (EXAFS) as the tool to probe internal aggregate order in ionic crosslinking....	42
2.6	Molecular Dynamics (MD) simulation as a powerful technique to confirm of aggregated environment obtaining from EXAFS analysis.....	46
III	RESEARCH METHODOLOGY.....	49
3.1	Apparatus and Materials.....	49
3.2	Experimental Part.....	50
3.2.1	Sample preparation.....	50
3.2.1.1	Preparation of SPS thin films.....	50
3.2.1.2	Preparation of SPEEK thin films.....	51
3.2.2	Sample Characterization.....	52
3.2.2.1	Nuclear Magnetic Resonance (NMR) Spectroscopy.....	52
3.2.2.2	Fourier Transform Infrared Spectroscopy (FT-IR).....	52
3.2.2.3	Thermo Gravimetric Analysis (TGA).....	53
3.2.2.4	Extended X-ray Absorption Fine Structure (EXAFS).....	53
3.3	Computational Part.....	55

CONTENTS (Continued)

	Page
3.3.1 Molecular Dynamics (MD).....	55
3.3.1.1 Bulk structures.....	55
3.3.1.2 Thin film.....	56
3.3.1.3 Benchmark models of sulfonated ionomers.....	56
IV RESULTS AND DISCUSSION	60
4.1 Experimental Part.....	60
4.1.1 Fourier Transform Infrared Spectroscopy (FT-IR) of Sulfonated Polystyrene (SPS) and Sulfonated poly- (ether-ether-ketone) (SPEEK).....	60
4.1.2 Nuclear Magnetic Resonance (NMR) of Sulfonated Polystyrene (SPS) and Sulfonated poly- (ether-ether-ketone) (SPEEK).....	62
4.1.3 Thermo Gravimetric Analysis (TGA) of Cation Neutralized SPS and SPEEK.....	64
4.1.4 Local structure analysis of ionomers by Extended- X-ray Absorption Fine Structure (EXAFS).....	67
4.1.4.1 Calcium neutralized Sulfonated polystyrene (K-SPS) and Sulfonated poly (ether-ether- ketone) (K-SPEEK) ionomers.....	67

CONTENTS (Continued)

	Page
4.1.4.2 Potassium neutralized Sulfonated polystyrene (K-SPS) and Sulfonated poly (ether ether- ketone) (K-SPEEK) ionomers.....	83
4.2 Computational Part.....	97
4.2.1 Molecular dynamic simulations of Polystyrene and Poly (ether-ether-ketone).....	97
4.2.1.1 Radial distribution function.....	97
4.2.1.2 Neutron and X-ray structure factor.....	101
4.2.1.3 Cohesive energy and solubility Parameters.....	103
4.2.1.4 Surface energy.....	104
4.2.1.5 Diffusion of water molecules in polymer matrix	106
4.2.2 MD simulations of benchmark models of sulfonated Ionomers.....	108
4.2.2.1 MD simulation of Ca-ionomer benchmark model.....	110
4.2.2.2 MD simulation of the K-ionomer benchmark model.....	117
4.2.2.3 Diffusion coefficient of H_3O^+ and H_2O in the benchmark models of sulfonated ionomers.....	123

LIST OF TABLES

Table	Page	
2.1	Ionic conductivity data (in mS/cm) for Nafion® 117 membranes exchanged with various cations and equilibrated with specific dipolar solvents at $T = 23^{\circ}\text{C}$	25
2.2	Summary of Tensile Properties and SAXS Parameters for a Model PTMO-TDI Based Polyurethane Ionomer.....	39
3.1	Description of the PS and PEEK Simulated Cells.....	57
4.1	Weight % and molar ratio of water and sulfonic group in 3.4 mol % SPS and 24.59 mol % SPEEK ionomers.....	67
4.2	EXAFS parameters of cationic doped sulfonated polystyrene and poly (ether-ether-ketone) ionomers.....	74
4.3	Fit results of Ca-SPS by using pseudo calcium methanesulfonate dehydrate model.....	80
4.4	Hildebrand solubility parameter of the simulated bulk polymer (the indicated limit is the standard deviation).....	105
4.5	The contribution of the potential energy to the surface energy.....	106
4.6	Description of the benchmark models of sulfonated ionomers. All MD simulations were performed at 227°C under NVT condition...	109
4.7	Parameters characterizing the first peak of the RDF from MD simulation of Ca^{2+} -ionomer.....	115

LIST OF TABLES (Continued)

Table		Page
4.8	Parameters characterizing the first peak of the RDF from MD simulation of K-Ionomer.....	121
4.9	Description of the benchmark models of sulfonated ionomers. All MD simulations were performed at 127 °C under NVT condition.....	124
4. 10	Diffusion coefficients of atomic species in the benchmark NVT simulation at 127 °C for 1.5 ns.....	125

LIST OF FIGURES

Figure	Page	
1.1	The repeating unit of (a) Sulfonated polystyrene (SPS) and (b) Sulfonated poly (ether-ether-ketone) (SPEEK).....	2
1.2	Schematic representation of (a) PEM-FC and (b) ionic cluster in PEM-FC.....	3
2.1	Schematic view of a PEM fuel cell.....	13
2.2	Schematic representations for the reaction of sulfonation of polystyrene and poly (ether ether ketone).....	16
2.3	Schematic representation of ionic cluster in PEM-FC.....	17
2.4	Sematic representation of the microstructures of Nafion and a sulfonated Polyetherketone.....	20
2.5	Models of H ⁺ transport mechanisms within ionomer membranes (a) Grotthuss (hopping) and (b) vehicle mechanisms. (a) is a simplified model of the Grotthuss mechanism, where the proton hopping direction deals with only one dimension.....	22
2.6	Optimized geometries of the X ⁺ (H ₂ O) _n clusters. B3LYP/6-311+G**// B3LYP/6 311+G**	28
2.7	Influence of barium-exchange fraction on the permselectivity of the barium-exchanged SPEKK membranes normalized with respect to the permselectivity of Nafion®.....	34
2.8	Derivative TGA curves of the barium-exchanged SPEKK (1.7 meq/g) membranes for various exchange fractions.....	34

LIST OF FIGURES (Continued)

Figure	Page
2.9 Influence of temperature and barium-exchange fraction on the water sorption at 25°C of barium-exchanged SPEKK membranes. The numbers in parentheses represent the mol % of H ⁺ neutralized by Ba ²⁺ . The IEC of the untreated SPEKK was 1.7 meq/g.....	35
2.10 Stress-strain curves for PTMO (1000)-TDI based ionomers with different neutralking cations.....	38
2.11 Mooney-Rivlin plots of the stress-strain data of PTMO (1000)-TDI based polyurethane ionomers. The neutralizing cations for curves from the top to the bottom are Ni ²⁺ , Na ⁺ , Eu ³⁺ , Cd ²⁺ , and Zn ²⁺	41
3.1 Schematic of the neutralization reaction of acidic SPS membranes.....	50
3.2 Schematic chemical structures of SPEEK.....	51
3.3 Schematic of the neutralization reaction of acidic SPEEK membranes	52
3.4 Thin films of ionomers casted from glass disk.....	52
3.5 Bulk structures of PS and PEEK used in molecular dynamics calculation.....	58
3.6 Thin film models of PS and PEEK used in molecular dynamics calculation.....	59
3.7 Diagram of the fragments featured in the molecular models: (a) sulfonate fragment, (b) potassium ion, (c) calcium ion, (d) hydroxonium ion and (e) water molecule. The outlines show the partial charges assigned to each atom.....	59

LIST OF FIGURES (Continued)

Figure	Page
4.1 FTIR spectra of (a) polystyrene and (b) sulfonated polystyrene.....	61
4.2 FTIR spectra of (a) poly(ether ether ketone) and (b) sulfonated poly- (ether-ether-ketone).....	61
4.3 ¹ H-NMR spectra of (a) polystyrene and (b) sulfonated polystyrene....	63
4.4 ¹ H-NMR spectrum of sulfonated poly (ether-ether-ketone).....	64
4.5 TGA curves of Ca-SPS and K-SPS samples.....	66
4.6 TGA curves of Ca-SPEEK and K-SPEEK samples.....	66
4.7 EXAFS data expressed as $k^2\chi$ for Ca-SPS and Ca-SPEEK ionomers...	69
4.8 Radial structure function for Ca-SPS and Ca-SPEEK ionomers.....	69
4.9 EXAFS data for the first shell of CaO (a) $k^2\chi$ and (b) radial structure function.....	70
4.10 Fit to the first shell of the Ca-SPS ionomer using CaO model (a) $k^2\chi$ and (b) radial structure function.....	71
4.11 Fit to the first shell of the Ca-SPEEK ionomer using CaO model (a) $k^2\chi$ and (b) radial structure function.....	72

LIST OF FIGURES (Continued)

Figure	Page
4.12 Structure of the local environment around nickel which contains two waters of hydration. (a) Two sulfonate groups share two nickel atoms. (b) Each sulfonate group which has one oxygen coordinated to a nickel atom has a different nickel atom for the other coordinating oxygen atom. The small filled circles represent nickel atoms, the larger filled circles represent sulfur atoms, and the largest unfilled circles represent oxygen atoms.....	76
4.13 Crystal structure with atomic distance for each bond in cadmium methanesulfonate dehydrate (Å).....	78
4.14 Comparison of $k^2\chi$ and radial structure function between Ca-SPEEK and the proposed 5-fold oxygen models. The solid line representing the experimental data (same for all the plots) and the dashed line representing the FEFF6 simulation.....	81

LIST OF FIGURES (Continued)

Figure	Page
4.15 Structures of 5-fold oxygen atom used to generate EXAFS peaks in Fig.4.17 (a) two water molecule with three sulfonate groups, two sulfonate group which has one oxygen coordinated to a calcium atom has a different calcium atom for the other coordinating oxygen atom. (b) one water molecule with four sulfonate groups, two sulfonate group which has one oxygen coordinated to a calcium atom has a different nickel atom for the other coordinating oxygen atom. (c) one water molecule with four sulfonate groups, two sulfonate groups share two calcium atoms.....	82
4.16 EXAFS data expressed as $k^2\chi$ for K-SPS and K-SPEEK ionomers....	86
4.17 Radial structure function for K-SPS and K-SPEEK ionomers.....	86
4.18 EXAFS data for $K_2S_2O_6$ used for fitting (a) $k^2\chi$ and (b) radial structure function.....	87
4.19 Fit to the first shell of the K-SPS ionomer using $K_2S_2O_4$ model (a) $k^2\chi$ and (b) radial structure function.....	88
4.20 Fit to the first shell of the K-SPEEK ionomer using $K_2S_2O_4$ model (a) $k^2\chi$ and (b) radial structure function.....	89
4.21 Possible structure for ZnSPS. Symbols as in Fig.4.14.....	91

LIST OF FIGURES (Continued)

Figure	Page
4.22 Structures of 4-fold oxygen atom used to generate EXAFS peaks in Fig.4.22 and 4.23 (a) two water molecule with two sulfonate groups, two sulfonate group which has one oxygen coordinated to a potassium atom has a different potassium atom for the other coordinating oxygen atom. (b) one water molecule with three sulfonate groups, two sulfonate group which has one oxygen coordinated to a potassium atom has a different potassium atom for the other coordinating oxygen atom. (c) four sulfonate groups, each sulfonate group which has one oxygen coordinated to a potassium atom has a different potassium atom for the other coordinating oxygen atom. (d) four sulfonate groups, two sulfonate groups share two potassium atoms.....	93
4.23 Comparison of $k^2\chi$ and radial structure function between K-SPS and the proposed 4-fold oxygen models. The solid line representing the experimental data (same for all the plots) and the dashed line representing the FEFF6 simulation.....	95
4.24 Comparison of $k^2\chi$ and radial structure function between K-SPEEK and the proposed 4-fold oxygen models. The solid line representing the experimental data (same for all the plots) and the dashed line representing the FEFF6 simulation.....	96
4.25 Elemental pair distribution function for all carbon atoms in PS.....	98

LIST OF FIGURES (Continued)

Figure	Page	
4.26	Elemental pair distribution function for all carbon atoms with all hydrogen atoms in PS.....	99
4.27	Elemental pair distribution function for all hydrogen atoms in PS.....	99
4.28	Elemental pair distribution function for all carbon atoms in PEEK.....	100
4.29	Elemental pair distribution function for all carbon atoms with all hydrogen atoms in PEEK.....	100
4.30	Elemental pair distribution function for all hydrogen atoms in PEEK.	101
4.31	(a) Neutron scattering factor and (b) X-ray scattering intensity for PS.....	103
4.32	(a) Neutron scattering factor and (b) X-ray scattering intensity for PEEK.....	103
4.33	Mean-square displacement of H ₂ O as a function of time in PS at 27°C.....	107
4.34	Mean-square displacement of H ₂ O as a function of time in PEEK at 30°C.....	108
4.35	Simulated Ca-O (H ₂ O) RDF of Ca-ionomer.....	112
4.36	Simulated Ca-S (-SO ₃ ⁻) RDF of Ca-ionomer.....	112
4.37	Simulated Ca-O (-S-O _{#1}) RDF of Ca-ionomer.....	113
4.38	Simulated Ca-O (-S-O _{#2}) RDF of Ca-ionomer.....	113
4.39	Simulated Ca-O (-S-O _{#3}) RDF of Ca-ionomer.....	114
4.40	Simulated Ca-O (H ₃ O ⁺) RDF of Ca-SPS ionomer.....	114

LIST OF FIGURES (Continued)

Figure	Page
4.41 Typical snapshots of a Ca-ionomer from MD simulation.....	116
4.42 Simulated K-O (H ₂ O) RDF of K-ionomer.....	118
4.43 Simulated Ca-S (-SO ₃ ⁻) RDF of K-ionomer.....	118
4.44 Simulated Ca-O (-S-O _{#1}) RDF of K-ionomer.....	119
4.45 Simulated Ca-O (-S-O _{#2}) RDF of K-ionomer.....	119
4.46 Simulated Ca-O (-S-O _{#3}) RDF of K-ionomer.....	120
4.47 Simulated Ca-O (H ₃ O ⁺) RDF of K-SPS ionomer.....	120
4.48 Typical snapshots of K-ionomer from MD simulation.....	122
4.49 Mean square displacements of water molecules in H, K ⁺ and Ca ²⁺ -from membranes at 127°C.....	124
4.50 Mean square displacements of hydronium ions in H, K ⁺ and Ca ²⁺ -from Membranes at 127°C.....	125
4.51 Comparison of the cumulative RDF between sulfonate fragments over a 1.5 ns NVT simulation at 127°C.....	127
4.52 Comparison of the cumulative cation-sulfonate RDF over a 1.5 ns NVT simulation at 127°C	127

LIST OF ABBREVIATIONS

PEM-FC	Polymer Electrolyte Membrane Fuel Cell
DMFC	Direct Methanol Fuel Cell
PS	Polystyrene
PEEK	Poly (ether-ether-ketone)
SPS	Sulfonated polystyrene
SPEEK	Sulfonated poly (ether-ether-ketone)
E-AA	Ethylene Acrylic Acid
E-MAA	Ether Methacrylic Acrylic Acid
TDI	Toluene Diisocyanate
DPE	Diphenyl Ether
DPK	Diphenyl Ketone
DMF	N, N-Dimethyl Formamide
DMTA	Dynamic Mechanical Thermal Analysis
EXAFS	Extended X-ray Absorption Fine Structure
MD	Molecular Dynamics
MM	Molecular Mechanics
FT-IR	Fourier Transform Infrared
NMR	Nuclear Magnetic Resonance
TGA	Thermogravimetric Analysis
DS	Degree of Sulfonation
DSS	Degree of Sulfonate Substitution

LIST OF ABBREVIATIONS (Continued)

RSF	Radial Structure Function
RDF	Radial Distribution Functions
<i>MSD</i>	Mean Square Displacement
SAXS	Small Angle X-ray Scattering
IEC	Ion Exchange Capacity
Meq/g	Milliequivalent/gram
S/cm	Siemen/centimeter
<i>D</i>	Diffusion Coefficient
°C	Degree Celcius
(μ)	Absorption Coefficient
K	Degree Kelvin
σ^2	Debye-Waller Factors
S_0^2	Amplitude Reduction Factor
$g(r)$	Pair Distribution Functions
δ	Hindebrand's Solubility Parameter
γ	Surface Energy
Å	Angstroms
<i>et al.</i>	et alia (and other)

CHAPTER I

INTRODUCTION

The concept of polymer electrolyte membrane fuel cells (PEM-FC) has been well established since early 1960s, and PEM-FCs are successfully commercialized for niche applications, such as electrical power sources in space crafts and submarines. During the last decade, however, the use of PEM-FCs as power sources in mass products, such as the electrical vehicles and portable electrical devices, was also brought into focus. This puts new demands on the materials being used, and is in particular true for the separator membrane material, which, traditionally, is a hydrated perfluorosulfonic polymer such as Nafion®, a perfluorinated sulfonated ionomer developed by DuPont. The perfluorosulfonic acid membranes cost US\$ 800 per meter² and the power generated costs approximate to US\$ 150 per kW. Since the technical feasibility of fuel cells has been to a large extent successfully demonstrated, the industry is currently engaged in field trials, lowering costs and determining manufacturing strategies. Hence, despite the superior performance of the membranes currently used in fuel cells, their inherently high cost of production and high methanol crossover in DMFC limit their usage in future mass-produced appliances including automobiles. From the application point of view, any membrane even the one without fluorine chemistry, but having high temperature resistance, greater mechanical strength and high proton conductivity would be useful.

Recently, the focus has been directed towards membranes based on aromatic polymers and especially sulfonated ones, *i.e.* aromatic polymers with the sulfonic acid group attached both to the polymer main chain and side chain via a reaction of sulfonation with different reagents. Alternatively, polymers containing an aromatic backbone such as polystyrene (PS) and poly (ether-ether-ketone), [PEEK] might be considered. The sulfonated polystyrene ionomer is a high performance thermoplastic and less expensive material while the sulfonated poly (ether-ether-ketone) exhibits stability in thermal and acidic environments. These polymers can be sulfonated (Fig.1.1) in the form of free acid ($-\text{SO}_3\text{H}$), a salt (e.g. $-\text{SO}_3^-\text{Na}^+$) or an ester ($-\text{SO}_3\text{R}$) through the use of some sulfonating agents such as concentrated sulfuric acid and chlorosulfonic acid .

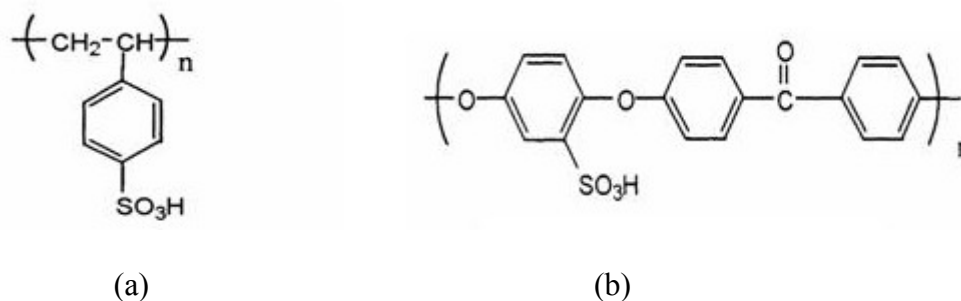


Figure 1.1 The repeating unit of (a) Sulfonated polystyrene (SPS) and (b) Sulfonated poly (ether-ether-ketone) (SPEEK).

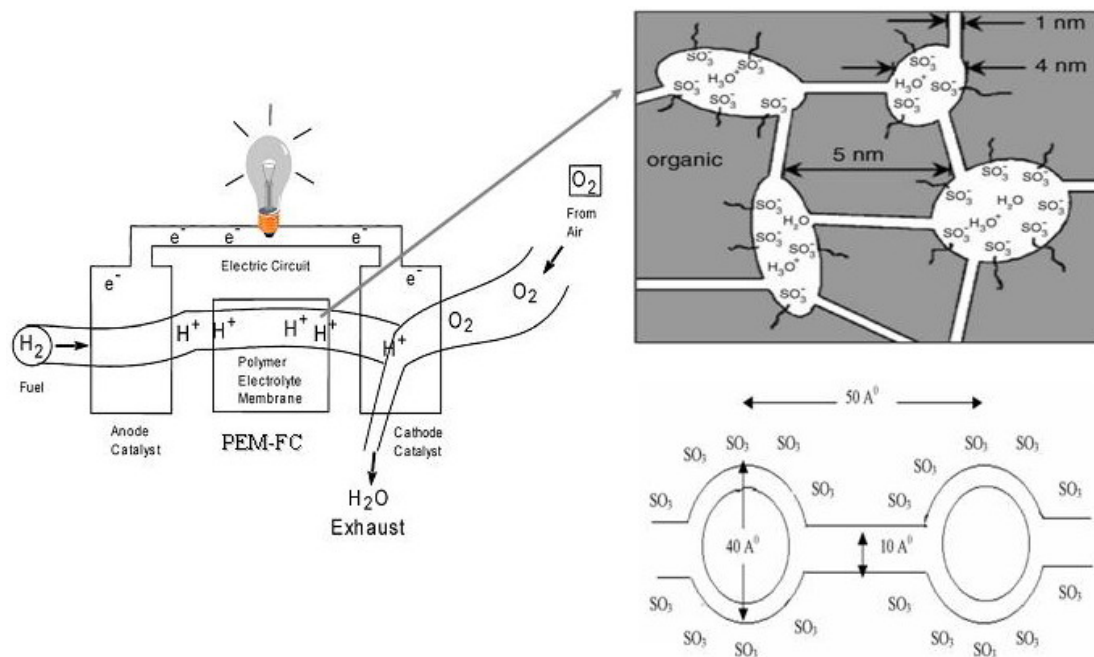


Figure 1.2 Schematic representation of (a) PEM-FC and (b) ionic cluster in PEM-FC (Hsu and Gierke, 1982).

The central component of PEM-FC is an ion conducting membrane, which, in fuel cells, is simultaneously an electrolyte for the proton transport from the anode to the cathode, and a barrier between the fuel (usually hydrogen or methanol for direct methanol fuel cells) and the oxygen fed to the cathode side. This membrane belongs to the class of polymers so-called “ionomers”. Ionomers are polymeric materials which have the capacity to form intermolecular ionic bonds. The presence of even small quantities of ionic groups (under 10 mol %) in materials such as polyethylene and polystyrene gives rise to dramatically elevated glass transition temperatures, anomalous viscoelastic properties, prodigious water uptake and order of magnitude increases in conductivity. By now, it is generally agreed that the often dramatic differences in material properties between ionomers and their non-ionic precursors are

due to the aggregation of ionic groups into microdomains, which can act as physical cross-links and define ion transport pathways in the material. With increasing ion content, the partially immobilized regions begin to overlap. Eventually, for high ion content, the immobilized regions begin to form sufficiently large domains, so-called “cluster” (Fig.1.2).

In the presence of water, the polymers swollen and the sulfonic groups dissociate into SO_3^- (fixed charge) and H^+ (mobile charge). Thus, the protons, which are the responsible for the ion conductivity, encounter a low resistance in moving across the membrane under a potential gradient. Hence, it can be implied that the water management of the membrane is a fundamental key. The performance of PEM-FC is strongly influenced by conductivity, and the conductivity is strongly influenced by the state of hydration of the membrane. If the membrane is too dry, its conductivity falls resulting in a reduced cell performance. An excess of water in the fuel cell can lead to cathode flooding problems, also resulting in less than optimal performance. Investigations dealing with hydration and swelling of membranes have been carried out to analyze the influence of hydration conditions on transport properties of polymer. In ionic polymers, hydration makes that adjacent cluster to be interconnected through channels that enhances ion and water transport. From this fact, the clusters arrangement has a marked influence on the physical properties of ionomers.

Although the crosslinking reduced the proton conductivity of membranes, the methanol permeability and methanol sorption were reduced significantly. Moreover, thermal and mechanical properties were increased when the crosslinking occurs. There seemed to have an optimum degree of crosslinking where the ratio of the proton conductivity to the methanol permeability, water swelled, was highest. It was found in

the previous that SPEEK with relatively moderate to high levels of sulfonation (*ca.* IEC > 1.7 meq/g) had proton conductivities comparable to that of Nafion[®]. However, these membranes exhibited poor dimensional, mechanical, and barrier properties in an aqueous environment at elevated temperatures (*ca.* 60–90°C), which are typical operating conditions in a DMFC. The poor properties were attributed to the excessive water sorption of the membranes at high water activities (*ca.* > 50 wt% of water at 98% relative humidity). In the work reported earlier, the objective is to reduce the water and methanol sorption by crosslinking the membrane. The idea of crosslinking of PEM is not new, but most of the crosslinking studies done previously pertain to chemical (covalent) crosslinking. The crosslinking procedure discussed in this work is a relatively less studied technique, which is ionic crosslinking. The approach is to exchange with mono and divalent cations *i.e.* Na⁺, K⁺, Zn²⁺, Cd²⁺, Ca²⁺. The salt produced by the exchange reaction should have very low water solubility and form a stable crosslink. To the best of the authors knowledge, the application of the above mentioned crosslinking procedure to PEMs is a novel idea. As an aggregation by these cationic donor act as both reinforcing filler and cross-links, leading to improvement in such properties as mechanical strength, abrasion and tear resistance, and impact strength. Thus, determining of the structure inside these domains is extremely important in ionomer research, since this information is necessary to understand the correlation between phase separated structure and physico-chemical properties of ionomers.

The remarkable improvement in mechanical properties of polymers having a small number of ionic groups covalently bonded to the polymer backbone is due to phase separation of the ionic groups into nanometersize ionic-rich aggregates. The

aggregates act as both reinforcing filler and cross-links, leading to improvement in mechanical strength. The fundamental driving force for phase separation in these systems is the favorable energetics of ionic group association. This work is designed to elucidate the internal atomic structure of these aggregates. However, the precise manifestation of remain in question at present. Unfortunately, methods to probe internal phase structure which have been applied to other microphase separated systems cannot be successfully utilized on ionomers. Differential scanning calorimetry, which is sensitive to the glass and/or melting temperature of each phase, does not exhibit any features from an ionic phase transition due to the well-known fact that ionic aggregates are thermodynamically stable to the degradation temperature of the polymer. Wide-angle X-ray scattering curves do not have peaks from crystalline ordering inside the ionic phase because the aggregates are very small; hence, even if the aggregates are crystalline on a local scale, only two or three unit cells can exist in any direction. Dynamic mechanical thermal analysis (DMTA) does have a high-temperature feature which is attributed to the presence of ionic groups, but a recent theory attributes this transition to the motion of immobilized polymer chains rather than ionic groups.

One of the few morphological probes which has been successfully applied to help understand internal aggregate order has been extended X-ray absorption fine structure (EXAFS). EXAFS is the measure of oscillations in the absorption coefficient (μ) about its mean value at energies between 50 and 1000 eV above an atomic absorption edge. An absorption edge occurs when the energy of an X-ray is sufficient to cause the ejection of a photoelectron; the K-edge corresponds to the ejection of a 1s electron. Oscillations occur because the outgoing photoelectron wave can be

backscattered by neighboring atoms which leads to interference between the outgoing and backscattered waves. Qualitatively, the shape and period of the oscillations will be a function of the absorbing atom as well as the type, distance, and number of atoms around the absorbing atom. Generally, the distance between the central atom and the backscattering atom must be less than 5 Å in order for the interference to be significant.

Recently, it was found that many papers present advances in the use of molecular simulations and EXAFS spectroscopy, which enable us to understand solvated ions in solution. A molecular-level understanding of ion-water and water-water interactions in solvation processes is essential to understanding the chemical and physical properties and transport mechanism of ions in aqueous solutions. Molecular dynamics (MD) and Monte Carlo (MC) simulation techniques provide a powerful approach to probing such processes in condensed phase environments. A detailed description of the solvent structure around an ion in solution can be obtained from a variety of experimental and theoretical techniques. MD simulations provide a detailed picture of structure and dynamics for complex systems that may not be tractable by other methods. Due to the advance of modern EXAFS algorithms and the availability of more accurate ion and solvent potential models, the number of studies that combine MD with EXAFS has increased considerably. The accuracy of the existing theoretical models for the interatomic potential in solid and liquid simple ionic systems was discussed in through direct comparison of EXAFS and molecular-dynamics (MD) results.

In this work, EXAFS technique was applied to study surrounded environments of cations including water and sulfonic groups. The systems chosen to study are

sulfonated poly (styrene) (SPS) and sulfonated poly (ether-ether-ketone) (SPEEK) neutralized with cation i.e. calcium ion (Ca^{2+}) and potassium ions (K^+). The results to indicate an aggregation aspects are (1) Distance between cation and oxygen atoms of sulfonic groups or water molecules and (2) Coordination number which indicates the average amount of water molecules and sulfonic groups around hydrophilic domains. It is obvious that these two parameters are the keys related to proton conducting properties and physico-chemical properties of polymer electrolyte materials. To gain more understanding about the thermodynamics and mechanism of phase separation in these materials, this research has applied molecular simulation techniques to discuss the results obtained from EXAFS experiments. Molecular Dynamics (MD) was used to estimate distance and an average coordination numbers of the probed atom and applied to interpret the results obtained from EXAFS.

Research Objectives

1. To study the atomistic structure of sulfonated poly (styrene) (SPS) and poly (ether-ether-ketone) (SPEEK) by EXAFS and molecular simulation methods.
2. To explain the correlation between atomistic structure and physico-chemical properties of cation doped SPS and SPEEK ionomers.

Scope and Limitations

This research work is divided into 3 main parts:

1. Sample Preparation

SPS and SPEEK thin films were prepared by solution casting technique. Then, metal ions such as potassium ion (K^+) or calcium ion (Ca^{2+}) were added to investigate the effect of doping metal ion on aggregate structure of ionomers.

2. Sample Characterization

The experimental techniques which were employed in this section are as follows:

2.1 Fourier Transform Infrared Spectroscopy (FT-IR): to verify an entering of sulfonation on ionomer backbone.

2.2 Nuclear Magnetic Resonance (NMR) Spectroscopy: to determine the microstructure and degree of sulfonation (DS) of ionomers.

2.3 Extended X-ray Absorption Fine Structure (EXAFS): to study the atomistic structure of ionomers such as distance and coordination number of probed atoms in ionomers.

2.4 Thermogravimetric Analysis (TGA): to estimate the ratio of $H_2O:SO_3H$ in ionomers.

3. Computational Molecular Modeling

The simulation techniques employed to study structures and properties of sulfonated ionomers for the system of SPS and SPEEK are as follows:

3.1 Molecular Dynamics (MD): to estimate the distance and coordination numbers between the probed and surrounding atoms. Moreover, other properties including structural, thermodynamic and dynamic properties of ionomers were investigated.

CHAPTER II

LITERATURE REVIEW

2.1 Polymer Electrolyte Membrane Fuel Cell (PEM-FC)

Fuel cells (FCs) have emerged strongly as a viable alternative source of power owing to their high-energy efficiency and eco-friendly nature. The proton exchange membrane (PEM) in fuel cells have been well established for over five decades and are successfully commercialized as electrical power sources in spacecrafts and submarines (Larminie and Dicks, 2000). During the last decade, the compatibility of PEM-FCs as power source in mass production of automobiles and portable electrical devices is well fathomed. This has lead to an increasing interest in materials being used as electrolytes.

Currently, the most conducting membranes are made of sulfonated polymers (Savadogo, 1998; Inzelt, Pineri, Schulze and Vorotyntser, 2000; Rikukawa and Sanui, 2000). Among them, Nafion[®], a perfluorinated sulfonated ionomer developed by DuPont, is chosen for several electrochemical applications because of its high proton conductivity and stability. The perfluorosulfonic acid membranes cost US\$ 800 m⁻² and the power generated costs approximate to US\$ 150 kW⁻¹. Since the technical feasibility of fuel cells has been to a large extent successfully demonstrated, the industry is currently engaged in field trials, lowering costs and determining manufacturing strategies.

Although such membranes show superior performance in fuel cells operating at moderate temperature ($< 90^{\circ}\text{C}$) and high relative humidity with pure hydrogen as a fuel, their inherently high cost of production makes their use in cost critical applications, such as fuel cells for electrical vehicles, unlikely. In addition the properties of such polymer membranes are insufficient if higher temperatures and/or fuels different from pure hydrogen are used

Currently, there is an increasing interest in using hydrogen-rich gases produced by reforming methanol or even gasoline. Such gases contain traces of different gases in particular CO, which reduces the activity of platinum or platinum-alloys (e.g. Ianniello, Schmidt, Stimming, Stumper and Wallan, 1994), which are generally used as anode catalysts. The CO tolerance, however, increases with increasing temperature, and therefore, fuel cell operation at somewhat higher temperature is desirable. Also the direct electrochemical oxidation of methanol is significantly promoted with increasing temperature. For direct liquid methanol fuel cells (DMFC), however, water and methanol cross-over significantly increases with temperature, which reduces the fuel efficiency and requires an expensive water management systems (e.g. Sundmacher and Scott, 1999). In short, limited operation temperature due to the humidification requirements, water and methanol cross-over and cost are severe disadvantages of plain perfluorosulfonic polymers.

These limitations have already stimulated a variety of approaches in the development of alternative polymeric proton exchange membranes (for a recent review see [Savadogo, 1998]). Most of them are sulfonated polymers, but also sulfamides have been used as thermally more stable acid functional groups (Desmarteau *et al.*, 2004). In any case, proton conductivity relies on proton solvation

by water at high water activities, and the limitations of their use in fuel cells are generally similar to those of NAFION. Modification of such membranes by the inclusion of small inorganic particles such as silica (Arico, Creti, Antonucci and Antonucci, 1998; Zoppi, Yoshida and Nunes, 1997; Bonnet *et al.*, 2000) or zirconiumphosphates sulfophenylphosphonates (Bonnet *et al.*, 2000) leads to some improvement of the performance of such membranes especially in pressurised fuel cells operating at temperatures up to 140°C. Also the morphological stabilisation of acidic polymers by either acid/base blending or covalent cross-linking (Kerres, Ullrich, Meier and Haring, 1999; Zhang *et al.*, 1998) appears to reduce swelling and water and methanol cross-over. But reduced conductivity and brittleness in the dry state emerge as new problems.

Distinctly different approaches are based on the complexation of basic polymers, such as polybenzimidazole, with oxo-acids (e.g. Lassegues, 1992; Wainright *et al.*, 1994), especially for phosphoric acid, high acid to polymer ratios lead to conductivities close to that of the pure acid. As in the case of pure phosphoric acid (Dippel, Kreuer, Lusseques and Rodriguez, 1993), proton conductivity of such adducts is predominantly carried by structure diffusion, i.e. proton transfer between phosphate species and phosphate reorientation. Phosphoric acid is successively immobilised with decreasing acid/polymer ratio, while proton conductivity still remains relatively high (Bozkurt, Ise, Kreuer, Meyer and Wegner, 1999). Due to the low transport coefficients of other species in the highly viscous phosphoric matrix and the low solubility of methanol at high temperatures, methanol cross-over is drastically reduced compared to hydrated acidic polymers (Wang, Wasmus and Savinell, 1996).

Recently, the focus has been directed towards membranes based on aromatic polymers and especially sulfonated ones, *i.e.* aromatic polymers with the sulfonic acid group attached both to the polymer main chain (Acosta, Garcia-Fierro, Linares and Canovas, 2000; Karlsson and Jannasch, 2005) and side chain (Smitha, Slidhar and Khan, 2003; Canovas, Sobrados, Sanzb, Acosta and Linares, 2006) via a reaction of sulfonation with different reagents. Alternatively, polymers containing an aromatic backbone such as polystyrene (PS) and poly (ether-ether-ketone), [PEEK] might be considered.

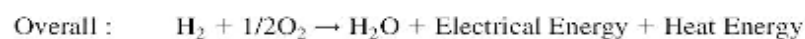
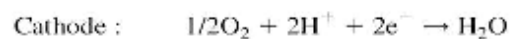
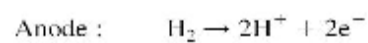
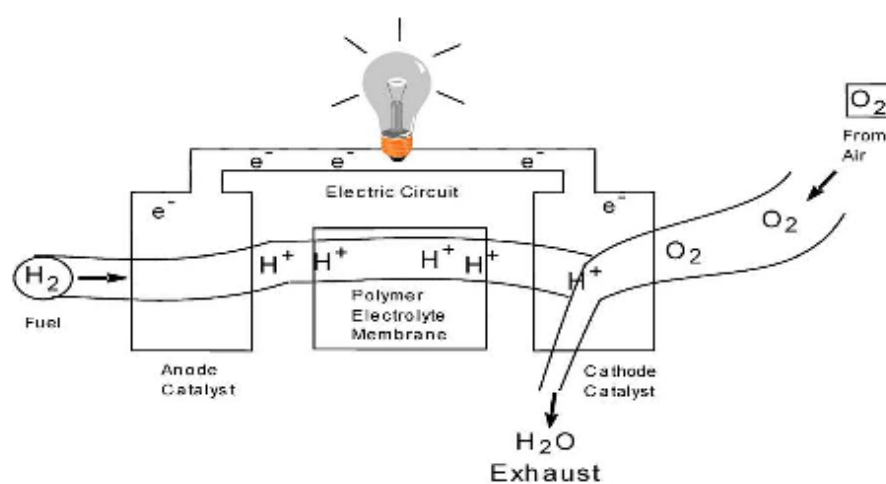


Figure 2.1 Schematic view of a PEM fuel cell.

2.2 Sulfonated poly (styrene) (SPS) and Sulfonated poly (ether-ether-ketone) (SPEEK)

Polystyrene are the low cost, disposable, high thermal stability and low methanol permeability material and provide moderate sulfonation process of the aromatic ring (Carretta, Tricoli and Picchioni, 2000) reported that a membrane made from sulfonated polystyrene which is rigid in nature shows the methanol permeability of about 70% lower than that of Nafion. This membrane has the advantages of low price and better water uptake, thus, a high proton conductivity, but has the disadvantages of poor chemical and thermal stability (Vielstich and Ives, 1970; Costamagna and Srinivasan, 2001). It is known that General Electric's battery employed the electrolyte based on sulfonated polystyrene equipped in the NASA's Gemini flight.

Non-fluorinated membranes based on the hydrophobic poly (ether-ether-ketone) (PEEK) have been presented as materials with excellent chemical and mechanical resistance, high thermo-oxidative stability and low cost (Jin, Bishop, Ellis and Kavasz, 1985; Kobayashi, Rikukawa, Sanui and Okata, 1998). This polymer can be easily made hydrophilic by sulfonation reactions, being the sulfonation degree (SD) controlled by the reaction time and temperature. Recently, Li, Zang and Wang, (2003) reported better DMFC performances for the SPEEK membranes (SD = 39 and 47%) compared to Nafion115, at 80°C. It was found that SPEEK membranes have a lifetime of more than several thousand hours under fuel cell conditions (Kreuer, 2001). Like other sulfonated aromatic main-chain polymers, these SPEEKs require a certain acidic groups to achieve high proton conductivity. However, too high loading of acidic groups induces excessive water swelling and methanol diffusion, which will

weaken the membranes and limit their practical application in DMFCs. Although the DS of the SPEEK sample obtained by post sulfonation is limited to low degree, the membrane with too high DS is not suitable for DMFCs due to poor mechanical stability. According to the results acquired in different laboratories (Cui, Kerres and Eigenberger, 1998; Ise, Kreuer and Maier, 1999; Bonnet *et al.*, 2000) PEEK functionalized by electrophilic sulfonation possesses many of the required properties, including chemical inertness and high proton conductivity, which makes it promising as an alternative material for PEMFC application. Considering that SPEEK is known to be thermally stable and it exhibits lower methanol crossover than Nafion in DMFC (Trotta, Drioli, Moraglio and Poma, 1998; Yang and Manthiram, 2003; Xing *et al.*, 2004). As mentioned, it has been shown that sulfonated poly (ether-ether-ketone) (SPEEK) is very promising for fuel cell application as it possesses a good thermal stability, mechanical strength and adequate conductivity. SPEEK membranes with good performance for hydrogen fuel cells are described in several reports (Bauer *et al.*, 2000). Recently, Kreuer (2001) reported that the absorptive amount of methanol in SPEEK membranes was lower than that of Nafion membranes, which may help to reduce the problems associated with high water drag and high methanol crossover in DMFC.

These polymers can be sulfonated (Fig.2.2) in the form of free acid ($-\text{SO}_3\text{H}$), a salt (e.g. $-\text{SO}_3^-\text{Na}^+$) or an ester ($-\text{SO}_3\text{R}$) (Noshay and Robenson, 1976) through the use of some sulfonating agents such as concentrated sulfuric acid (Nagarale, Gohil and Shahi, 2006) and chlorosulfonic acid (Nolte, Ledjeff, Bauer and Molhaupt, 1993).

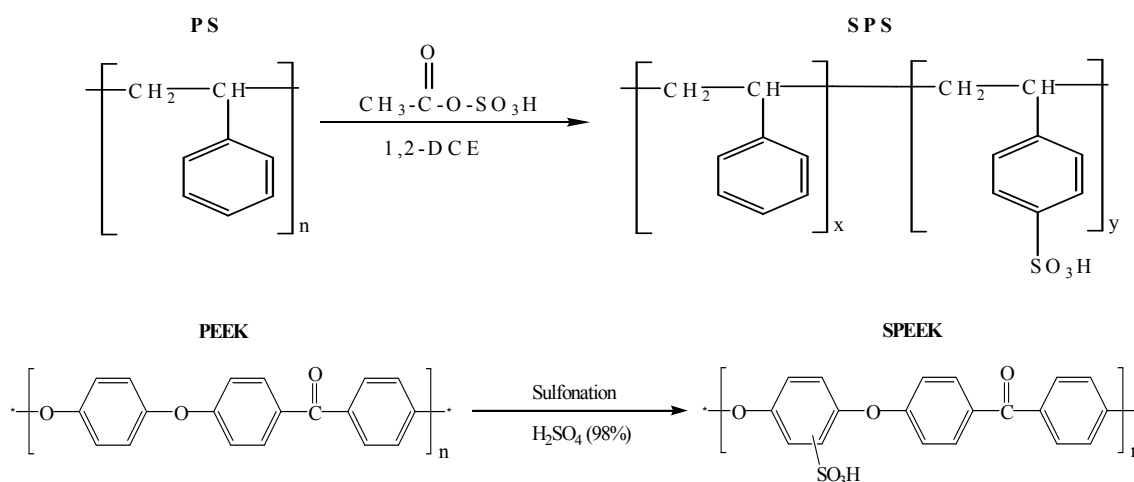


Figure 2.2 Schematic representations for the reaction of sulfonation of polystyrene and poly(ether-ether-ketone).

2.3 Ionic aggregation and Proton transport pathway in PEM-FCs

The central component of PEM-FC is an ion conducting membrane, which, in fuel cells, is simultaneously an electrolyte for the proton transport from the anode to the cathode, and a barrier between the fuel (usually hydrogen or methanol for direct methanol fuel cells) and the oxygen fed to the cathode side. This membrane belongs to the class of polymers so-called “ionomers”. Ionomers are polymeric materials which have the capacity to form intermolecular ionic bonds. The presence of even small quantities of ionic groups (under 10 mol %) in materials such as polyethylene and polystyrene gives rise to dramatically elevated glass transition temperatures, anomalous viscoelastic properties, prodigious water uptake and order of magnitude increases in conductivity (Wu, Lin and Yang, 2006; Smita and Montgomery, 2007). By now, it is generally agreed that the often dramatic differences in material properties between ionomers and their non-ionic precursors are due to the aggregation of ionic

groups into microdomains, which can act as physical cross-links and define ion transport pathways in the material. With increasing ion content, the partially immobilized regions begin to overlap. Eventually, for high ion content, the immobilized regions begin to form sufficiently large domains, so-called “cluster” (Fig. 2.3).

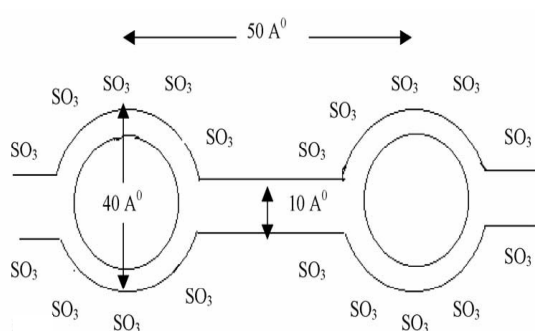
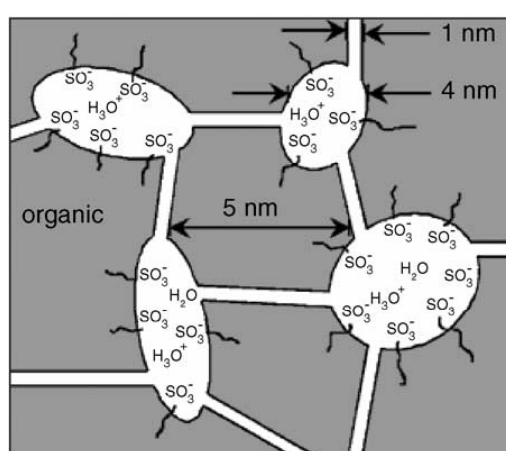


Figure 2.3 Schematic representation of ionic cluster in PEM-FC (Hsu and Gierke, 1982).

In the presence of water, the polymers swollen and the sulfonic groups dissociate into SO₃⁻ (fixed charge) and H⁺ (mobile charge). Thus, the protons, which are the responsible for the ion conductivity, encounter a low resistance in moving across the membrane under a potential gradient. Hence, it can be implied that the

water management of the membrane is a fundamental key. The performance of PEM-FC is strongly influenced by conductivity, and the conductivity is strongly influenced by the state of hydration of the membrane. If the membrane is too dry, its conductivity falls resulting in a reduced cell performance. An excess of water in the fuel cell can lead to cathode flooding problems, also resulting in less than optimal performance. Investigations dealing with hydration and swelling of membranes have been carried out to analyze the influence of hydration conditions on transport properties of polymer (Ludvigsson, Lingren and Tegenfeldt, 2000; Yang, Jablonsly and Mays, 2002; Kim and Kim 2003). In ionic polymers, hydration makes that adjacent cluster to be interconnected through channels that enhances ion and water transport (Gebel, 2000; Serpico *et al.*, 2000; Wang, Kawano, Aubochon and Palmer, 2003). From this fact, the clusters arrangement has a marked influence on the physical properties of ionomers.

By comparison to Polyetherketone, perfluorosulfonic polymers naturally combine, in one macromolecule, the extremely high hydrophobicity of the perfluorinated backbone with the extremely high hydrophilicity of the sulfonic acid functional groups. Especially in the presence of water, this gives rise to some hydrophobic/hydrophilic nano-separation. The sulfonic acid functional groups aggregate to form a hydrophilic domain. When this is hydrated, protonic charge carriers form within inner space charge layers by dissociation of the acidic functional groups, and proton conductance assisted by water dynamics occurs. While the well connected hydrophilic domain is responsible for the transport of protons and water, the hydrophobic domain provides the polymer with the morphological stability and prevents the polymer from dissolving in water. The situation in sulfonated

polyetherketones was found to be distinctly different with respect to both transport properties and morphological stability. As a result of the smaller hydrophilic/hydrophobic difference (the backbone is less hydrophobic, and the sulfonic acid functional group is less acidic and therefore, also less polar) and the smaller flexibility of the polymer backbone, the separation into a hydrophilic and a hydrophobic domain is less pronounced. This can directly be inferred from the results of small angle X-ray scattering (SAXS) experiments. For a hydrated sulfonated polyetherketone compared to Nafion the ionomer peak is broadened and shifted towards higher scattering angles and the scattering intensity at high scattering angles (Porod-regime) is higher (Ise, 2000). This indicates a smaller characteristic separation length with a wider distribution and a larger internal interface between the hydrophobic and hydrophilic domain for the hydrated sulfonated polyetherketone.

The SAXS data and water self-diffusion coefficients obtained by pulsed-field-gradient (PFG) - NMR have been used to consistently parameterise a simple model for the microstructure, which is based on a cubic hydrophilic channel system in a hydrophobic matrix. Data for channel diameter, channel separation, degree of branching and number of dead-end channels have been obtained for both type of polymers (Ise, 2000). As schematically illustrated in Fig. 2.4, the water filled channels in sulfonated PEEKK are narrower compared to those in Nafion. They are less separated and more branched with more dead-end “pockets”. These features correspond to the larger hydrophilic/ hydrophobic interface and, therefore, also to a larger average separation of neighboring sulfonic acid functional groups. The stronger confinement of the water in the narrow channels of the aromatic polymers leads to a significantly lower dielectric constant of the water of hydration (about 20 compared to

almost 64 in fully hydrated Nafion [Bender, 1999; Paddison, Bender, Kreuer, Nicoloso and Zawodzinski, 2000]).

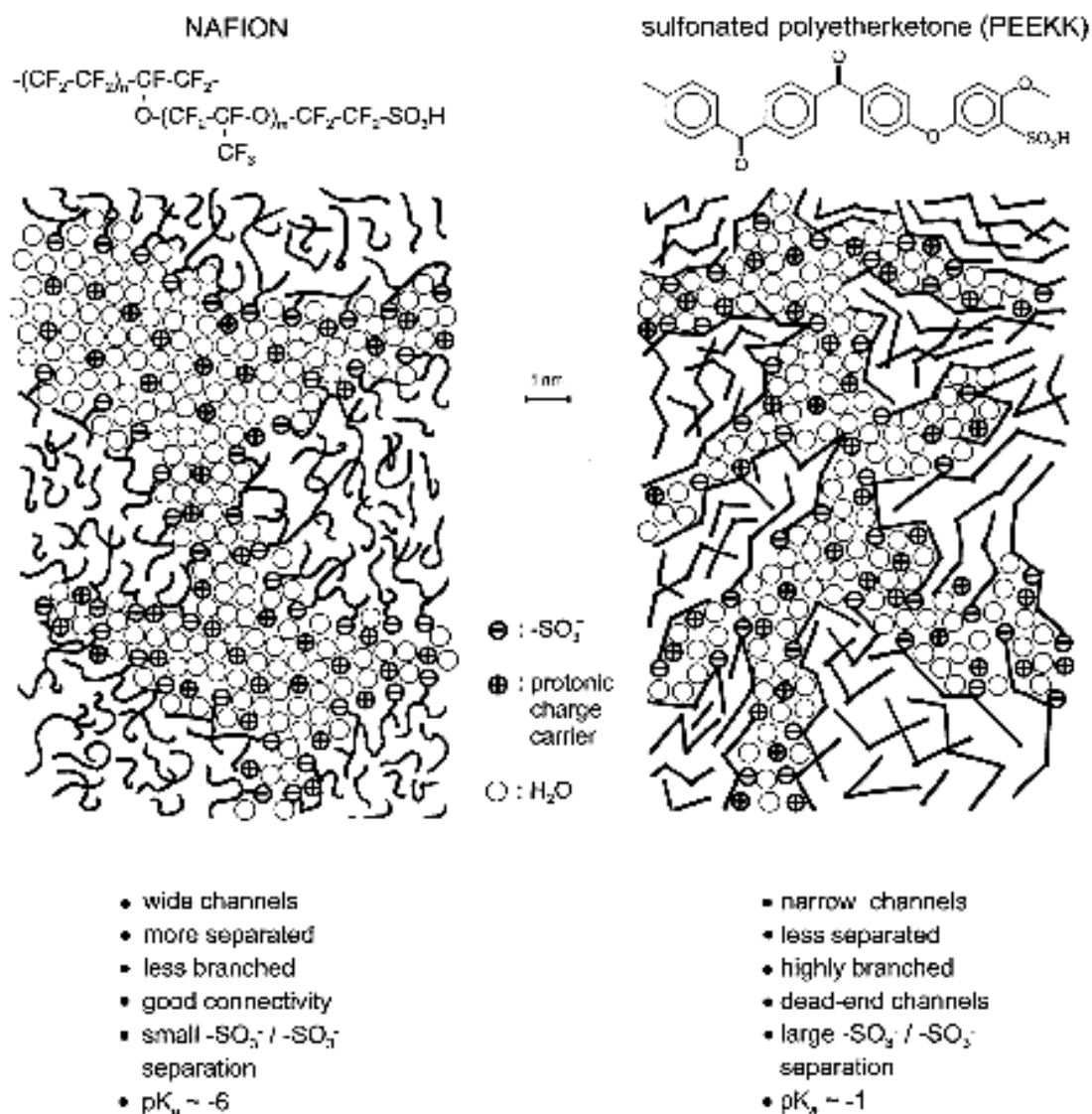


Figure 2.4 Sematic representation of the microstructures of Nafion and a sulfonated polyetherketone (derived from SAXS experiments, Ise, 2000, illustrating the less pronounced hydrophobic/hydrophilic separation of the latter compared to the first).

There are two limiting proton-conduction mechanisms to describe proton diffusion in such a way that the proton remains always shielded by some electron density along the entire diffusion path. The most trivial case is the assistance of proton migration by the translational dynamics of bigger species (vehicle mechanism) (Kreuer, Rabenan and Wepper, 1982). In this case, the proton diffuses together with a vehicle (e.g. as H_3O^+). In the other case, the “vehicles” display local dynamics but reside on their sites, the proton being transferred within hydrogen bonds from one “vehicles” to the other. Additional reorganization of the proton environment, which comprises, e.g. reorientation of individual species or even more extended ensembles, results in the formation of an uninterrupted trajectory for proton migration. This mechanism is frequently termed the Grotthuss (hopping) mechanism or structure diffusion, indicating that the reorganization of the structural pattern is an inherent part of the diffusion path (Kreuer, 1996). In many cases, Grotthuss type mechanism is progressively dominated by vehicle-type mechanisms at increasing temperature, *i.e.* there is a gradual transition from Grotthuss to vehicle type conductivity. Investigations dealing with hydration and swelling of membranes have been carried out to analyze the influence of hydration conditions on transport properties of polymer (Ludvigsson, Lindgren and Tegenfeldt, 2000; Kim and Kim, 2003). In ionic polymers, hydration makes that adjacent cluster to be interconnected through channels that enhances ion and water transport (Gebel, 2000; Siroma, Ioroi, Fujiwara and Yasuda, 2002; Wang, Cavano, Aubuchon and Palmer, 2003). From this fact, the clusters arrangement has a marked influence on the physical properties of ionomers.

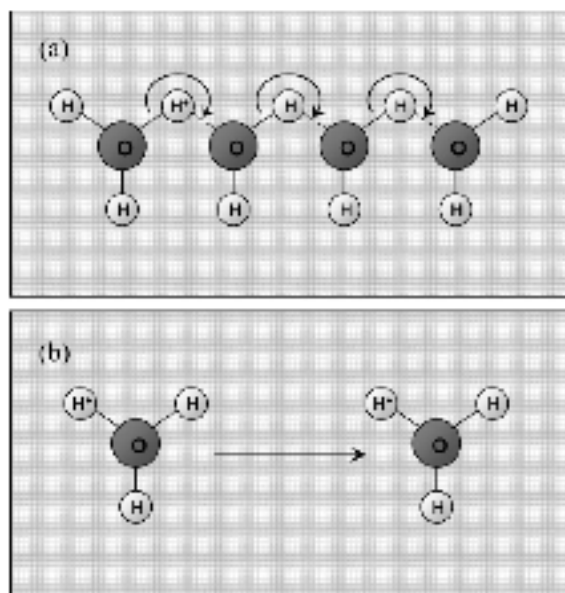


Figure 2.5 Models of H^+ transport mechanisms within ionomer membranes (a) Grotthuss (hopping) and (b) vehicle mechanisms. (a) is a simplified model of the Grotthuss mechanism, where the proton hopping direction deals with only one dimension (Saito, Hayamizu and Okada, 2005).

2.4 Ionomer crosslinking by Cationic donors

The idea of crosslinking of PEM is not new, but most of the crosslinking studies done previously pertain to chemical (covalent) crosslinking (Kerres, Cui and Junginger, 1998; Guo, Pintauro, Tand and O'connor, 1999; Chen *et al.*, 2005). The crosslinking procedure discussed in this work is a relatively less studied technique, which is ionic crosslinking. The approach is to exchange with divalent cations some of the protons in acidic membranes. The salt produced by the exchange reaction should have very low water solubility and form a stable crosslink. To the best of the authors knowledge, the application of the abovementioned crosslinking procedure to PEMs is a novel idea.

In general, crosslinking alters several important properties of polymers. Although decrease ionic conductivity, the vantage effects of crosslinking are reduction in the sorption in swelling solvents, increase in transition temperatures, and increase in plateau modulus. In some cases, crosslinking can also enhance the tensile strength and toughness of the polymer. It can also alter the permeability and permselectivity of the polymer.

2.4.1 Ionic conductivity in cationic doped-ionomers

It has been found by Koter, Piotrowskia and Kerres (1999) that crosslinked ionomer membranes based on sulfinated and sulfonated PSU in aqueous solutions of HCl, NaCl and KCl are more compact and their conducting paths are of smaller dimension than that of the Nafion[®] 117. Similarly as for aqueous solutions the conductivity of membranes changes in the order NaCl < KCl < HCl. Okada, Arimura, Satou, Yuasa and Kikuchi (1999) investigated ion and water transport characteristics of perfluorosulfonated ionomer membranes in the mixed cation form of H/Fe, H/Ni, and H/Cu systems. Membrane cationic composition showed that trivalent cations had more affinity than divalent cations. Also larger valence cations caused less water content in the membrane. The membrane ionic conductivity was markedly influenced by counterions and H⁺ mobility μ_{H^+} was altered according to the nature of coexisting cations. In the presence of Cu²⁺, μ_{H^+} increased from its inherent value, while in the presence of Fe³⁺, μ_{H^+} decreased to a large extent, Ni²⁺ bringing about nearly no change in μ_{H^+} . The ionic transference number of H⁺ was also influenced by coexisting cations in several ways. The interaction between adjacent cationic species in the membrane ion exchange sites, although plausible in general for multivalence cations, appeared to be not specific due probably to the shielding of the cationic charge by

water molecules or by sulfonic acid groups. The water transference coefficient $t_{\text{H}_2\text{O}}$ as measured by streaming potential measurements showed unique changes with membrane ionic composition, and $t_{\text{H}_2\text{O}}$ increased from 2.5 to over 13 by the presence of impurity ions. These impurity ions were found to result in more water molecules dragged than in the case of individual ions, when coexisting with the H^+ ion. Overall, it was noted that the water molecules within the influence of impurity cations appeared to play a large role in the H^+ movement in the membrane. Doyle, Lewittes, Roelofs, Perusich and Lowrey (2001) measured Ionic conductivity of Nafion® perfluorinated ionomeric membranes in nonaqueous solvents and solvent mixtures. The ionic conductivity of cationic forms of the membranes are measured and found to have influences to a varied extent depending on the choice of solvent with the relative order of conductivities being similar to those in water: $\text{H}^+ > \text{Ag}^+; \text{NH}_4^+ > \text{Na}^+ > \text{Li}^+ > \text{K}^+ > \text{Rb}^+ \gg \text{divalent cations} > \text{Cs}^+ \gg \text{trivalent cations} \gg \text{tetrabutylammonium}^+$. An ionic conductivity data for Nafion® 117 membranes exchanged with various cations and equilibrated with specific dipolar solvents at $T = 23^\circ\text{C}$ are showed in Table 2.1. While membrane solvent properties are important in determining ionic conductivity, polymer structural properties are also critical. As cation dissociation can be the rate-limiting step in ionic conductivity in poor solvating media, the basicity of the fixed anion group is expected to be a strong factor influencing conductivity.

Table 2.1 Ionic conductivity data (in mS/cm) for Nafion® 117 membranes exchanged with various cations and equilibrated with specific dipolar solvents at $T = 23^{\circ}\text{C}$

(Doyle, Lewittes, Roelofs, Perusich and Lowrey (2001).

Cation type	Ionic conductivity in water	Ionic conductivity in TEP	Ionic conductivity in NMC	Ionic conductivity in GBL	Ionic conductivity in DMSO
H ⁺	90.20	0.087	5.56	0.827	5.62
NH ₄ ⁺	74.95	0.521	4.98	0.509	7.94
Ag ⁺	25.10	0.387	5.85	0.185	3.05
Li ⁺	16.10	0.345	4.60	0.475	1.60
Na ⁺	18.68	0.321	3.82	0.518	0.564
K ⁺	15.79	0.141	4.10	0.022	0.797
Rb ⁺	19.12	0.078	3.87	0.012	0.895
Cs ⁺	5.65	0.007	3.59	0.013	1.65
Mg ²⁺	8.87	$<1 \times 10^{-2}$	2.50	0.001	0.192
Ca ²⁺	9.09	$<1 \times 10^{-2}$	2.79	0.01	0.45
Sr ²⁺	8.03	$<1 \times 10^{-2}$	3.29	0.025	0.319
Ba ²⁺	7.34	$<1 \times 10^{-2}$	2.56	0.012	0.368
Pb ²⁺	8.2	$<1 \times 10^{-2}$	3.60	0.006	0.69
Ni ²⁺	9.13	$<1 \times 10^{-2}$	2.15	0.001	0.129
Cu ²⁺	9.08	0.001	2.86	0.012	0.258
Zn ²⁺	9.45	0.001	3.62	0.008	0.17
Fe ²⁺	2.56	$<1 \times 10^{-2}$	1.88	$<1 \times 10^{-2}$	$<1 \times 10^{-2}$

Saito, Arimura, Hayamizu and Okada (2004) studied mechanisms of ion and water transport in perfluorosulfonated ionomer membranes for fuel cells. Various membranes, such as one Nafion, two Aciplex, and four Flemion types, having different equivalent weight values (EW) were examined. H, Li and Na-form samples were prepared for each membrane by immersion in 0.03 M HCl, LiCl, and NaCl aqueous solutions, and their properties in the fully hydrated state were investigated systematically. The water content of the membranes showed the tendency that the size and/or the number of ionic cluster region increases with decreasing EW value and the Li-form membranes have the most largely expanded ionic cluster regions. The ionic conductivity of the H-form membranes was considerably higher than that of the Li and Na-form membranes. It was suggested that the proton in the membranes transports by the hopping mechanism and the Li⁺ and Na⁺ ions by the vehicle mechanism. In addition, the ionic conductivity of all membranes increased with

increasing water content within the same kinds of membranes. Although the cation concentration in the membranes is insensitive to the EW value, the cation mobility increased with decreasing EW value. This means that the increased mobility of the carrier cations is the major factor to enhance the ionic conductivities due to the expansion of the ionic cluster regions. The water transference coefficients for the Li and Na-form membranes showed higher values than those of the H-form membranes, while the water permeabilities gave the inverse tendency. This means that the water molecules in the Li and Na-form membranes interact with the Li^+ and Na^+ cations more strongly than the proton when the cations move in the membranes, and as a result the diffusion of the water molecules is reduced. With the same ionomers (Saito, Hayamisu and Okada, 2005), the ionic conductivity, water self-diffusion coefficient ($D_{\text{H}_2\text{O}}$), and DSC were measured in the fully hydrated state as a function of temperature. The ionic conductivity of the membranes was reflected by the cation transport through the intermediary of water. Clearly, H^+ transports by the Grotthuss (hopping) mechanism, and Li^+ and Na^+ transport by the vehicle mechanism. The $D_{\text{H}_2\text{O}}$ in the membranes exhibited a tendency similar to the ionic conductivity for the cation species and the EW value. The increase in the ionic conductivity with decreasing EW value arises from the increase in the water content in the membranes, which is due to the increase in the number of cations and sulfonic acid groups having high hydrophilic properties. In addition, water transport in the membranes is strongly influenced by the interaction with the ionic species, *i.e.*, cations and sulfonic acid groups. Especially the cation species and their hydrophilic property are quite important for the water content and mobility. However, no remarkable difference of $D_{\text{H}_2\text{O}}$ between H and the other cation-form membranes was observed as compared with the ionic conductivity. This

indicates that water in each membrane diffuses almost in a similar way; however, H^+ transports by the Grotthuss mechanism so that conductivity of H^+ is much higher than that of the other cations. Moreover, the D_{H_2O} and DSC curves suggested that completely free water (bulk water) does not exist in the membranes, and water weakly interacting with the cation species. DFT calculation of the interaction (solvation) energy between the cation species and water molecules suggested that the water content depend strongly on the cation species penetrated into the membrane. The size of the interaction energies (ΔE_{int}) values of the clusters including the same number of water molecules (Fig.2.6) followed the trend $Li^+ \geq H_3O^+ > Na^+$. This electrostatic interaction between the cation and water molecules strongly influences the amount of water uptake into the membranes.

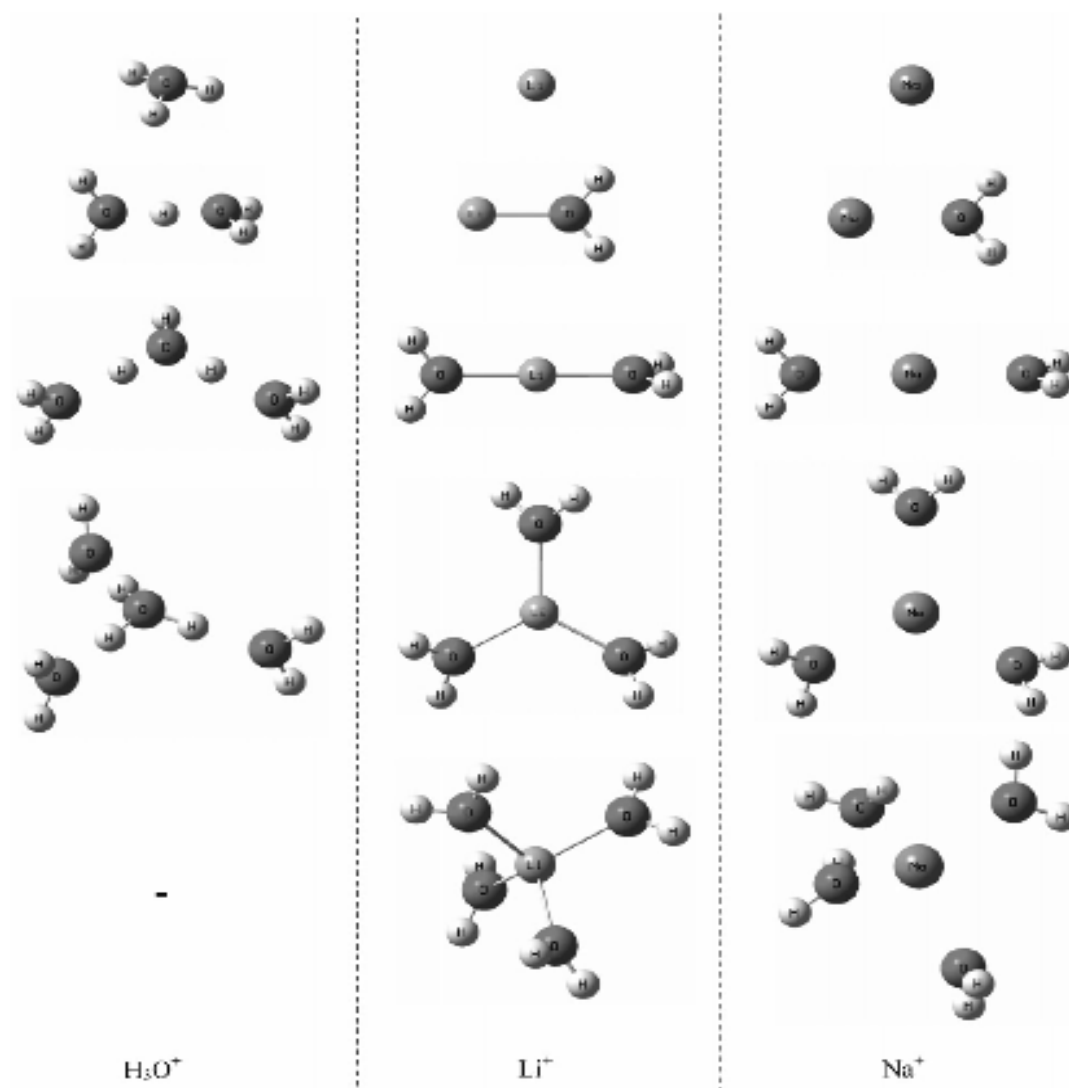


Figure 2.6 Optimized geometries of the $X^+(H_2O)_n$ clusters. B3LYP/6-311+G**//
 B3LYP/6 311+G** (Okada, Arimura, Saton, Yuasa and Kikuchi, 2005).

Transport characteristics of binary cation systems with Li^+ and alkali metal cations in perfluorosulfonated ionomers were studied by Okada, Arimura, Saton, Yuasa and Kikuchi, 2005. Nafion ionomer membranes were exchanged with series of pair of cation mixtures between Li^+ and other alkali metal cations, and investigated for equilibrium and transport characteristics of ion and water. The alkali metal cations, especially those of larger atomic number, revealed higher affinity to sulfonic acid groups than Li^+ , but less water content and higher density of the membrane. It was found that the mobility of cations followed the order of $\text{Li}^+ < \text{Na}^+ > \text{K}^+, \text{Rb}^+ > \text{Cs}^+$. The water transference coefficient (electro-osmosis drag coefficient) of Li^+ was ca. 15, but decreased to 10 for Na^+ and even less when other alkali metal cations existed. In the mixed systems, Li^+ and alkali metal cations showed tendency to drag more water molecules than in the individual ions, which indicated that ionic conductivity decreases when cations are coexisting in the membrane.

Zhang, Dou, Colby and Runt, 2005 investigated glass transition and ionic conduction in plasticized and doped poly (ethylene glycol)_n-co-5-sulfoisophthalate lithium) ionomers. They found that plasticization with a poly (ethylene glycol) oligomer significantly increases the ionic conductivity, despite a decrease in lithium concentration. Doping with LiClO_4 leads to much lower conductivity, despite the increase in Li^+ content. Atorngitjawat *et al.*, 2007. used broadband dielectric relaxation spectroscopy to study the dynamics of sulfonated polystyrene ionomers. In their work, sulfonated polystyrene ionomers were prepared from the precursor sulfonic acid polystyrene, having 1 and 7 mol % sulfonic acid, by exchanging the protons of the acid functionality with Na, Cs, and Zn cations. The dielectric relaxations were observed above the glass transition temperature. The relaxation

strengths of ionomers were suppressed by interaction with the cations that create physical cross-links, and the relaxation times decreased with increasing strength of the electrostatic interaction of the ion pairs.

Chen *et al.* (2007) studied the effects of dissolved iron and chromium on the performance of direct methanol fuel cell. To evaluate the influences of Fe^{3+} and Cr^{3+} on the performance of DMFC, the cell was fed with 1 mol L⁻¹ methanol solution containing different concentrations of Fe^{3+} or Cr^{3+} for 24 h. The results show that the cell performance decreased remarkably when the concentration of Fe^{3+} or Cr^{3+} exceeded 1x10⁻⁴ mol L⁻¹. Fe^{3+} displayed a strong negative effect on the catalytic oxidation of methanol, while Cr^{3+} affected the cell performance primarily by exchanging with protons of the membrane/ionomer and resulted in ionic conductivity losses. Gasa, Weiss and Shaw (2007) studied Ionic crosslinking of ionomer polymer electrolyte membranes using barium cations. In their work, the protons in acidic SPEKK membranes were partially exchanged with divalent barium cations to create ionic crosslinks between the sulfonate groups attached to the aromatic rings of the PEKK to reduce the water sorption of the membranes and improve their mechanical properties and dimensional stability. This is because acidic polymer electrolyte membranes (PEM) based on sulfonated poly (ether ketone ketone) (SPEKK) with relatively moderate to high levels of sulfonation (ion-exchange capacity (IEC) > 1.7 meq/g) have excellent proton conductivities (< 0.1 S/cm), but they absorb excessive amounts of water at elevated temperatures (*ca.* 60-90°C). The degree of crosslinking was varied by changing the degree of neutralization of the ionomer. The conductivity was reduced by crosslinking, but the thermal stability, swelling, and barrier properties were improved. Crosslinking reduced the water swelling at room temperature by

nearly a factor of two and prevented membrane dissolution at temperatures up to 80°C. In a water/methanol mixture (72/28, v/v), swelling was reduced by a factor of four. The balance of transport and mechanical properties could be varied to produce a viable PEM for a direct methanol fuel cell by adjusting the crosslink density.

From the review of ionic conductivity in ionomers exchange with cationic, it is obvious that the ionic conductivity of the H-form membranes was higher than that of the cationic-form membranes. The conductivity values of clusters followed the trend $H^+ > \text{monovalent} > \text{divalent cation}$. This is due to the trivalent cations had more affinity than divalent and monovalent cations. This means that the water molecules in cationic-form membranes interact with the cations more strongly than the proton when the cations move in the membranes, and as a result the diffusion of the water molecules is reduced. Also larger valence cations caused less water content in the membrane. As it was suggested earlier that the proton in the membranes transports by the hopping mechanism and the cations by the vehicle mechanism. These two mechanisms have water molecules as the charge carrier. Thus, reduction of carrier mobility, in the same way, reduce ionic conductivity in cationic-form membranes.

2.4.2 Improving of PEM properties by cationic crosslinking

Effect of monovalent (Na^+ , K^+) and divalent (Ca^{2+} , Ba^{2+}) cations on volume variation of ionic gels in water solution was studied by Jar and Wu, 1997. The results confirmed the reported theoretical prediction on how ion concentration affects the gel swelling behavior. In addition to the gel swelling, gel shrinkage was observed during the hydrolysis in solutions with divalent cations. The gel shrinkage was attributed to the formation of ionic crosslinks that change elastic modulus of the gel.

Replacing the divalent cations by monovalent cations, the shrunk gel swelled to a size larger than that before the hydrolysis. The results suggest that gel swelling and shrinkage can be controlled by valency for the cations in the solution. The valency for the cations affects density of ionic crosslinks, resulting in variation of elastic modulus for the gel. The balance between the osmotic pressure difference and the elastic modulus of the gel provides a way to control the gel deformation behaviour. As the study reveals that the ionic crosslinks, due to ionic clusters, affect the elastic modulus of the gel, they suggested that further study using small angle X-ray scattering should be carried out to provide evidence of the ionic clustering, especially for the gels with divalent cations.

To reduce the water sorption of the membranes and improve their mechanical properties and dimensional stability, the protons in acidic SPEKK membranes were partially exchanged with divalent barium cations to create ionic crosslinks between the sulfonate groups attached to the aromatic rings of the PEKK. (Gasa, Weiss and Shaw, 2007). Although the crosslinking reduced the proton conductivity of SPEKK membranes, the methanol permeability and methanol sorption were reduced significantly. There seemed to be an optimum degree of crosslinking, about 14% barium exchange, where the ratio of the proton conductivity to the methanol permeability, the selectivity, was highest (Fig.2.7). But, more samples with various degrees of crosslinking need to be tested to confirm the statistical significance of this optimum crosslink density. Statistical analysis of the data obtained in this study showed that there is a decreasing relationship between selectivity and the degree of crosslinking. However, when a highly sulfonated PEKK was used (e.g., IEC = 2.06 meq/g), a barium exchange of 10%, still yielded a membrane with a proton

conductivity comparable to that of Nafion®, but with a methanol permeability 80% lower than that of Nafion®. Crosslinking with barium ions also greatly improved the thermal stability of the SPEKK membranes under dry conditions (Fig.2.8), and crosslinking mitigated the problem of excessive water sorption of SPEKK membranes at elevated temperatures (Fig.2.9).

With a divalent cation (e.g., barium), intermolecular crosslinks that form from the ion-bridge due to the metal sulfonate, renders the polymer less swellable by water and also may improve the membranes mechanical properties. However, investigation is needed into the question of the durability of the crosslinks in a working fuel cell. In the materials area, additional work is needed to determine whether other cations also may work to improve membrane selectivity and mechanical properties. In this case, dipole–dipole aggregation of the metal sulfonate groups, similar to what occurs in metal salt ionomers of much lower ion-exchange capacity, may provide the crosslinks. Similarly, other divalent cations or higher valency ions such as Al (III) or Ti(IV) may be of interest. The higher valency cations may provide stronger crosslinking and better water resistance and mechanical properties using less exchange of the protons.

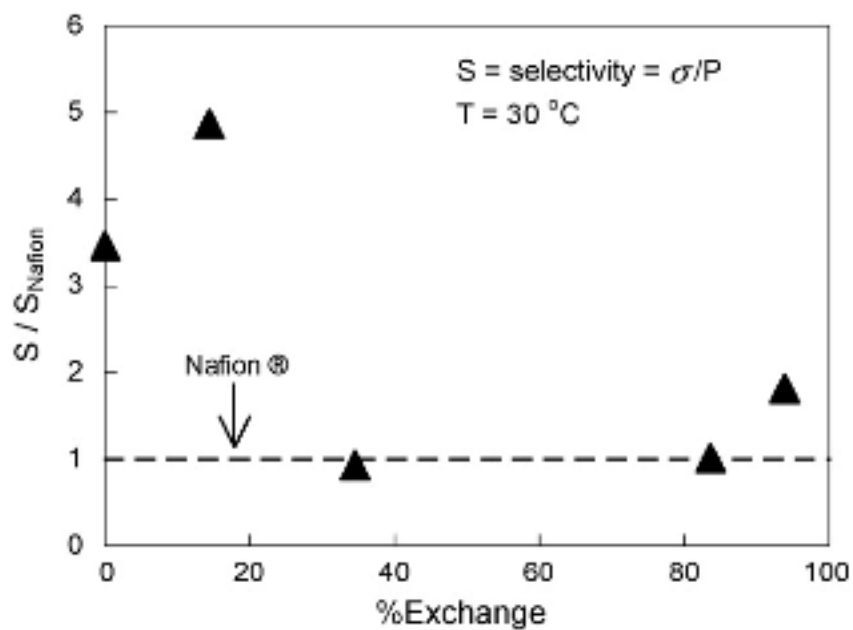


Figure 2.7 Influence of barium-exchange fraction on the permselectivity of the barium-exchanged SPEKK membranes normalized with respect to the permselectivity of Nafion® (Gasa, Weiss and Shaw, 2007).

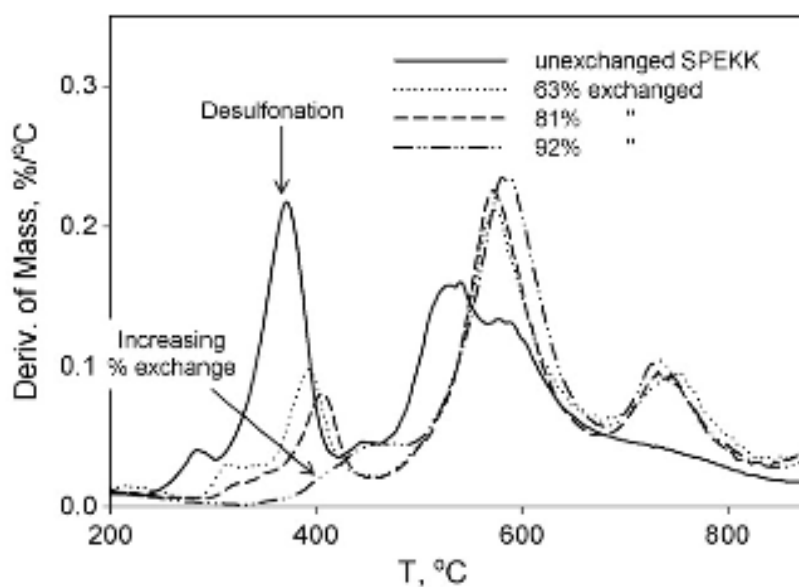


Figure 2.8 Derivative TGA curves of the barium-exchanged SPEKK (1.7 meq/g) membranes for various exchange fractions (Gasa, Weiss and Shaw, 2007).

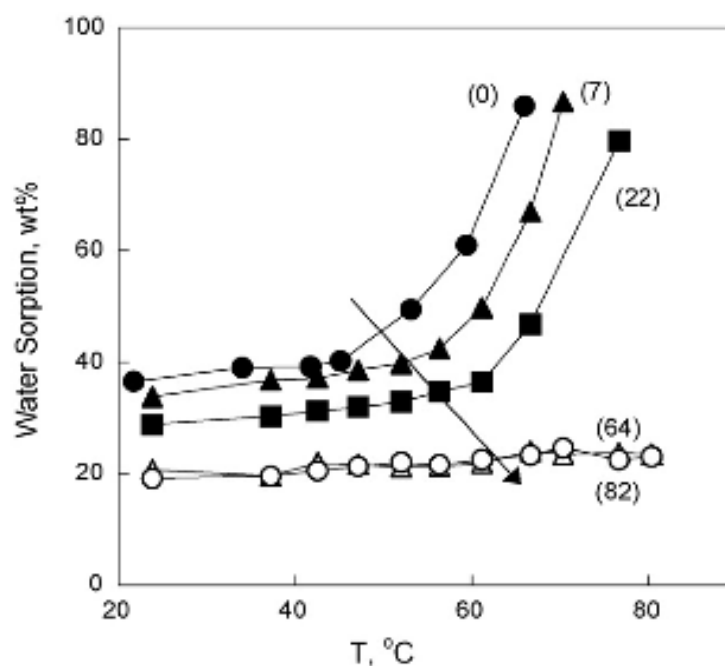


Figure 2.9 Influence of temperature and barium-exchange fraction on the water sorption at 25°C of barium-exchanged SPEKK membranes. The numbers in parentheses represent the mol % of H^+ neutralized by Ba^{2+} . The IEC of the untreated SPEKK was 1.7 meq/g (Gasa, Weiss and Shaw, 2007).

Ionomers have hydrophobic polymer structures with ionic groups randomly located along the hydrocarbon backbone. The number, type, and locations of these charged groups are based on the monomer composition and polymerization process used to produce the copolymer. To form an ionomer from a polymer containing acid groups, part or all of the copolymer's acid groups are neutralized with a cation. These species form ion pairs that will phase separate into nanometer-size aggregates. These aggregates impart remarkable properties to ionomers including exceptional clarity and toughness (Eisenberg and Kim, 1998).

Farrell and Grady (2001) studied copolymers of ethylene and either acrylic and methacrylic acid (E-AA or E-MAA). Both have significant commercial

applications, including food packaging materials, automobile parts, and golf ball covers. The vast majority of commercial E-AA or E-MAA ionomers are neutralized with zinc, sodium, or both zinc and sodium. The properties of zinc-neutralized and sodium-neutralized carboxylate copolymer ionomers are very different; these differences include the following:

(1) Sodium-neutralized ionomers absorb significantly more water.

(2) Sodium-neutralized ionomers are typically harder than the zinc counterparts, which is a result of higher fractional crystallinities. This crystallinity difference is also typically reflected in a higher melting point for the sodium-neutralized material, although the melting points of both ionomers are typically very low (90°C) compared to polyethylene homopolymer.

(3) Zinc ionomers show excellent adhesion to a variety of solid surfaces, while sodium ionomers do not.

These differences are the result of differences in aggregate characteristics, i.e., size, shape, and composition. They have extensively studied the zinc aggregate in both E-MAA and E-AA copolymer ionomers (Grady, Floyd, Genetti, Vanhoorne and Register, 1999; Grady, 2000; Farrell and Grady, 2000). Their studies, as well as the properties listed above, are consistent with the conclusion that zinc aggregates are thermodynamically highly favored. Experimental evidence from their studies to support this conclusion are the following:

(1) Adding water does not break the aggregate apart when absorption is carried out at room temperature. A recent study from Ishioka *et al.* confirmed this observation (Ishioka, Shimuzu, Watanabe, Kawauchi and Harada, 2000). Through

detailed inductive analysis, they concluded that water absorbs only at the edges of aggregates.

(2) Heating the material to near the degradation temperature of the polymer without any applied stress does not significantly affect the aggregate structure.

(3) Aggregates in E-AA and E-MAA ionomers have essentially the same structure.

(4) A significant amount of isolated zinc ions appear only at neutralizations less than about 20% of stoichiometric.

The structure of the aggregate does not change as a function of neutralization; however, the average size increases with increasing neutralization amount.

Ding (1986) studied sulfonated polyurethane ionomers (M1) based on toluene diisocyanate (TDI) and either poly(tetramethylene oxide), poly(propylene oxide) or polybutadiene (PTMO, PPO, or PBD) polyols doped with various cation types (*i.e.* Na^+ , Cs^+ , Ca^{2+} , Ni^{2+} , Zn^{2+} , Cd^{2+} and Eu^{3+}).

Stress-strain curves for ionomers neutralized with different cations are presented in Fig. 2.10. Tensile properties are summarized in Table 2.2. Figure 2.10 and Table 2.2 show that the strength and extensibility of the materials are remarkably high. Based on previous SAXS, IR and dynamic mechanical analysis, the superior tensile properties of these ionomers are attributed to the development of a two phase morphology. The ionic phase serves as a crosslinking point and gives the materials mechanical strength, while the PTMO matrix provides the material's extensibility at temperatures above its T_g ($\sim -70^\circ\text{C}$). A most interesting feature revealed from Fig. 2.10 and Table 2.2 is the strong dependence of tensile properties on the neutralizing cation and sample preparation method. The tensile strength followed the trend:

Ni(methano1) > Ca(DMF) > Ni(DMF) > Na(DMF) > Eu(DMF) > Cd(methano1) > Zn(methano1) > Cd(DMF) > Zn(DMF) > Cs(methano1). Young's modulus followed a similar trend. There is presently no apparent rationalization of the tensile properties data based on the difference in cation radius, charge, or coordination number.

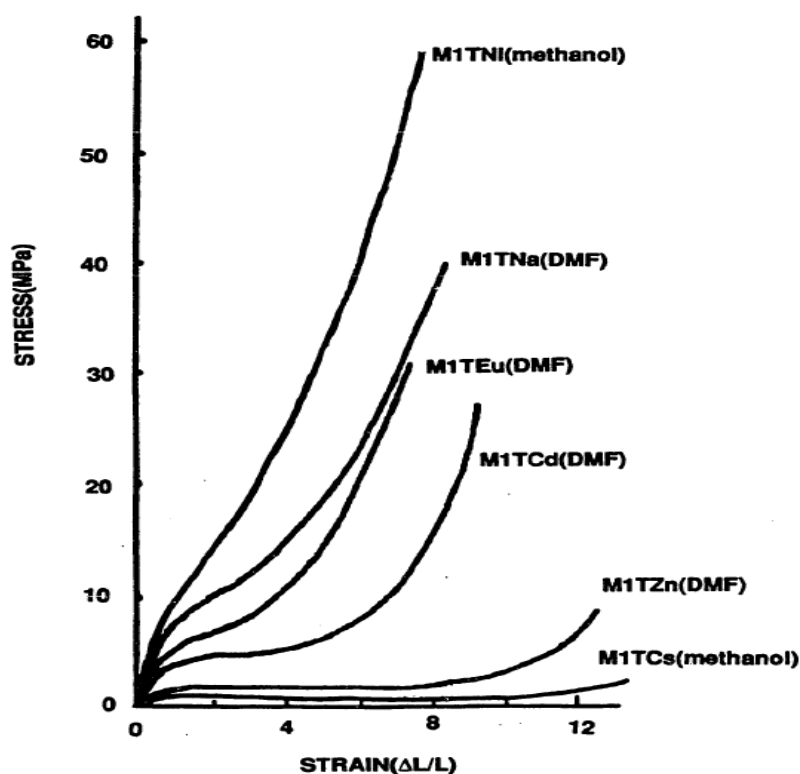


Figure 2.10 Stress-strain curves for PTMO (1000)-TDI based ionomers with different neutralizing cations (Ding, 1986).

Table 2.2 Summary of Tensile Properties and SAXS Parameters for a Model PTMO-TDI Based Polyurethane Ionomer (Ding, 1986).

Sample	Tensile Properties			SAXS Parameters (Liquid Model)			
	Young's Modulus (MPa)	Tensile Strength (MPa)	Strain at Break (%)	R_1 (nm)	V_p (nm ³)	A (nm ⁻¹)*	$\Delta\rho_1$ (nm ⁻³)
M1TCa/DMF	18.2	55.5	780	1.26	157	0.127	197
M1TNI/DMF	19.4	19.0	375	1.63	326	0.102	226
M1TNa/DMF	17.5	40.5	375	1.40	186	0.132	198
M1TEu/DMF	16.1	30.5	700	0.99	121	0.102	299
M1TCd/DMF	13.7	26.0	830	1.32	203	0.108	361
M1TZn/DMF	8.2	9.7	1130	1.42	262	0.098	251
M1TNI/methanol	20.0	63.0	650	1.15	174	0.096	336
M1TZn/methanol	12.5	25.8	650	1.31	205	0.105	306
M1TCs/methanol	2.5	2.4	1340	1.97	467	0.104	286

$$* A = 4\pi R_1^2 / V_p$$

Previous SAXS analysis of these ionomers suggested that the size and concentration of the ionic aggregates do not strongly depend on the neutralizing cation. A comparison of the tensile properties of the ionomers and their structural parameters based on SAXS analysis can be found in Table 2.2. It is not apparent if the effect of cation on tensile properties can be explained by the size and concentration of the aggregates, or by the aggregate specific surface area, which presumably is related to the chain density in these materials. Regarding the effect of sample preparation method on tensile behavior, it appears that samples with a higher electron density contrast tend to have higher tensile properties. A higher electron density would be related to a more compact ionic domain, and thus better domain cohesion.

EXAFS analysis of the local coordination structures of these ionomers provides a possible explanation for the tensile behavior. Ionomers with a higher degree of local order in the coordination environment surrounding the cation, such as Ca^{2+} , Ni^{2+} and Eu^{3+} , tend to be stronger. Those ionomers with a lower degree of local order, such as Cd^{2+} , Zn^{2+} and Cs^+ , tend to be weaker. Strong ion-ion interactions inside the aggregate provide a high degree of local order and enhance domain cohesion. This enhances the tensile behavior of these ionomers, especially at high strain levels.

A Mooney-Rivlin plot of the stress-strain data shown in Fig.2.11 reveals an interesting feature in the tensile behavior of the polyurethane ionomers. Strain hardening in these polymers occurred at different elongation levels for ionomers neutralized with different cations. Strain hardening behavior is related to strain induced crystallization or high level of chain orientation. Ionomers with stronger intradomain cohesion should have less domain disruption and chain relaxation, allowing strain hardening to take place at a lower elongation level. From EXAFS, M1Ni and M1Eu have clear second-shell peaks in their RSFs; M1Ca and M1Cd may or may not have weak second shell peaks; the M1Zn RSF clearly has only a single peak; and the M1Cs RSF has only one peak. Therefore, it seems that in the dry samples, the postulate that aggregate cohesiveness controls the large-strain tensile properties is verified.

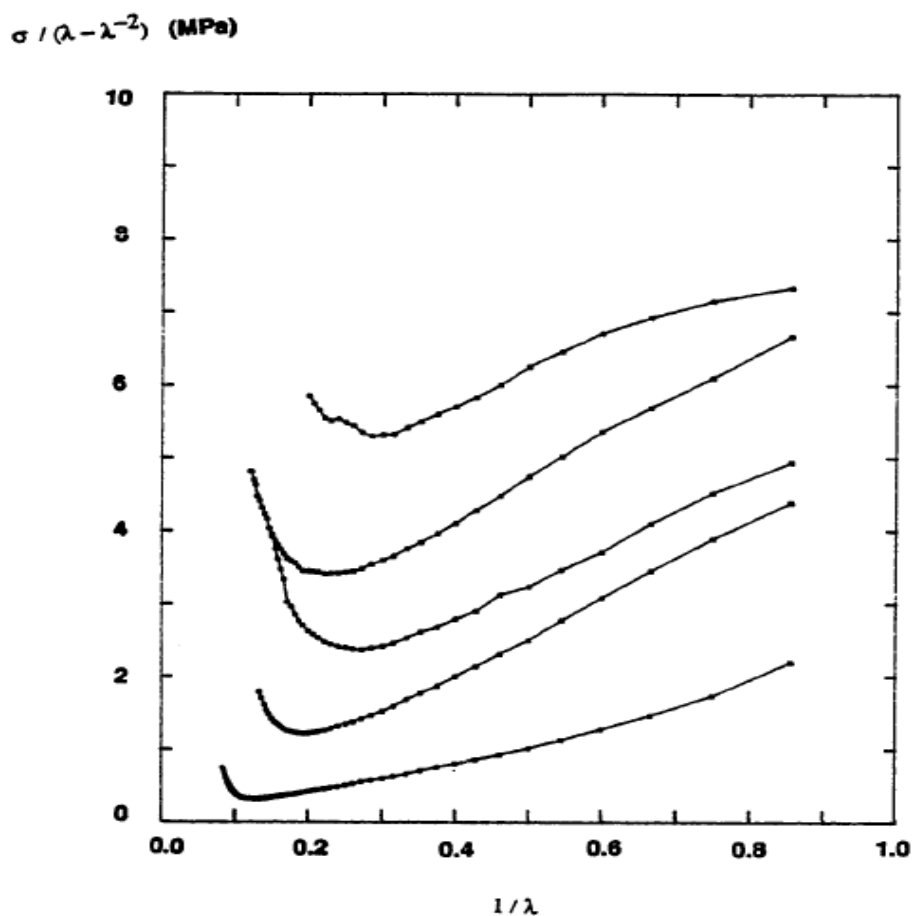


Figure 2.11 Mooney-Rivlin plots of the stress-strain data of PTMO (1000)-TDI based polyurethane ionomers. The neutralizing cations for curves from the top to the bottom are Ni^{2+} , Na^+ , Eu^{3+} , Cd^{2+} and Zn^{2+} (Ding, 1986).

Also in a previous investigation of non-crystallizable carboxy-telechelic polyisoprenes (Register, Foucart, Jerome, Ding and Cooper, 1988) it was found that the strain hardening behaviour observed when the neutralizing cation was divalent nickel or calcium could be explained by the presence of a second coordination shell in the EXAFS data due to a well defined cation-cation distance. It was inferred that the higher degree of order present in these aggregates made them more cohesive, and therefore the stressed chains could not relax by “ion-hopping”, where ionic groups are

transported between aggregates (Ward and Tobolsky, 1967; Sakamoto, Macknight and Porter, 1970; Hara, Eisenberg, Storey and Kennedy, 1986).

2.5 Extended X-ray Absorption Fine Structure (EXAFS) as the tool to probe internal aggregate order in ionic crosslinking

Determining the structure inside these domains is extremely important in ionomer research, since this information is necessary to understand the thermodynamics and mechanism of phase separation in these materials. Unfortunately, methods to probe internal phase structure which have been applied to other microphaseseparated systems cannot be successfully utilized on ionomers. Differential scanning calorimetry, which is sensitive to the glass and/or melting temperature of each phase, does not exhibit any features from an ionic phase transition due to the well-known fact that ionic aggregates are thermodynamically stable to the degradation temperature of the polymer. Wide-angle X-ray scattering curves do not have peaks from crystalline ordering inside the ionic phase because the aggregates are very small; hence, even if the aggregates are crystalline on a local scale, only two or three unit cells can exist in any direction. Dynamic mechanical thermal analysis (DMTA) does have a high-temperature feature which is attributed to the presence of ionic groups, but a recent theory (Eisenberg, Hird and Moore, 1990) attributes this transition to the motion of immobilized polymer chains rather than ionic groups.

One of the few morphological probes which has been successfully applied to help understand internal aggregate order has been extended X-ray absorption fine structure (EXAFS) (Grady and Cooper, 1994). EXAFS is a powerful technique for

determining the local atomic environment about a specific atom, and has been profitably applied to numerous ionomers (Pan, Knapp and Cooper, 1983; Jerome, Vlais and Williams, 1983; Galland *et al.*, 1986; Meagher *et al.*, 1986; Register *et al.*, 1988).

The EXAFS signal is a modulation of the X-ray absorption coefficient on the high energy side of an elemental absorption edge, and it contains information on the coordination shells surrounding that atom. The type and number of atoms in a shell, as well as the distance to and disorder within a shell, are all reflected in the EXAFS data. In a previous investigation of non crystallizable carboxy-telechelic polyisoprenes (Register, Foucart, Jarome, Ding and Cooper, 1988), it was found that the strain hardening behaviour observed when the neutralizing cation was divalent nickel or calcium could be explained by the presence of a second coordination shell in the EXAFS data due to a well defined cation-cation distance. It was inferred that the higher degree of order present in these aggregates made them more cohesive, and therefore the stressed chains could not relax by 'ion-hopping', where ionic groups are transported between aggregates (Sakamoto, MacKnight and Porter, 1970). Ion-hopping was discussed previously (Ding, Register, Yand and Cooper, 1989) in explaining the poorer physical properties observed with Cs^+ and Zn^{2+} cations relative to Ni^{2+} and Eu^{3+} cations. Therefore, it is of interest to see whether the mechanical properties in the ionomer series can be correlated with the degree of order within the ionic aggregates, as determined by EXAFS.

EXAFS theory: EXAFS is the measure of oscillations in the absorption coefficient (μ) about its mean value at energies between 50 and 1000 eV above an atomic absorption edge. An absorption edge occurs when the energy of an X-ray is

sufficient to cause the ejection of a photoelectron; the K-edge corresponds to the ejection of a 1s electron. Oscillations occur because the outgoing photoelectron wave can be backscattered by neighboring atoms which leads to interference between the outgoing and backscattered waves. Qualitatively, the shape and period of the oscillations will be a function of the absorbing atom as well as the type, distance, and number of atoms around the absorbing atom. Generally, the distance between the central atom and the backscattering atom must be less than 5 Å in order for the interference to be significant.

The simplest correct theoretical description of this phenomenon was originally developed by Stern, Sayers and Lytle, 1975 and has been labeled single-electron single-scattering theory. This theory assumes that multiple-scattering events are unimportant and that disorders, both thermal and static, are small. The fundamental equation from this theory assuming a completely isotropic sample is

$$\chi(k) = \frac{\mu(E) - \mu_0(E)}{\mu_0(E)} = \sum_j N_j S_0^2(k) \frac{F_j(k)}{kR_j^2} e^{-2\sigma_j^2 k^2} e^{-2R_j/\lambda_j} \sin[2kR_j + \phi_{ij}(k)] \quad (2.1)$$

where $\mu(E)$ and $\mu_0(E)$ are the measured and mean absorption coefficients, respectively, at the energy E , N_j is the number of atoms of type j in the j th shell, $S_0^2(k)$ is the amplitude reduction factor which is due to excitations of electrons other than 1s electrons (for a K -edge) in the X-ray absorbing atom, $F_j(k)$ is the backscattering amplitude (called the amplitude function) from the N_j atom, R_j is the root mean square distance between the central atom and the j th atom, σ_j is the Debye-Waller factor which measures the variation in R_j about its mean, λ_i is the electron mean free path, and ϕ_{ij} is the phase shift (called the phase function) experienced by the photoelectron,

which is a function of both the absorbing i atom and the backscattering atom. The k dependence of the amplitude reduction factor is usually quite small. In eq 1 it has been assumed that R_j and the type of atom are identical for all atoms in the j th shell. (Actually, R_j does not necessarily need to be identical, since slight variations in R_j between different atoms in the same shell can be accounted by the Debye-Waller factor.) If the material or the electric field polarization is isotropic, then the sum over l can be performed and the result is N_j , the number of atoms in the j th coordination shell. k is called the wave vector because $2\pi/k$ is the wavelength of the ejected photoelectron. Through a simple energy balance it can be shown that

$$k = \left[\frac{2m_e}{h^2} (E - E_0) \right]^{\frac{1}{2}} \quad (2.2)$$

where E_0 is the absorption edge energy, m_e is the mass of an electron, and h is Planck's constant divided by 2π . Equation 2.1 gives the expression for EXAFS oscillations as a function of wavevector, but generally a Fourier transformation is performed to yield the radial structure function (RSF). The RSF is similar to a radial distribution function in that peaks in the RSF correspond to distinct coordination shells. The units of the abscissa of the Fourier transform are angstroms, but the peaks are shifted from the interatomic distances as indicated by eq 2.1; hence a subscript F will be used to distinguish this distance from the actual interatomic distance R .

2.6 Molecular Dynamics (MD) simulation as a powerful technique to confirm of aggregated environment obtaining from EXAFS analysis.

Over the past two decades, there have been extensive studies directed at understanding the unique properties of ionomers (Eisenberg and King, 1997; Capek, 2004; Mathew *et al.*, 2002; Schneider and Rivin, 2006; Kazimiera and Kowalonek, 2006). The early studies focused on random ionomers where the ionic groups are randomly placed along the polymer chain. This was followed by considerable interest in telechelic ionomers where the ionic groups are located at the ends of the chain. More recently, several groups have studied segmental ionomers (Visser and Cooper, 1991; Zhang, Dou, Collby and Runt, 2005) and block copolymer ionomers (Lu, Steckle and Weiss, 1993) one of the segments or blocks is fully or partially ionized. Despite numerous experimental and theoretical investigations, the basic features of ionomers are still not well understood. For example, ionic aggregation is a well-documented phenomenon in ionomers, but the spatial details of the ions is still unverified. The effect of aggregation on the chain conformation and size is also unknown. Various theories predict either an expansion of the ionomers chain upon aggregation (Forsman, MacKnight and Higgins, 1984; Dreyfus, 1985) or no change of the average chain dimensions as a result of ionic aggregation (Squires, Painter and Howe, 1987). With the current availability of sophisticated software and more powerful computers, it is instructive to evaluate the effect of ionic aggregation on the chain dimensions of ionomers using molecular simulations. This may provide some insight and guidance for evaluating the chain conformation of ionomers by experimentalists.

Recently, it was found that many papers present advances in the use of molecular simulations and EXAFS spectroscopy, which enable us to understand solvated ions in solution. (Dang, Schenter, Glazakou and Fulton, 2006). A molecular-level understanding of ion-water and water-water interactions in solvation processes is essential to understanding the chemical and physical properties and transport mechanism of ions in aqueous solutions. Molecular dynamics (MD) and Monte Carlo (MC) simulation techniques provide a powerful approach to probing such processes in condensed phase environments (Allen and Tildesley, 1987). A detailed description of the solvent structure around an ion in solution can be obtained from a variety of experimental and theoretical techniques. MD simulations provide a detailed picture of structure and dynamics for complex systems that may not be tractable by other methods. At the heart of a computational study are the potential functions that have been very successful in describing complex phenomena (Dang and Chang, 1997). It is important to show that the simulation not only reproduces important macroscopic properties but also the molecular structure and dynamics of the ions in real systems.

Due to the advance of modern EXAFS algorithms and the availability of more accurate ion and solvent potential models, the number of studies that combine MD with EXAFS has increased considerably (D'Angelo, Nola, Fillipponi, Pavel and Roccatano, 1994; Filipponi and Di Cicco, 1995; Hoffmann, Dara, Palmer and Fulton, 1999). The accuracy of the existing theoretical models for the interatomic potential in solid and liquid simple ionic systems was discussed in through direct comparison of EXAFS and molecular-dynamics (MD) results (Di Cicco *et al.*, 1996; 1997). In this respect, it is then possible to benchmark the performance of MD simulation by using (1) the highest level of theory possible in an atomic structure calculation of finite size

clusters, and (2) spectroscopic studies of the hydrated ions in bulk solution from EXAFS measurements. In this research, a powerful combination of these two different techniques was used to determine the aggregated structure of SPS and SPEEK ionomers under the induction role of K^+ and Ca^{2+} donors.

CHAPTER III

RESEARCH METHODOLOGY

3.1 Apparatus and Materials

- Magnetic stirrers and magnetic bars
- Vacuum oven
- Hot air oven
- Hot plate stirrer
- Polystyrene (PS MW 22,000, 64,000 and 430,000 g/mol), Aldrich
- Sulfonated polystyrene (3.4 mol % sulfonate substitution levels)
- Poly(sodium 4-styrene-sulfonate)(Na-SPS MW 70,000), Aldrich
- Poly(ether-ether-ketone)(PEEK, VICTREX 150PF), Victrex.
- Potassium Acetate(CH_3COOK), Aldrich
- Calcium Acetate Monohydrate($\text{C}_4\text{H}_6\text{CaO}_4 \cdot \text{H}_2\text{O}$) Aldrich
- Methanol (CH_3OH), Analytical Reagent, Merck
- Toluene ($\text{C}_6\text{H}_5\text{CH}_3$), Analytical Reagent, Merck
- N, N-Dimethyl Formamide(CH_3)₂NC(O)H), Analytical Reagent, Ajax
- Tetrahydrofuran (CH_2)₄O), Analytical Reagent, Aldrich
- Sulfuric acid (H_2SO_4)(95-97%), Analytical Reagent, Merck

3.2 Experimental Part

3.2.1 Sample preparation

3.2.1.1 Preparation of SPS thin films

3.4 mol % sulfonated Polystyrene (SPS) was dissolved in a 90/10 v/v mixture of toluene/methanol and neutralized with a stoichiometric amount of potassium acetate/ calcium acetate monohydrate to produce fully neutralized potassium/calcium sulfonated PS, respectively (the simple neutralization reaction of acidic ionomer is shown in Fig.3.1). Samples were stirred at room temperature until the solution became highly viscous. Then, this SPS solution was poured to the 45 mm disk (the amount of sample was adjusted to obtain a proper thickness calculating from equation 3.1, (*i.e.* in most cases about 0.5-1.0 mm.). Samples were then dried at room temperature in air for 1 week and then in a vacuum oven at 80°C for 3 days to get rid of residual solvent.

$$x = d \times \delta \times \pi \times (r^2) \quad (3.1)$$

where x is the weight of sample (g), d is the density of sample (SPS) (g/cm^3) and r is the radius of a circular disk (cm).

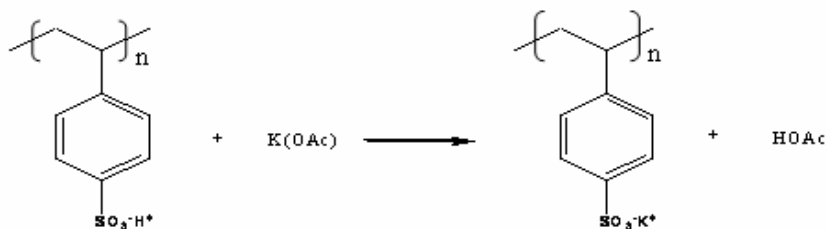


Figure 3.1 Schematic of the neutralization reaction of acidic SPS membranes.

3.2.1.2 Preparation of SPEEK thin films

About 6 g of the dried PEEK powder was carefully added to 200 mL of concentrated sulfuric acid (95-97%) at an ambient temperature in a reaction flask under vigorous stirring. The reaction was kept stirring at room temperature for further 120 h. After that, the reaction was terminated by slowly dropping into ice-cold deionized water under continuous stirring. The precipitated polymer was filtered and washed with de-ionized water until $\text{pH} \approx 6$. Then, the polymer was dried at room temperature in air for 3 day and then in a vacuum oven at 70°C for 12 h. Once the acid form of SPEEK has prepared, it was dissolved in a 90/10 v/v mixture of DMF /methanol and neutralized with a stoichiometric amount of potassium acetate/ calcium acetate monohydrate to produce fully neutralized potassium/calcium sulfonated PEEK, respectively. Sample was stirred at room temperature until the solution become highly viscous. The solution was then casted to thin film. After that, sample were dried at room temperature in air for 1 week and then in a vacuum oven at 90°C for 3 days to get rid of residual solvent. Sulfonation reaction of aromatic polyether ether ketones is shown in Fig.3.2.

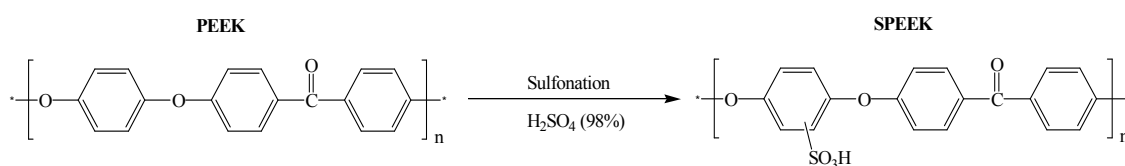


Figure 3.2 Schematic chemical structures of SPEEK.

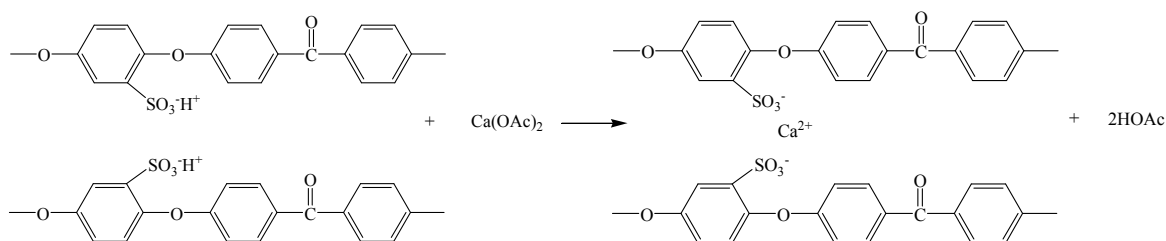


Figure 3.3 Schematic of the neutralization reaction of acidic SPEEK membranes.



Figure 3.4 Thin films of ionomers casted from glass disk.

3.2.2 Sample Characterization

3.2.2.1 Nuclear Magnetic Resonance (NMR) Spectroscopy

The ^1H experiments were performed on a Varian Unity INOVA NMR spectrometer operating at 300 MHz. The spectra were collected on SPS in CDCl_3 solvent and SPEEK in DMSO-d_6 solvent. The chemical shift of TMS was used as internal standard reference. 1D-NMR experiments were performed to determine the microstructure and find the degree of sulfonation (DS) of ionomers.

3.2.2.2 Fourier Transform Infrared Spectroscopy (FT-IR)

The infrared spectra of ionomers were obtained from the FT-IR spectrometer Perkin-Elmer model: spectrum GX. The numbers of scans were 4 at the

resolution of 1 cm^{-1} . The range of measurement was between 4000 cm^{-1} and 400 cm^{-1} for all samples.

3.3.2.3 Thermo Gravimetric Analysis (TGA)

TGA was performed on a SDT2960 simultaneous TA Instrument, for SPS systems, 20 mg of sample was heated from 25 to 600°C at a heating rate $10^\circ\text{C}/\text{min}$ under nitrogen gas blanket and, for SPEEK systems, from 25 to 600°C at a heating rate $10^\circ\text{C}/\text{min}$ under nitrogen gas blanket to determine weight loss and estimate amount of water contained in prepared ionomers.

3.2.2.4 Extended X-ray Absorption Fine Structure (EXAFS)

K-edge EXAFS spectra was collected at an X-ray Absorption Spectroscopy beam line (BL8), National Synchrotron Research Center (NSRC), Thailand. For both SPS and SPEEK systems, 2-eV steps were used in the pre-edge region, while 0.5-eV steps were employed from 30 eV below the edge to 100 eV above the edge. For the EXAFS region (100 eV above the edge to 800 eV), 1-eV steps were employed. Energy calibration was performed with the standard CaCO_3 and KI compounds. All measurements were performed under 250 mbar N_2 gas. A total of 3 scans (each scan lasted approximately 30 min) were collected, and these scans were added after E_0 determination before further data analysis to improve the signal to noise ratio.

AUTOBK (Newville, Livins, Yacoby, Rehr and Stern, 1993) a commercial software package was used to convert the measured μt vs E curves to $k^2\chi(k)$ vs k . To help this program determine the optimal background subtraction and edge locations, a hypothetical structure of the compounds having atomic positions analogous to the interested ionomers were modeled using the simulation package FEFF6 (Rehr,

Zabinsky and Albers, 1992). This package performs *ab initio* calculations of EXAFS patterns based on user-supplied XYZ coordinates of the atomic structure and includes single- and multiple-scattering curved wave paths. After isolation of the EXAFS oscillations, the data were Fourier transformed, which gave a result termed the radial structure function (RSF). The radial structure function is similar to a radial distribution function because peaks in the RSF usually correspond to distinct coordination shells. The abscissa of the RSF has units of angstroms, but the location of the peaks are shifted from the real distances as indicated in Eq 2.1; hence a subscript F was used to distinguish this distance from the actual interatomic distance R . Reduction procedures for all data sets were identical to enable direct comparison of results.

Many of the parameters appearing in Eq 2.1 were determined by FEFF6 directly. For the standards, the only free parameters in Eq 2.1 were the Debye-Waller factor for each shell and the amplitude reduction factor; all other terms either were determined by FEFF6 or were obtained from the known crystal structure. For our ionomers, the metal-oxygen distance and the number of oxygen atoms in the first shell were determined by the FEFFIT program (Newville, Haskel, Rehr, Stern and Yacoby, 1995), FEFFIT is a computer program for the analysis of XAFS data. It was designed to fit experimental XAFS spectra to theoretical calculations from FEFF6. Fitting can be done in both k and R space, and error analysis is automatically done, and a wide-range of options are given for modelling XAFS data. The fitting method calculates N/N_{ref} , $E_0 - E_{0,\text{ref}}$, $\sigma^2 - \sigma_{\text{ref}}^2$ and $R - R_{\text{ref}}$ where the subscript ref represents the value for the metal oxide reference. Although E_0 can be identified from a μt vs E plot, generally E_0 should be allowed to vary when applying the fitting method to correct for errors in

energy calibration and phase transferability (Teo, 1986). The amplitude reduction factor was assumed to be identical for the two samples when the ratio method was applied.

3.3 Computational Part

3.3.1 Molecular Dynamics (MD)

3.3.1.1 Bulk structures

Bulk structures of ionomers (shown in Fig.3.5) and water absorbed were generated and simulated by means of Accelrys commercial software (Materials Studio 4.1 provided by Computational Nanoscience Consortium, NANOTEC, Thailand) using the COMPASS force field. The composition of the system contained in each cell is summarized in Table 3.1 which all the MD simulations were performed under NVT conditions with the working temperature $T = 27$ and 30°C for the systems of PS and PEEK, respectively. The temperature was controlled by means of Andersen thermostat method with a collision ratio of 1.0. The standard Verlet algorithm was used to integrate Newton's law of motion with a time step of 1 fs (*i.e.*, 10^{-15} s). Van der Waals and Coulombic nonbonding interactions were calculated by the cell multipole method (CMM); the value of the update width parameter was 1.0 Å, and the accuracy parameter was set to medium to use third order in the Taylor series expansion and explicit interactions from more neighboring cells. 3D amorphous cells with periodic boundary conditions and containing different amounts of polymers and dopants were built using the Amorphous Cell module of the software.

3.3.2.2 Thin film

Thin films of PS and PEEK were constructed to investigate properties relating to the membrane characteristics. This was achieved by the confine layer method which allowed cells to behave like two dimension-boxes (Fig.3.6). The dimension of the periodic box along the z axis was increased by extending about 3 times the original length, and the other two dimensions were left unchanged. The relaxation and the data collecting stage of the films were achieved in the same way of amorphous cells.

3.3.2.3 Benchmark models of sulfonated ionomers

To study cation doped sulfonated PS and PEEK, systems containing molecular fragments of sulfonate group and metal cation Fig.3.7 were studied. This method is to represent the membranes with a suspension of such fragments rather than a fully connected polymer chain in order to produce higher molecular mobilities, so that a model could undergo significant structural reorganizations over the course of a simulation. The compositions of the benchmark models used in these simulations were obtained from TGA analysis of ionomers. This model corresponds to our samples under ambient humidity conditions, according to mass % from TGA analysis. In order to produce charge neutrality, hydroxonium ions were added in the box of sulfonate fragments and metal cation. To compare diffusion of H^+ in H-form ionomers, the cell which replaced cations by proton (H^+) was also studied. The requirement for mobile hydrogen ions required careful thought in order to achieve realistic results. Lone protons proved very destructive to the simulations due to their extremely high charge to mass ratio and small size. Each proton was therefore associated with a water molecule, to form a hydroxonium ion, as shown in Fig.3.8. In this way, the cations

were free to diffuse between sulfonate fragments in a natural way, as opposed to being bound to a particular site.

The size of the simulation box was adjusted in each case to give the correct overall density for the mass-weighted combination of ionomer and other molecular species in the box. Charges were calculated by the QEq_charged 1.1 module which is available in Materials Studio software. The structure of each system was first minimized with respect to all internal coordinates by conjugate gradient method until the maximum derivative smaller than 0.1 kcal/(Å mol), with a limit of 5000 steps. Then, the system was submitted to an equilibration process consisting on a 200 ps long MD run. The data collecting stage consisted of 1 ns MD runs for all systems. In all cases, the trajectories were saved each 5000 fs for subsequent analysis. Distance and coordination data were calculated from radial distribution function (RDF) analysis and used to discuss the results obtained from EXAFS technique.

Table 3.1 Description of the PS and PEEK Simulated Cells

Polymer	Chain length (Unit)	Temperature(K)	Box size(Å)	Density(g/cm ³)
PS	50	410	20.30	1.051
PEEK	20	303	19.76	1.260

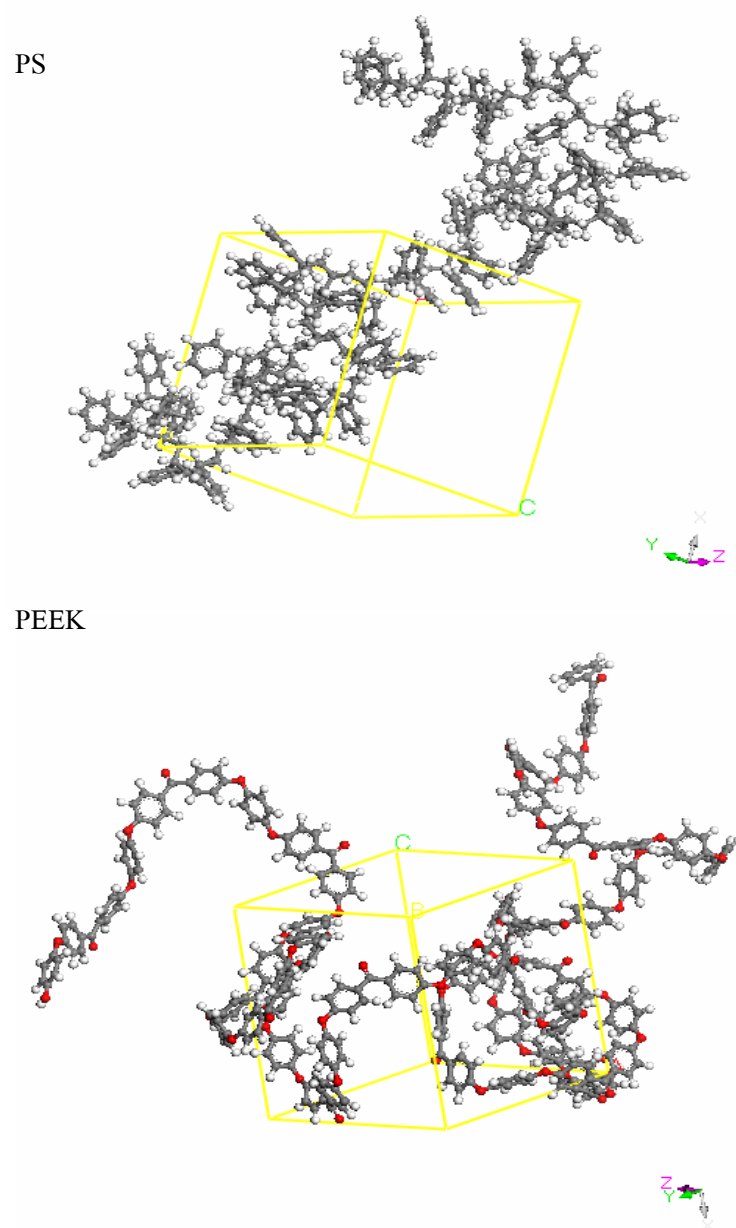


Figure 3.5 Bulk structures of PS and PEEK used in molecular dynamics calculation.

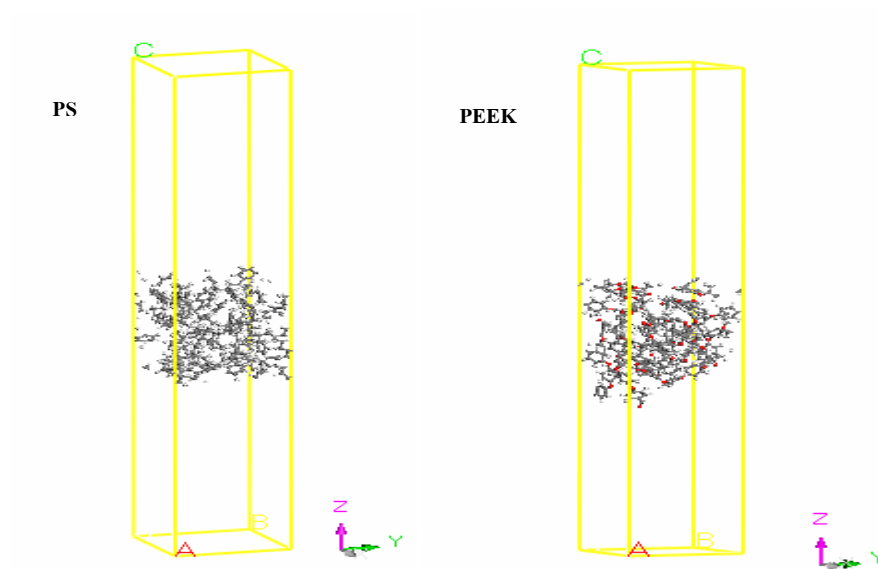


Figure 3.6 Thin film models of PS and PEEK used in molecular dynamics calculation.

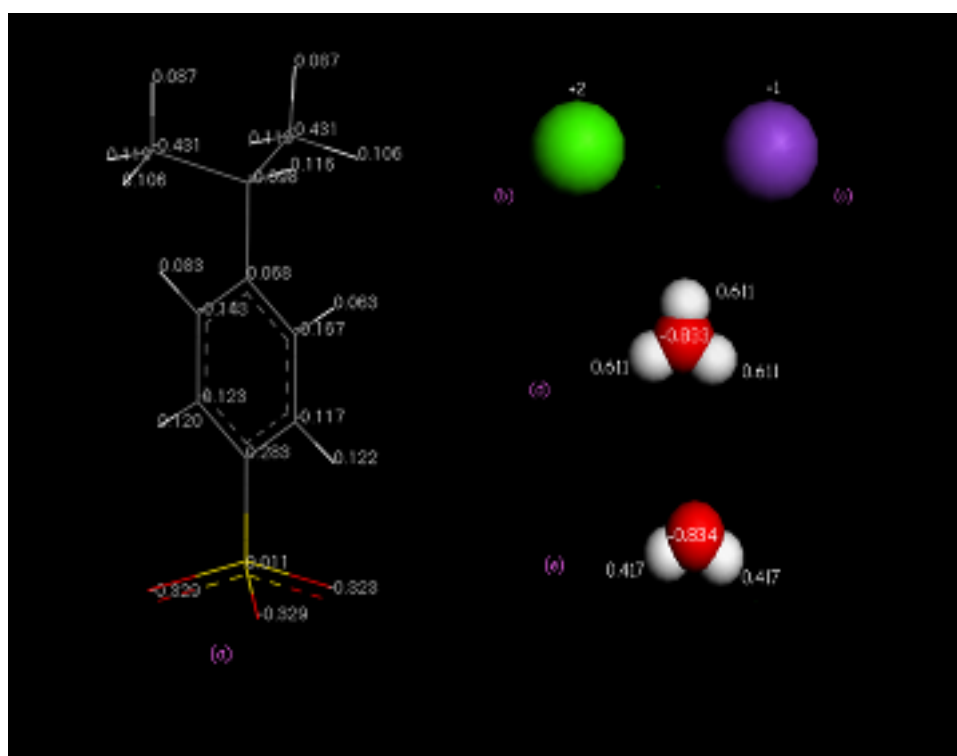


Figure 3.7 Diagram of the fragments featured in the molecular models: (a) sulfonate fragment, (b) potassium ion, (c) calcium ion, (d) hydroxonium ion and (e) water molecule. The outlines show the partial charges assigned to each atom.

CHAPTER IV

RESULTS AND DISCUSSION

4.1 Experimental Part

4.1.1 Fourier Transform Infrared Spectroscopy (FT-IR) of Sulfonated Polystyrene (SPS) and Sulfonated Poly(ether-ether-ketone) (SPEEK)

The FT-IR spectra of SPS taken from 400 to 4000 cm^{-1} was shown in Fig.4.1. The detection of a broad peak at approximately 3400 cm^{-1} has been ascribed to stretching modes of hydroxyl groups of $-\text{SO}_3\text{H}$ groups and water molecules retained by the sample. The absorption at 1030 cm^{-1} resulted from the symmetric stretching vibration of SO_3H groups and the absorption at 1125 cm^{-1} resulted from the sulfonate anion attached to a phenyl ring. Our results were in good agreement with the literature (Weiss, Ashish, Willisand and Pottick, 1991).

FT-IR spectra were also used to confirm the functional groups in SPEEK ionomers. As in Fig.4.2, the successful incorporation of sulfonate groups can be confirmed by their corresponding characteristic transmission bands. The observed bands at 1081 cm^{-1} were assigned to symmetric and asymmetric stretching vibrations of $\text{O}=\text{S}=\text{O}$. The strong and broad band for the OH group of sulfonic acid was also observed at 3415 cm^{-1} . Spectroscopic results of SPEEK were similar to one observed by the previous work (Gil *et al.*, 2004). So, it proved that the sulfonate groups were successfully introduced into PEEK as expected.

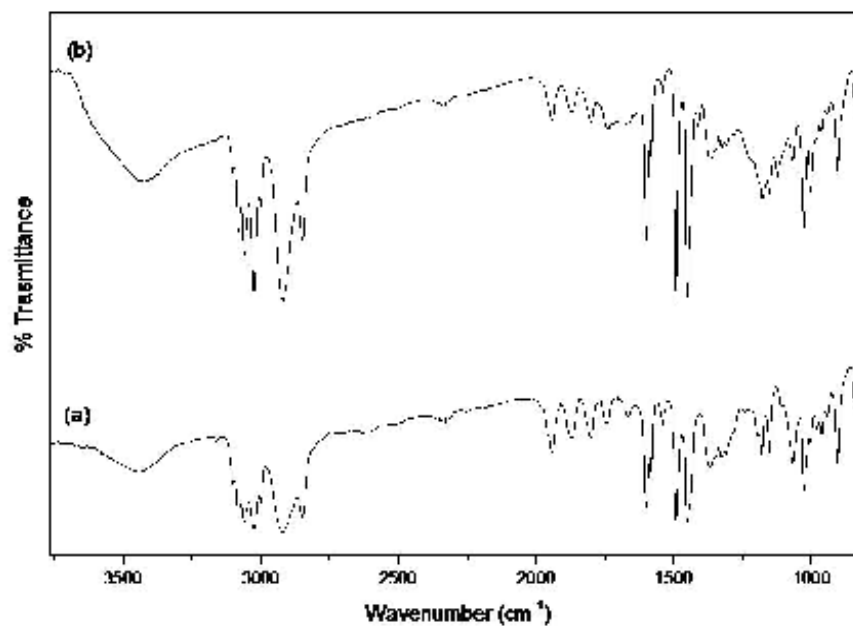


Figure 4.1 FTIR spectra of (a) polystyrene and (b) sulfonated polystyrene.

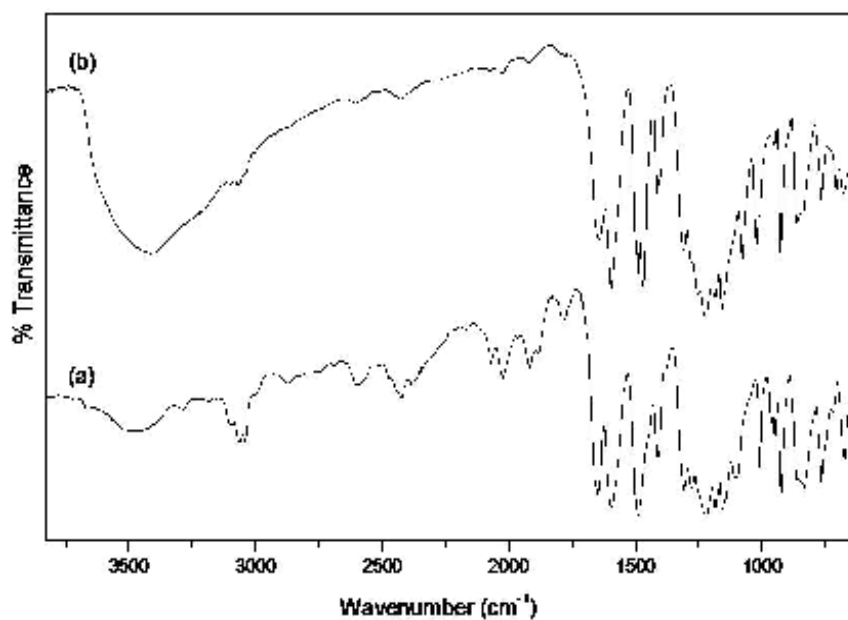


Figure 4.2 FTIR spectra of (a) poly(ether ether ketone) and (b) sulfonated poly(ether-ether-ketone).

4.1.2 Nuclear Magnetic Resonance (NMR) of Sulfonated Polystyrene (SPS) and Sulfonated Poly (ether-ether-ketone) (SPEEK)

¹H-NMR spectra of polystyrene before and after sulfonation was presented in Fig.4.3 The ¹H NMR spectrum of the starting polymer consists of two central peaks at 1.44 and 1.86 ppm, assigned to methylene (–CH₂–), and methyl (–CH–) protons, and other broad peaks at 6.59 and 7.07 ppm, that correspond to H of aromatic rings. A hump around 2.98 ppm indicates the presence of sulfonic acid linkage on the benzene ring.

¹H-NMR spectra of SPEEK sample dissolved in DMSO-*d*₆ was shown in Fig. 4.4. The degree of sulfonation can be determined quantitatively by the method presented in Robertson *et al.* (2003). The presence of the sulfonic acid group increases the deshielding effect for proton H_A, causing the H_A resonance to move to a higher chemical shift compared with protons H_B and H_C. Therefore, a distinct signal for H_A can be observed from NMR spectra. The ¹H-NMR signal for the sulfonic acid group cannot be recorded directly since the sulfonic acid proton is highly mobile. Nevertheless, the number of the H_A was exactly equal to that of the sulfonic acid protons. Thus, if the degree of sulfonation (DS) was defined as a ratio of sulfonated units to total units, the DS can be calculated as follows:

$$DS / (12 - 2DS) = \text{area}_{H_a} / \sum \text{area}_{H_{b,c,d,e,e'}} \quad (4.1)$$

The DS calculated from the ¹H-NMR spectra of SPEEK sample was 0.64. This value falls in the same range with the reported 0.62 DS by Ye, Janzen and Goward, (2006) of which SPEEK was prepared by reacting with H₂SO₄ at room temperature

for 125 h. The difference, however, could be attributed to the fact that the reaction time and concentration of the PEEK in acid solution were different. The 0.64 DS was corresponding to the ion exchange capacity (IEC) of 1.76 meq/g (Li, Zhang and Wang, 2003; Xue and Yin, 2006). From the IEC value it can be calculated to the degree of sulfonate substitution level (DSS) by the formula (Smitha, Slidhar and Khan, 2003):

$$DSS = \frac{120 \times IEC}{1000 + 120 \times IEC - 200 \times IEC} = 0.2459 \quad (4.2)$$

The 24.59 mol % sulfonate substitution levels in SPEEK was much more than 3.4 mol % in SPS ionomers. This value indicates that sulfonation reaction in PEEK polymer was much easier than that in PS polymers.

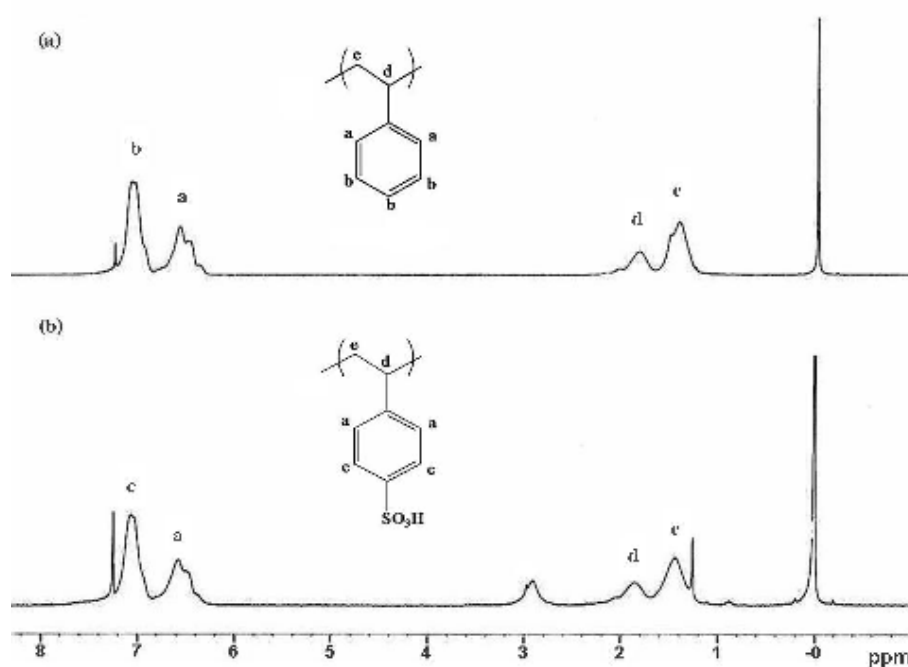


Figure 4.3 ^1H -NMR spectra of (a) polystyrene and (b) sulfonated polystyrene.

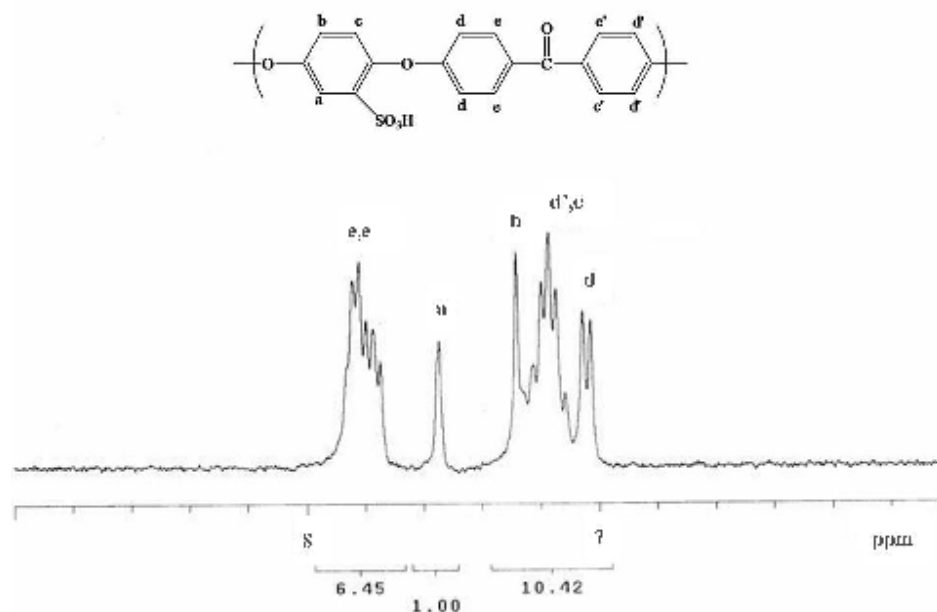


Figure 4.4 $^1\text{H-NMR}$ spectrum of sulfonated poly (ether-ether-ketone).

4.1.3 Thermo Gravimetric Analysis (TGA) of Cation neutralized SPS and SPEEK

Fig.4.5 shows the thermograms of SPS films neutralized with calcium and potassium cation. The films were dried at room temperature for several days and, before TGA analysis, they were exposed to air at an atmospheric condition. Two weight loss stages at $70^\circ\text{C} - 200^\circ\text{C}$ and $322^\circ\text{C} - 450^\circ\text{C}$ can be distinguished in the figure. According to Grady and Moore (1996) works, they found a very small amount (~ 0.3 wt %) of DMSO solvent (b.p. 189°C) presented in carboxylate ionomer after drying in a vacuum oven at 90°C for 5 days. Thus, for the films being exposed to air before subjecting to TGA, the weight loss in the first and second stage could be attributed to the loss of water absorbed in the ionomers and the combining decomposition of sulfonic groups and the main chains of the polymer. Though the

boiling point of the water was much less than the temperature in the weight loss zone, the fact that the polymer was in a rubbery state cannot be overlooked. An increase in free volume in the rubbery state and the excessive sliding of polymer chains one upon another with an increase in temperature would enhance evaporation of water entrapped in the polymer at glassy state resulting in weight loss at a temperature much higher than its boiling point (Smitha, Slidhar and Khan, 2003). Water content in Ca-SPS and K-PS were estimated to be 6.83 and 8.60%. The remaining 2.75 and 6.60% (w/w) should be attributed to the residual calcium and potassium metal as these metals have boiling point much higher than the range of measured temperature. Assuming that neutralizations by calcium and potassium acetate were completed, the % of sulfonate group in ionomers could be estimated from the remaining metal amount.

Fig.4.6 shows the TGA thermograms of SPEEK film neutralized with calcium and potassium cation. For Ca-SPEEK ionomer, the initial weight loss starts around 70°C - 190°C because of water loss (6.75% w/w). The second transition occurring over the temperature from 260°C - 450°C was attributed to loss of sulfonic groups from SPEEK (11.29% w/w) (Xue and Yin, 2005). The third weight loss occurred over 450°C could be ascribed to the decomposition of PEEK molecules. For K-SPEEK ionomer, a significant water loss, of about 6.08% (w/w), was recorded at 70°C - 180°C. The loss of sulfonate group (desulfonation) about 11.28% (w/w) occurs at 270°C - 420°C while the degradation process of the sulfonated polymer starts around 450°C. TGA results allowed the calculation of the weight% of water and sulfonic group in each sample. These results, shown in Table 4.1, will be considered again in MD simulation parts.

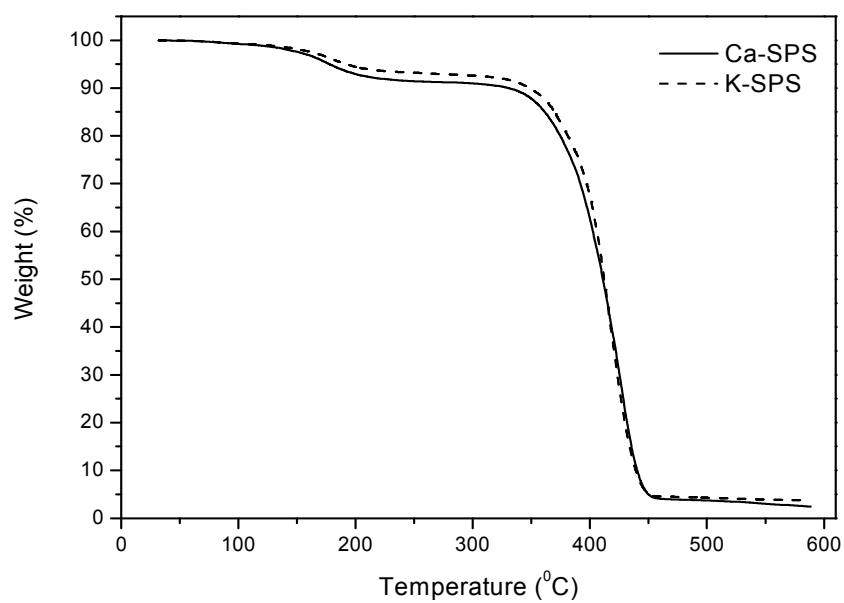


Figure 4.5 TGA curves of Ca-SPS and K-SPS samples.

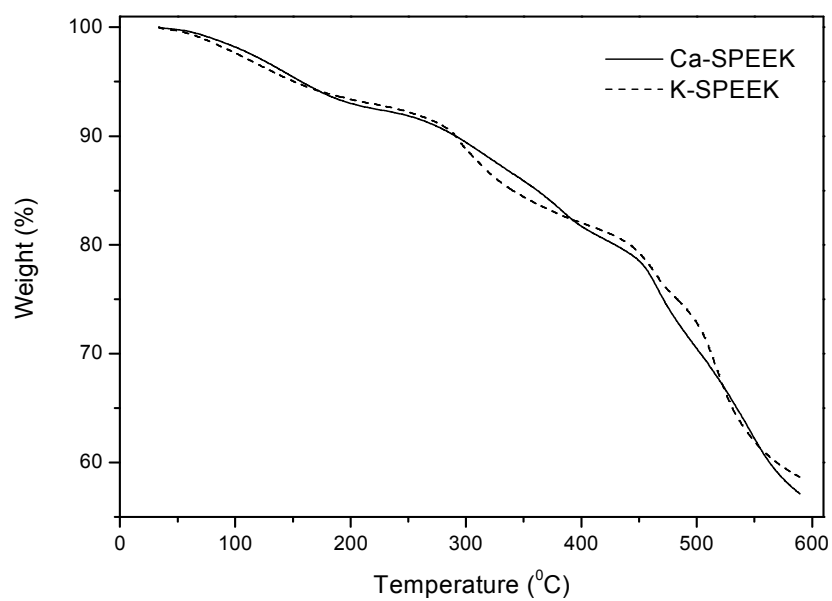


Figure 4.6 TGA curves of Ca-SPEEK and K-SPEEK samples.

Table 4.1 Weight % and molar ratio of water and sulfonic group in 3.4 mol% SPS and 24.59 mol % SPEEK ionomers

Ionomers	Weight% H ₂ O	Weight% SO ₃ H	nH ₂ O/SO ₃ H
Ca-SPS	6.83	11.13	2.76
K-SPS	8.60	13.71	2.83
Ca-SPEEK	6.08	11.28	2.42
K-SPEEK	6.75	11.29	2.69

4.1.4 Local structure analysis of ionomers by Extended X-ray Absorption

Fine Structure (EXAFS)

The sulfonated polystyrene (SPS) ionomer is a high performance thermoplastic and less expensive material while the sulfonated poly (ether-ether-ketone) (SPEEK) exhibits stability in thermal and acidic environments. These make them ideal for examining the effect of the cation on the aggregation aspects of sulfonate groups and their properties. The main structural difference between these ionomers is that the sulfonate groups of SPS are on the aromatic side chain while SPEEK has the ionic group on the aromatic main chain. A comparison of the local coordination structure around the cation in these ionomers is of interest and might help to elucidate the relationship between the polymer type, cation, ionomer and their physico-chemical properties.

4.1.4.1 Calcium neutralized Sulfonated polystyrene (Ca-SPS) and Sulfonated poly (ether-ether-ketone) (Ca-SPEEK) ionomers

The background subtracted and normalized EXAFS spectra for calcium cations in the Ca-SPS and Ca-SPEEK are plotted as $k^2\chi$ vs. k in Fig.4.7. Plots

of the radial structure function (RSF) for these two samples are shown in Fig. 4.8. A prominent first coordination shell at about 2 Å was observed in both samples. The peak about 0.7 Å in the RSF is an artifact due to the residual low-frequency background. The samples have a broad and skewed peak after 3 Å in the RSF. Both Fig.4.7 and 4.8 indicated that coordination distances, numbers of atoms and coordination structures were not much different in the Ca-SPS and Ca-SPEEK samples.

To model the local structure of Ca^{2+} in the sulfonated ionomers, Calcium Oxide (CaO) crystals were used as a reference material. The atomic positions of the atoms around the central Ca atom in calcium oxide are listed in Table A.1 of appendix A. Calcium oxide CaO possesses six-fold oxygen coordination in the first coordination shell and twelve-fold calcium coordination in the second shell. The normalized EXAFS and radial structure function of the first shell of calcium oxide standard are shown in Fig.4.9.

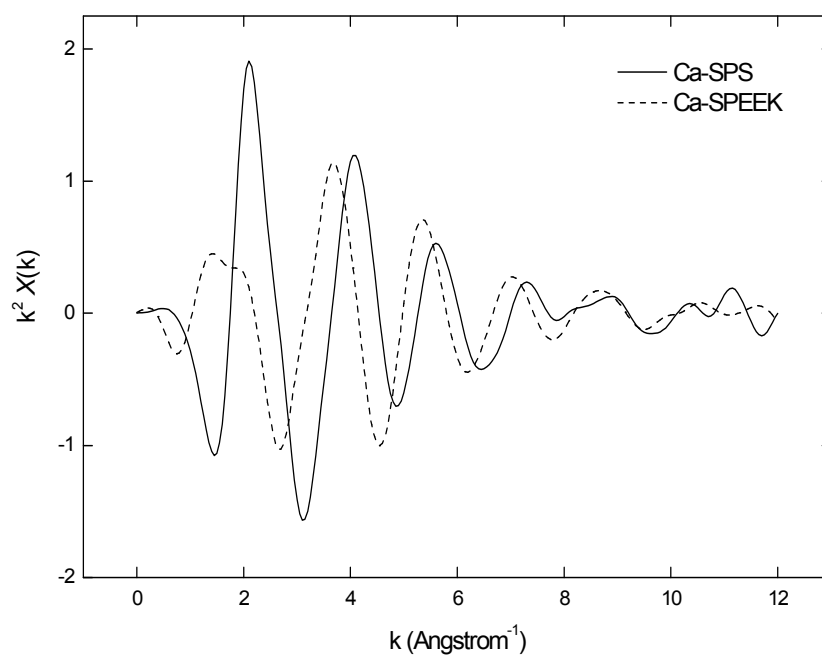


Figure 4.7 EXAFS data expressed as $k^2\chi$ for Ca-SPS and Ca-SPEEK ionomers.

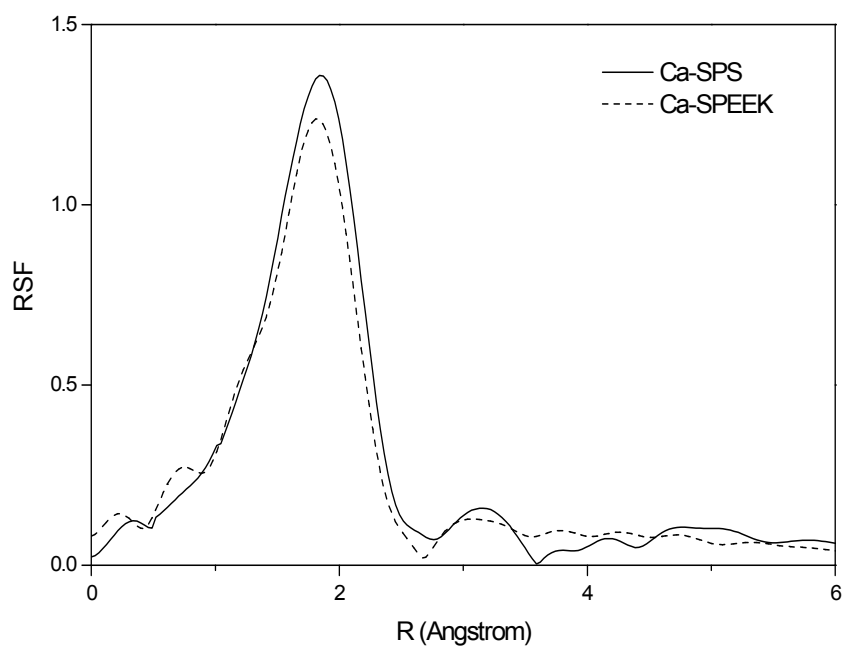


Figure 4.8 Radial structure function for Ca-SPS and Ca-SPEEK ionomers.

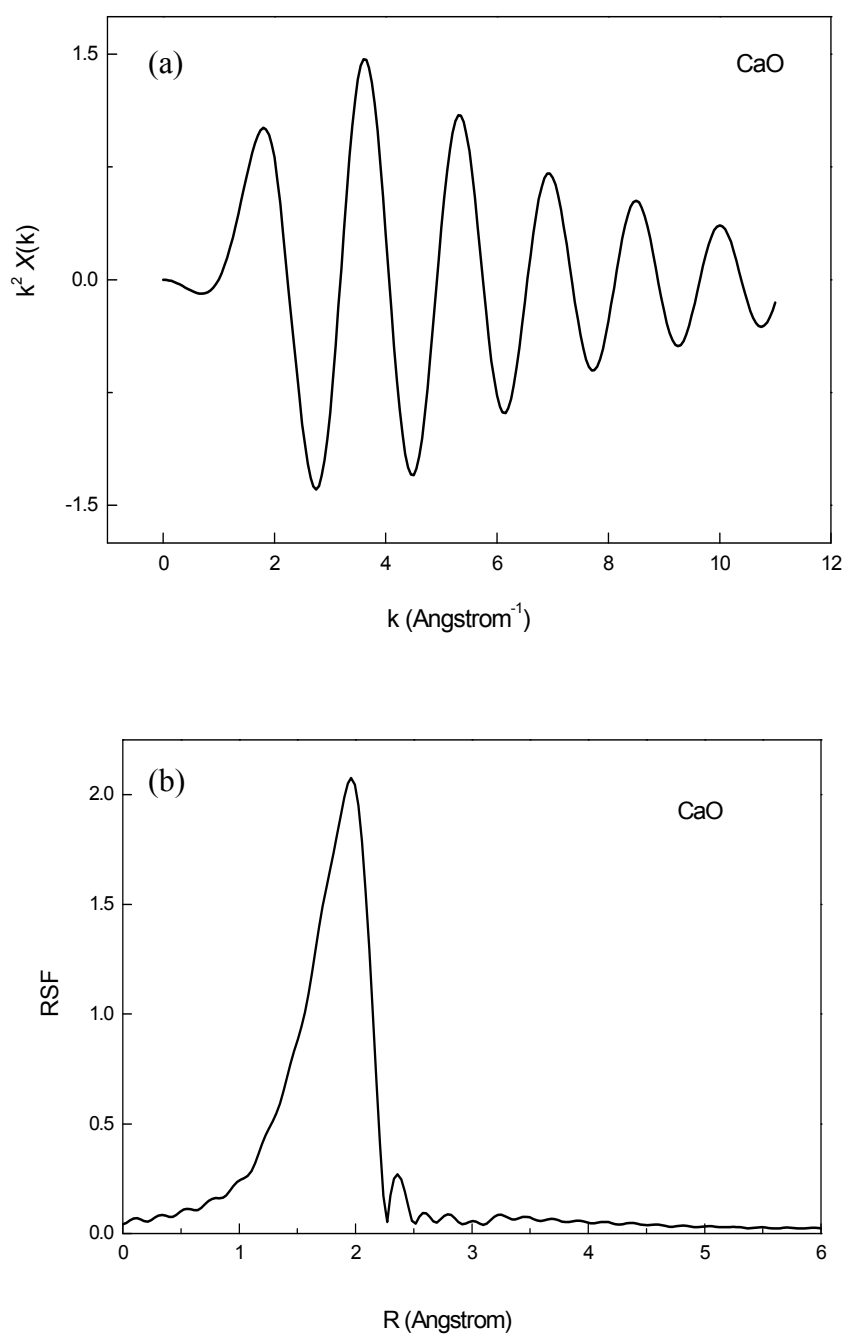


Figure 4.9 EXAFS data for the first shell of CaO (a) $k^2 \chi$ and (b) radial structure function.

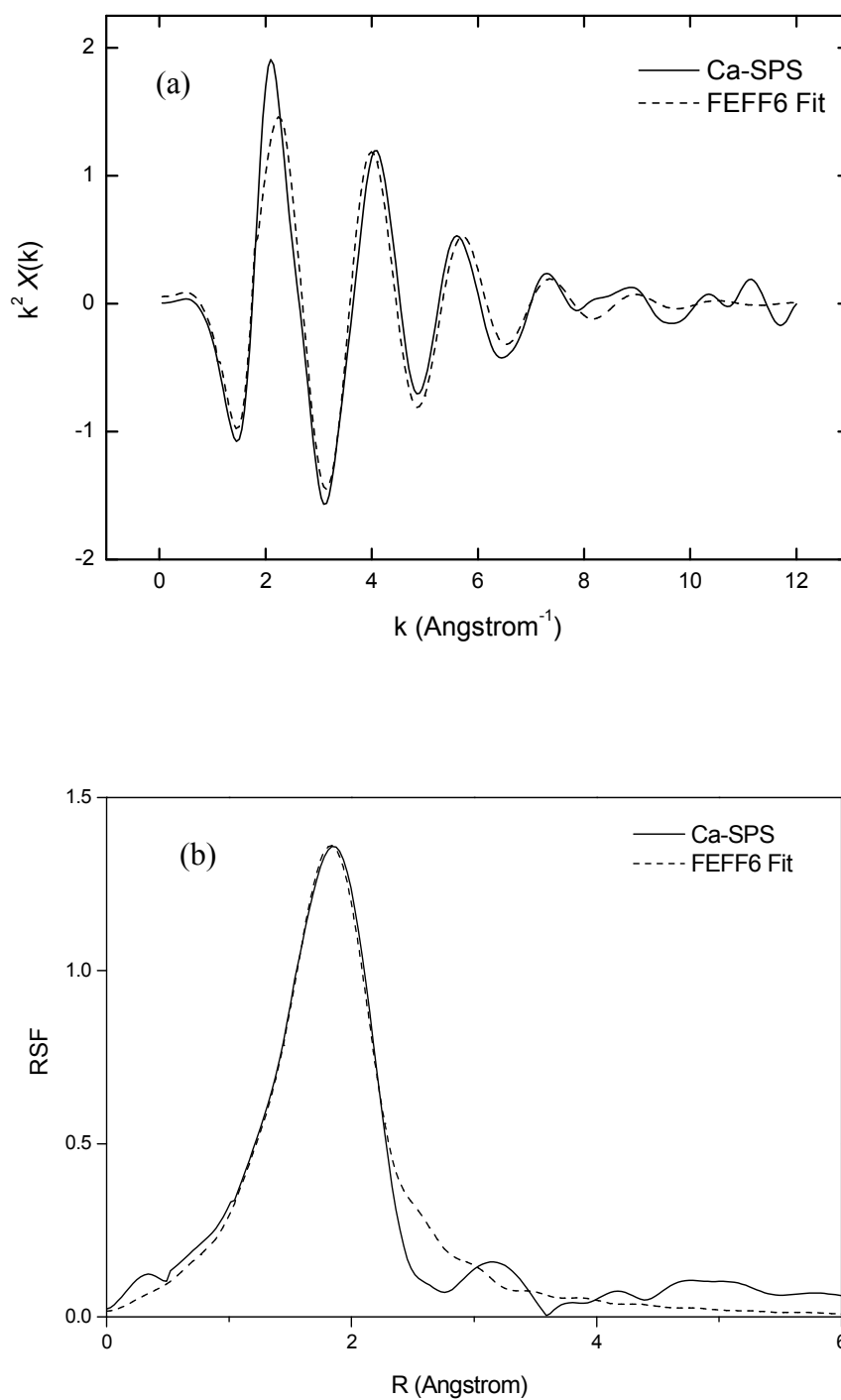


Figure 4.10 Fit to the first shell of the Ca-SPS ionomer using CaO model (a) $k^2 \chi$ and (b) radial structure function.

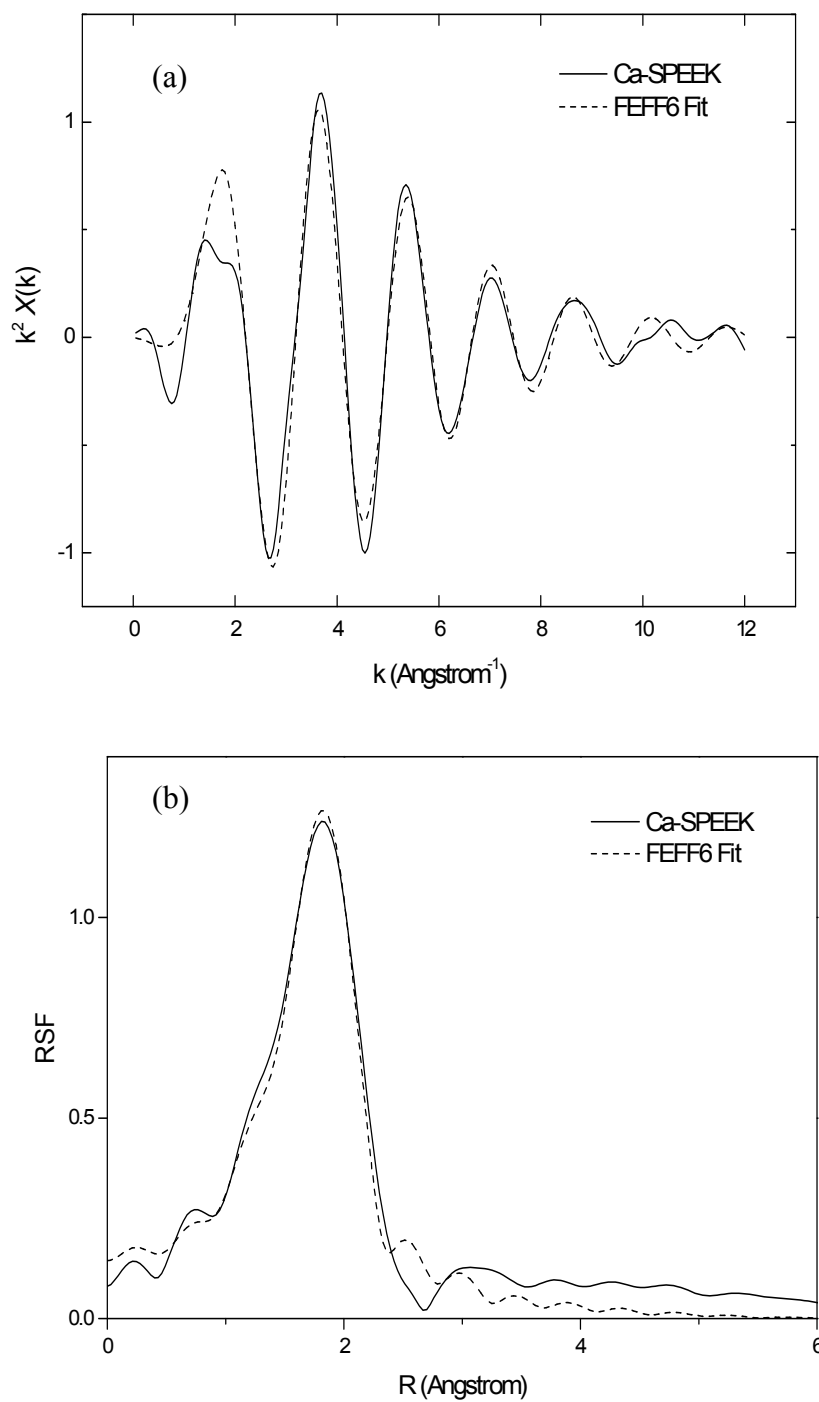


Figure 4.11 Fit to the first shell of the Ca-SPEEK ionomer using CaO model (a) $k^2\chi$ and (b) radial structure function.

FEFF simulations and best fits of the structure using the atomic positions of calcium oxide were shown in Fig.4.10 and 4.11 for Ca-SPS and Ca-SPEEK, respectively. In these curve-fitting procedures, the first-shell oxygen Debye-Waller factors, the amplitude reduction and the edge energy were adjustable. Therefore, three adjustable parameters (Debye-Waller factor, the amplitude reduction and the edge energy) were used in the fits of experimental data to theory for the sulfonate ionomers: In the FEFFIT documentation, it is strongly suggested that E_0 should be allowed to float to correct for problems such as incomplete core-hole shielding, angular variations in valence charge distribution, and charge transfer effects.

The quality of fit to the nearest-neighbor contributions of sulfonated ionomers are demonstrated in Fig.4.10 and Fig.4.11. The fit parameters are listed in Table 4.2. Oxygen atoms at 2.32 Å achieve the best fit of the first shell in Ca-SPS ionomer, which close to Ca-O distance in calcium oxide model compound. Using the mean-free-path value from calcium oxide model compound (4.8 ± 1.0 Å), the coordination number for this shell in Ca-SPS ionomer was estimated to 6. The Ca-O distance for Ca-SPEEK ionomer was 2.37 Å, which was close to the Ca-O distance in the Ca-SPS ionomer and calcium oxide model compound. The coordination number for the first solvation in Ca-SPEEK was estimated 5. An absent of one oxygen atom from the first coordination shell in Ca-SPEEK might due to linking sulfonate group at aromatic main chain which result in more steric and difficult to fill in the coordination sphere of Ca^{2+} ion. Therefore, it was possible that one oxygen atom disappeared from Ca-SPEEK first coordination shell may belong to the sulfonate group.

The average distance and coordination number of oxygen atom obtained from the fits agree very well with the results mentioned in sulfonated polyurethane

ionomers based on toluene diisocyanate neutralized with Ca^{2+} (Ding, Register, Yang and Cooper, 1989), which were found around 2.38 Å and 6, respectively. This local structure in sulfonated polyurethane ionomers neutralized with calcium ion appeared little affected when ionomers were changed from dry to hydration state.

Table 4.2 EXAFS parameters of cationic doped sulfonated polystyrene and poly (ether-ether-ketone) ionomers^a.

Sample	Shell No.	Atom	Distance	N	$\sigma^2(\text{Å}^2)$	$E^0\text{Shift(eV)}$
Ca-SPS	1	oxygen	2.32	6.3	0.015	+5.95
Ca-SPEEK	1	oxygen	2.37	5.4	0.009	-1.01
K-SPS	1	oxygen	2.69	4.4	0.025	-4.01
K-SPEEK	1	oxygen	2.65	3.6	0.024	-4.22

(a) Typical uncertainties for all cases for Distance and N are ± 0.03 Å and ± 1.0 , respectively. For K^+ , σ^2 is ± 0.004 Å² whereas for Ca^{2+} σ^2 is ± 0.002 Å².

In both Ca-SPS and Ca-SPEEK cases, the first shell was surrounded totally by oxygen atoms. These oxygen atoms could arise from either water or sulfonate groups. Although the presence of water in these materials was expected, completely surrounded by water molecule might be argued (based on the difficulty in drying sulfonated ionomers, as discussed previously [Ding, Register, Yang and Cooper, 1989]), This is because the structures should have at least two negative charges close to the metal cation to produce the charge neutrality in materials. This may also be confirmed by the structure of the hydrated calcium (II) ion in aqueous solution by EXAFS, large-angle X-ray scattering (LAXS) and molecular dynamics (MD) methods,

which concluded that there are eight coordination of the hydrated calcium(II) ion in aqueous solution with the Ca-O bond distances centered around 2.46 Å (Jalilehvand, F. *et al.*, 2001). These distance and coordination number are different from our fitting results. This was because there are sulfonate group in Ca-SPS and Ca-SPEEK which their site are bigger than water that might cause the oxygen coordination number different. This reference suggests that oxygen atoms in the first salvation shell do not all belonged to water molecules.

Grady and Cooper (1994) provided very insightful pictures of ionic aggregation in SPS ionomers neutralized with a divalent Ni^{2+} and Cd^{2+} ion. They suggested that both Ni-SPS and Cd-SPS ionomers had two waters of hydration in the coordination sphere, with the remaining oxygens from the sulfonate anions. Their studies illustrated the importance of incorporating interference of phase and amplitude functions to simulate EXAFS patterns. From this fact, four oxygen atoms from sulfonate group were proposed. Many structures of the local environment were drawn to simulate the RSFs and to prove the experimental results. As described above, it leads to the conclusion that the cations in the sample are coordinated by a mixture of water and sulfonate groups. Fig.4.12 shows the proposed pictures of ionic aggregation in SPS ionomers neutralized with a divalent Ni^{2+} and Cd^{2+} ion.

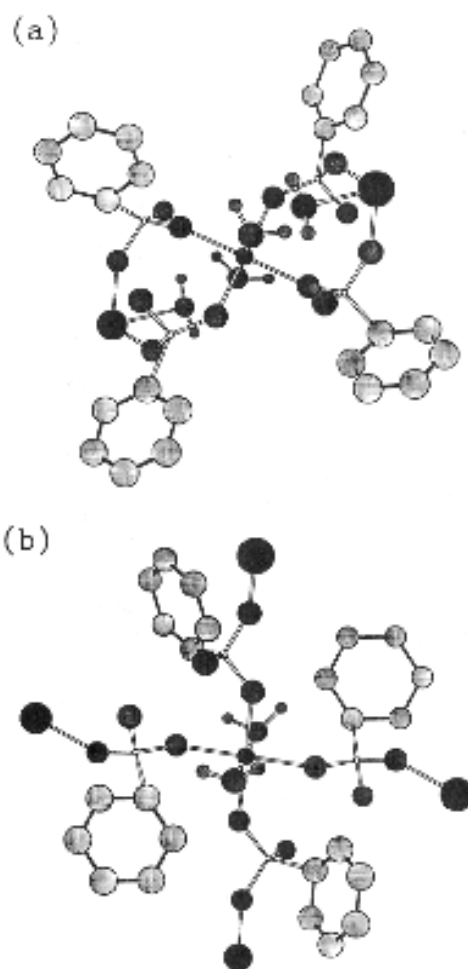
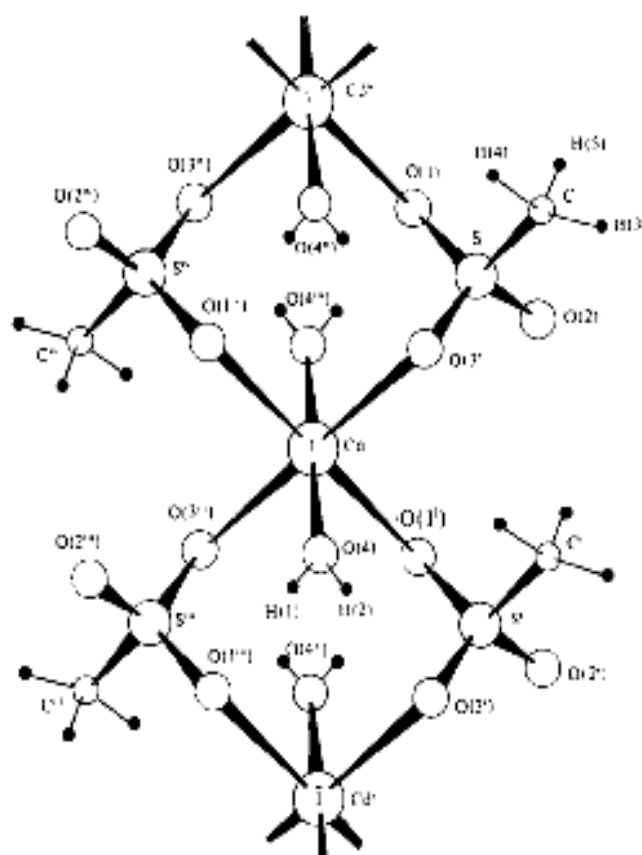


Figure 4.12 Structure of the local environment around nickel which contains two waters of hydration. (a) Two sulfonate groups share two nickel atoms. (b) Each sulfonate group which has one oxygen coordinated to a nickel atom has a different nickel atom for the other coordinating oxygen atom. The small filled circles represent nickel atoms, the larger filled circles represent sulfur atoms, and the largest unfilled circles represent oxygen atoms (Grady and Cooper, 1994).

For the systems of sulfonated polystyrene neutralized with cadmium studied by Grady and Moore (1996). It was found that the sulfonate ionomers had six oxygen atoms in the first coordination shell and the structure of the ionomer was successfully modeled using the crystal structure of cadmium methanesulfonate dehydrate. The results of this work are consistent with the postulate that the local arrangement of atoms around the transition metal cation in a dried ionomer is very similar to the arrangement which exists in the corresponding small-molecule analogue. For the limited number of materials studied, the identity of the polymer matrix and the ionic level had no effect on the local environment within the ionic aggregates. Simulations suggest that the sulfonate ionomers had two waters of hydration in the coordination sphere, with the remaining oxygens from the anions. For a crude approximation to predict EXAFS spectra from a model crystal, calcium atom was placed into the atomic position of cadmium atom in cadmium methanesulfonate dehydrate. Then, the crystal structure of pseudo calcium methanesulfonate dehydrate was used to fit with the Ca-SPS and Ca-SPEEK ionomers. The structures of cadmium methanesulfonate dehydrate is shown in Fig.4.13 and an atomic coordinates for this structure is presented in Table A.2.



Cd—O(3)	2,261 (4)	S—C	1,754 (6)
Cd—O(4)	2,270 (4)	O(4)—H(1)	0,83 (9)
Cd—O(1 ⁱ)	2,295 (4)	O(4)—H(2)	0,96 (9)
S—O(1)	1,460 (4)	C—H(3)	0,96 (14)
S—O(2)	1,436 (5)	C—H(4)	1,01 (14)
S—O(3)	1,463 (4)	C—H(5)	0,70 (13)

Figure 4.13 Crystal structure with atomic distance for each bond in cadmium-methanesulfonate dihydrate (Å) (Charbonnier and Loiseleur, 1978).

In this curve-fitting procedure, the first-shell oxygen and second shell sulfur Debye-Waller factors were adjustable, while the remainder of the higher shell Debye-Waller factors were arbitrarily set to 0.007 \AA^2 . Changing these higher shell Debye-Waller factors essentially had no impact on the quality of fit. The amplitude reduction

parameter could be set to 1.0 in this simulation. Allowing S_0^2 to vary improved the agreement between theory and experiment slightly; however, in all cases, the range of the error in the determination of the amplitude reduction factor included 1.0. Therefore, only three adjustable parameters were used in the fits of experimental data to theory for the sulfonate ionomers: two Debye-Waller factors and the edge energy. However, fitting by CaO suggests a Ca-O distance of the first shell is 2.32 Å. Thus the atomic positions for each path in the fit were shifted according the difference of distance between CaO and calcium methanesulfonate dehydrate so that the maxima of the first-shell peaks were identical for the simulation and the experimental data. Best fit results for the first- and second-shell parameters using the pseudo calcium methanesulfonate dihydrate crystal structure to fit the Ca-SPS ionomer experimental EXAFS data are shown in Table 4.3. From this fit, it was successfully confirm that local arrangement of atoms around the calcium metal cation in a dried Ca-SPS ionomer has the structure very similar to the arrangement which exists in the corresponding small-molecule analogue.

Table 4.3 Fit results of Ca-SPS by using pseudo calcium methanesulfonate dehydrate model

Path	Scatter	Deg.	{reff + delr}	E ⁰ Shift(eV)	$\sigma^2(\text{\AA}^2)$
1	O	2	2.32	11.045	0.0108
2	O	2	2.32	11.01	0.0109
3	O	2	2.32	10.98	0.0109
4	S	2	3.40	11.79	0.0382
5	S	2	3.48	-18.36	0.0141
6	S -->O	4	3.57	1.25	0.0070
7	S -->O	4	3.63	-8.11	0.0070
8	O	2	3.71	-15.96	0.0070
9	C	2	3.89	-3.09	0.0070
10	O	2	3.91	0.12	0.0070
11	O	2	3.92	0.04	0.0070
12	O	2	4.15	-15.57	0.0070
13	O-->O	2	4.55	-8.91	0.0070
14	O-->O	2	4.57	-8.55	0.0070

For Ca-SPEEK, as expected, using atomic position of pseudo calcium methanesulfonate dehydrate did not successfully fit. This is because fitting by CaO crystal suggested that they are five oxygen atoms in the first coordination shell. In this case, Grady and Cooper tried to prove where these five oxygen atoms come from. Simulations of all the possible structures of 5-fold oxygen models (based on losing 1 water molecule or 1 sulfonated group) were attempted. The Ca-O distance of the first coordination shell was set to 2.32 Å as the fitting suggested. Then, FEFF simulation was used to generate scattering parts and fit K- and R-space EXAFS with the Ca-SPEEK experimental result. Fig.4.14(a)-(c) show K- and R-space EXAFS of Ca-SPEEK ionomer fitted by the proposed models. The models used to generate the

atomic coordinates are shown in Figure 4.15(a)-(c), respectively. Lists of atomic coordinates used to generate feff paths for model 4.15(a)-(c) are presented in Table A.3 - A.5 of appendix.

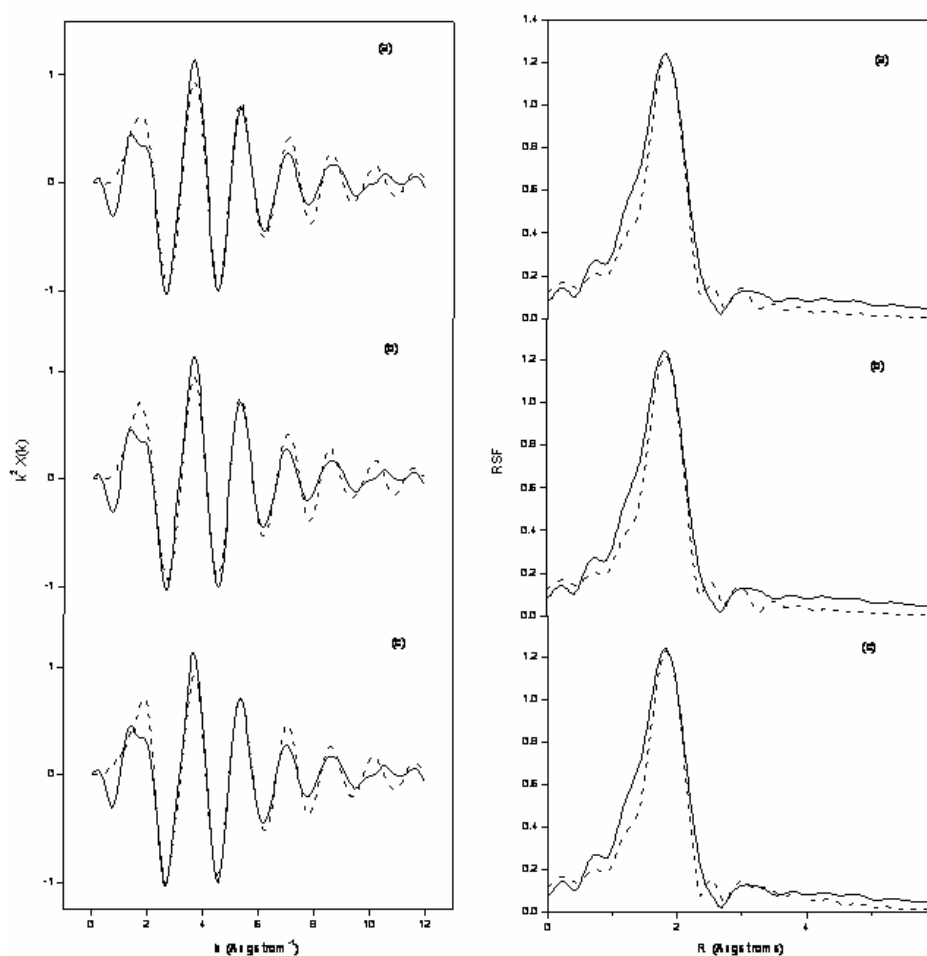


Figure 4.14 Comparison of $k^2\chi$ and radial structure function between Ca-SPEEK and the proposed 5-fold oxygen models. The solid line representing the experimental data (same for all the plots) and the dashed line representing the FEFF6 simulation.

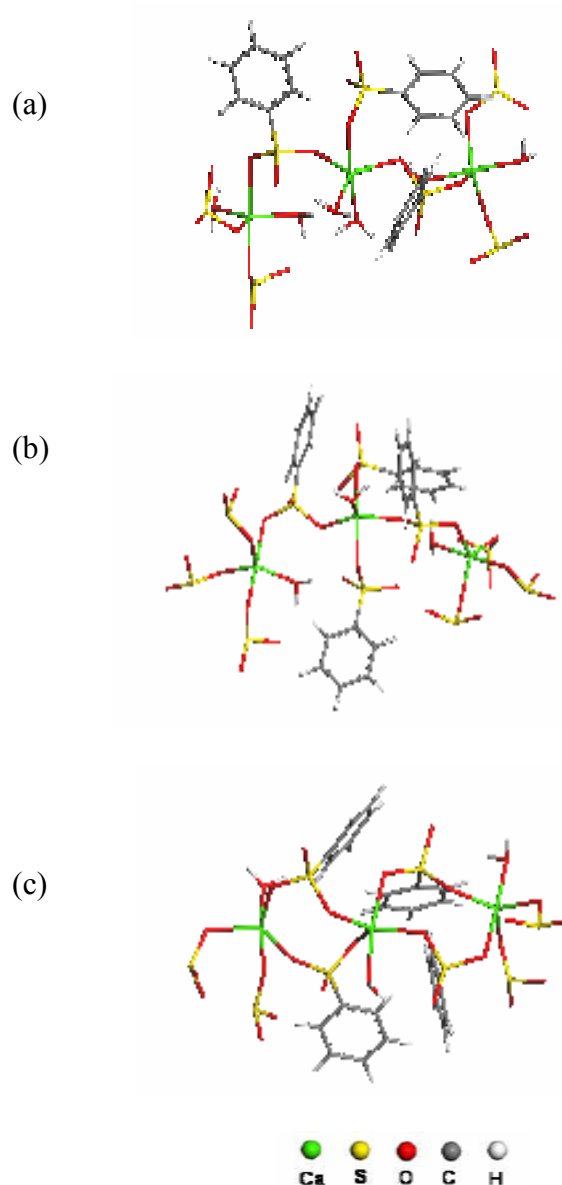


Figure 4.15 Structures of 5-fold oxygen atom used to generate EXAFS peaks in Fig.4.17 (a) two water molecule with three sulfonate groups, two sulfonate group which has one oxygen coordinated to a calcium atom has a different calcium atom for the other coordinating oxygen atom. (b) one water molecule with four sulfonate groups, two sulfonate group which has one oxygen coordinated to a calcium atom has a different nickel atom for the other coordinating oxygen atom. (c) one water molecule with four sulfonate groups, two sulfonate groups share two calcium atoms.

Considering both K- and R-space, it can be seen that the features of K and R-EXAFS from the dashed lines in Figure 4.14(a), (b) and (c) are not much different. However, the best-fit for Ca-SPEEK structure should be the dashed lines in Figure 4.14(c). This fit indicates that the preferred structure of Ca-SPEEK is four sulfonate groups and one water molecule around calcium atom in the first solvation shell.

An important factor when considering the internal aggregate structure is the overall shape and the form of an aggregate. SAXS modeling results (Ding, Hubbard, Hadgson, Register and Cooper, 1988) indicate that the aggregates are on the order of approximately 1-2 nm. When one considers the size of the structures presented in this work, it becomes clear that these aggregates can only contain a few metal cations. The real purpose of water in ionomers may be to provide a coordination site for the metal cations located on the edges of the aggregates. Hence, the finite aggregate size may explain the high resistance to dehydration found in TGA analysis of ionomers. Finally, the finite size of aggregates suggests that water or some other small coordinating molecule must be present in order to satisfy the coordination needs of the metal cation at the aggregate boundaries where the repeat structure terminates. The structures of Ca-SPS and Ca-SPEEK sample will be considered again through the MD simulations of these ionomers. This will give the theoretical view of local structures and help to confirm the structures proposed by EXAFS analysis.

4.1.4.2. Potassium neutralized Sulfonated polystyrene (K-SPS) and Sulfonated poly (ether-ether-ketone) (K-SPEEK) ionomers

The background subtracted and normalized EXAFS spectra plotted as $k^2\chi$ vs. k for potassium (1+) ions in the K-SPS and K-SPEEK ionomers are shown in

Fig.4.16. Plots of the radial structure function (RSF) for these samples are shown in Fig.4.17. The strong first coordination shell peak at 2 Å in the RSF was about the same for both samples, but the amplitude in K-SPS sample was slightly larger than in the K-SPEEK sample. This might indicate that the coordination number of oxygen atom around cation in the K-SPS sample was higher than in the K-SPEEK sample. The skewed and broad second shell peak of the K-SPS sample located at about the same position as in the K-SPEEK sample.

Potassium Dithionate ($K_2S_2O_6$) crystals were chosen as a reference material to an analogous atomic structure. The atomic positions of the atoms around the central K atom in potassium dithionate are listed in Table A.4. Potassium atom in $K_2S_2O_6$ possesses two-fold sulfur coordination in the first coordination shell and 6-fold oxygen coordination in the second shell. Only the atomic coordinates of the second shell oxygen from potassium dithionate were employed to fit the EXAFS spectra of K-SPS and K-SPEEK ionomers. The normalized EXAFS and radial structure function of potassium dithionate standard are shown in Fig.4.18.

Analysis of the first shell coordination was relatively straightforward. The fits of the $k^2\chi$ vs. k and the radial structure function data of K-SPS and K-SPEEK ionomers are shown in Fig.4.19 and 4.20, respectively. The relatively small size of the peak around 3-5 Å in the K-SPS and K-SPEEK samples causes the fitting difficult; the smaller the peak is, the more its shape is distorted by background noise. Therefore, the second shell coordination number in the samples cannot be determined accurately. The fit parameters were listed in Table 4.2. The potassium atom was found to be coordinated by 4 oxygen atoms located at a distance of 2.69 Å in K-SPS ionomer while it was 4 oxygen atoms at 2.65 Å from the potassium central atom in K-SPEEK

ionomer. By comparing cation-oxygen distance, the radius of the first coordination sphere of potassium neutralized ionomers is larger than those in calcium neutralized ionomers. This result was reasonable because the size of Ca^{2+} ion (Van der Waals radius of Ca^{2+} and K^+ are 2.00 and 2.75 Å) was smaller and it should decrease the optimum radius that oxygen atoms can enter. Different cation also affects the number of oxygen atoms in the first coordination shell of K-SPEEK ionomers. Since the size of K^+ ion was larger and has lower electro-negativity than Ca^{2+} ion, the number of oxygen atoms around K^+ ion should be lower than that of Ca^{2+} as shown in the fitting results.

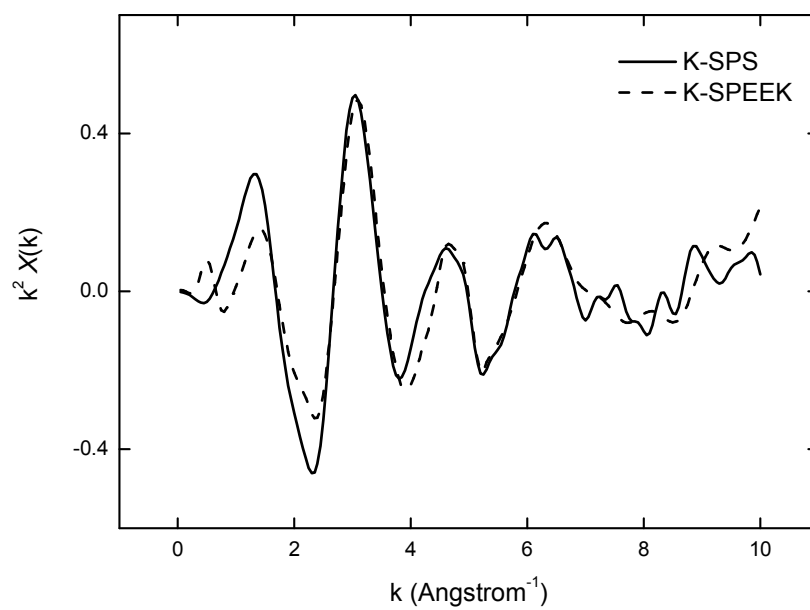


Figure 4.16 EXAFS data expressed as $k^2\chi$ for K-SPS and K-SPEEK ionomers.

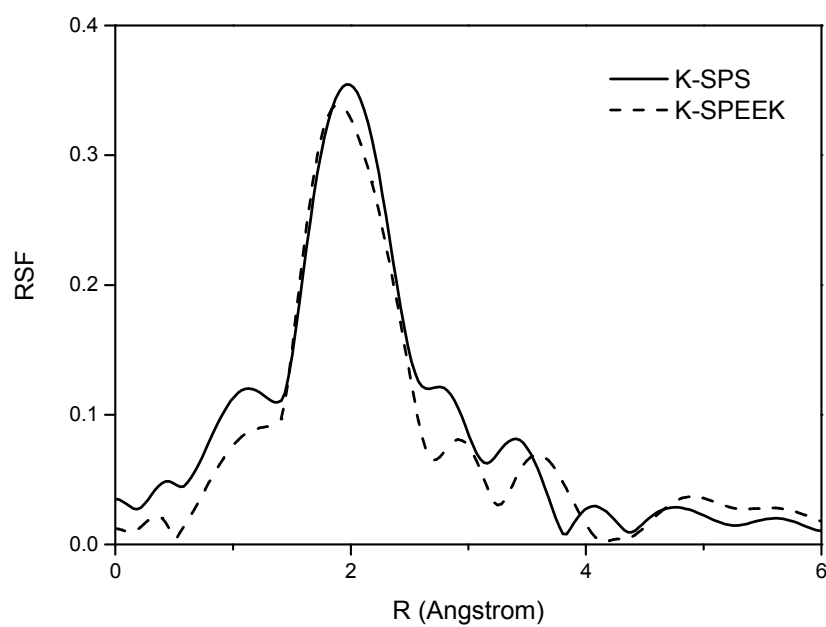


Figure 4.17 Radial structure function for K-SPS and K-SPEEK ionomers.

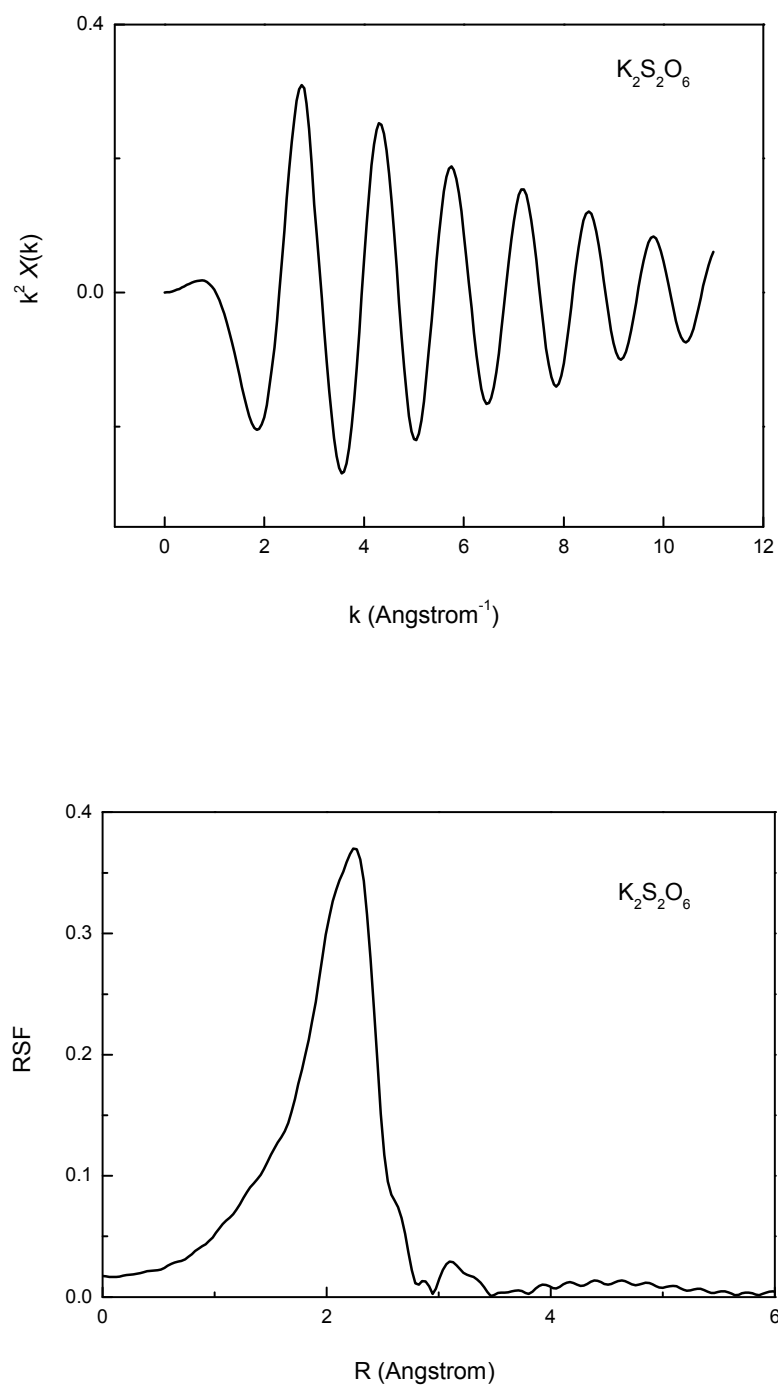


Figure 4.18 EXAFS data for $K_2S_2O_6$ used for fitting (a) $k^2 \chi$ and (b) radial structure function.

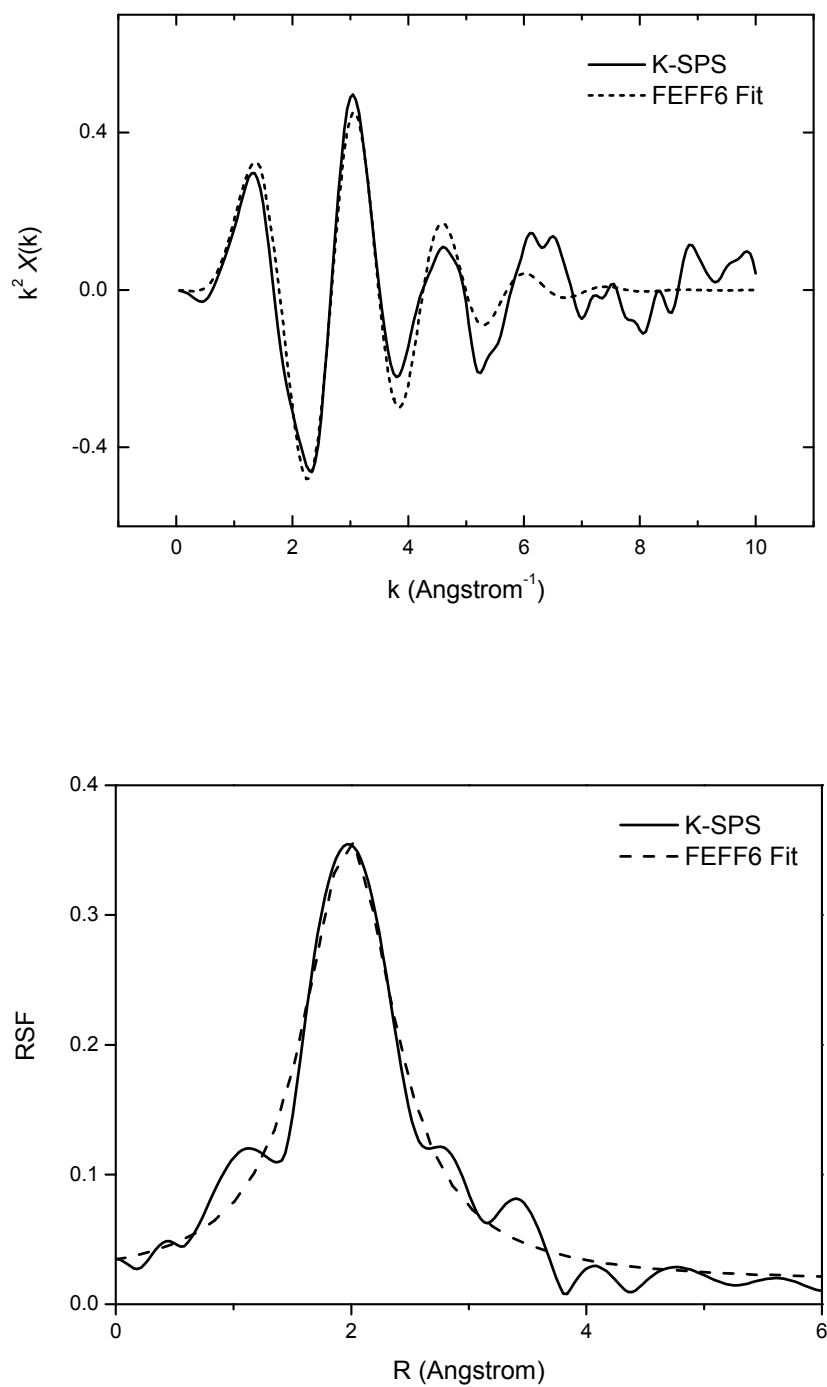


Figure 4.19 Fit to the first shell of the K-SPS ionomer using $K_2S_2O_4$ model (a) $k^2\chi$ and (b) radial structure function.

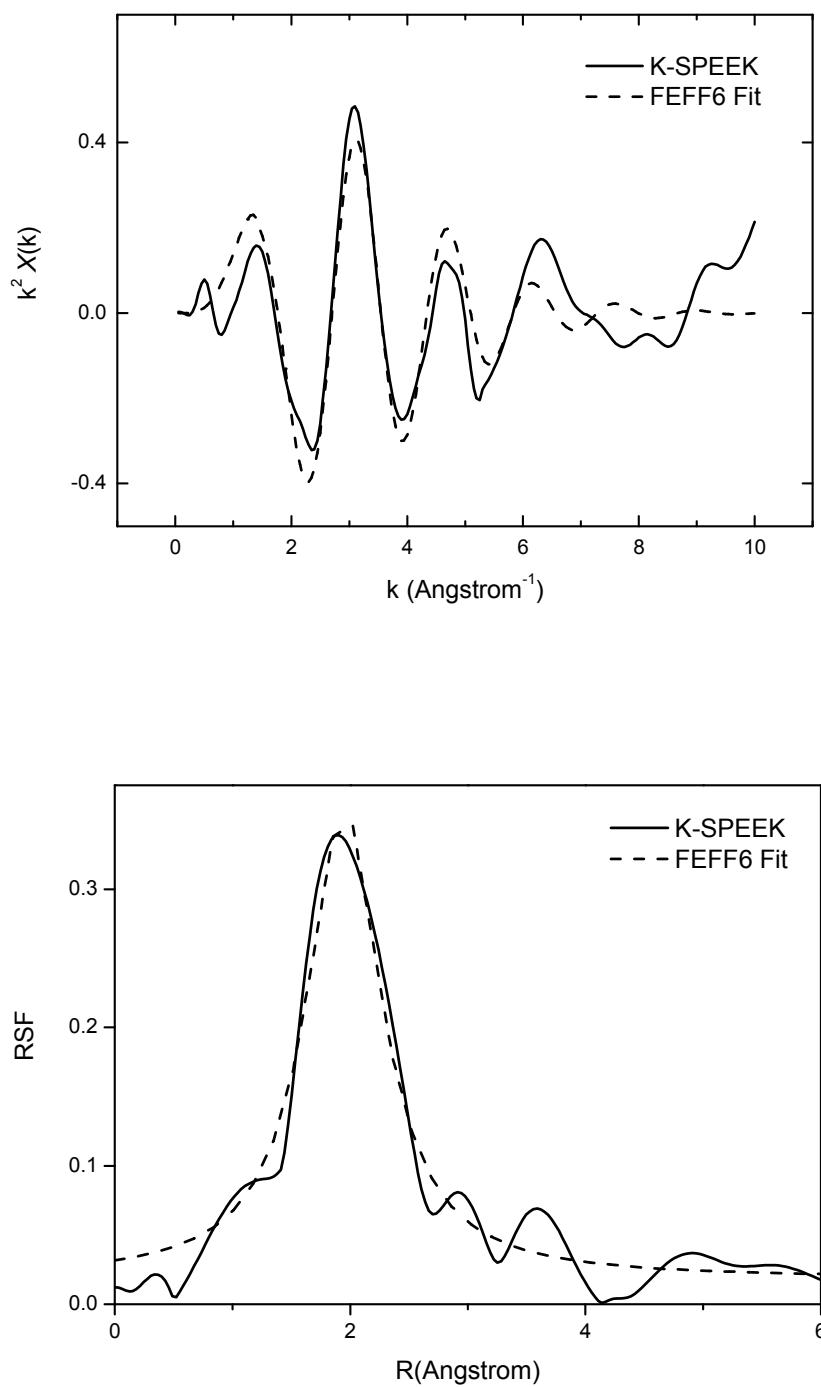


Figure 4.20 Fit to the first shell of the K-SPEEK ionomer using $K_2S_2O_4$ model (a) $k^2\chi$ and (b) radial structure function.

For K-SPS and K-SPEEK ionomers, MD simulation work with polarized QM-based force field by Borodi, Bell, Li, Bedrov and Smith (2001) for K^+ ion in water was employed to compare the number and distance of oxygen atoms around K^+ ion. This simulation suggests that there are about 6-7 oxygen atoms at the distance of 2.68-2.75 Å around K^+ ion. This is also confirmed by the experimentally observed values ranging from 2.6-2.8 Å (Marcus, 1988). In both cases, the distance and coordination number fall in the same range with our fitting results, especially for the system of K-SPS ionomers. Nevertheless, Grady and Cooper (1994) suggested that the best model compound for SPS with water in the first coordination shell is toluene sulfonate hexahydrate. In this compound, the oxygen in second coordination shell is over 4 Å away from the metal cation. The RSFs of SPS ionomers in this study clearly show features from a coordination shell closer than 4 Å. Thus, although it is still unclear which element involving the skewed and broad second shell peaks, it is strongly suggests that cations are not surrounded completely by water molecule. Charge neutrality is an important reason to indicate that at least one sulfonate anion must be in the first shell of K cation. Other 4-coordination models are still possible for the local coordination structure of K-ionomers. It is also possible that the four oxygen atoms are from four sulfonate groups. This structure was postulated by Grady and Cooper (1994) for the local coordination structure of zinc in Zn-SPS as shown in Fig. 4.21.

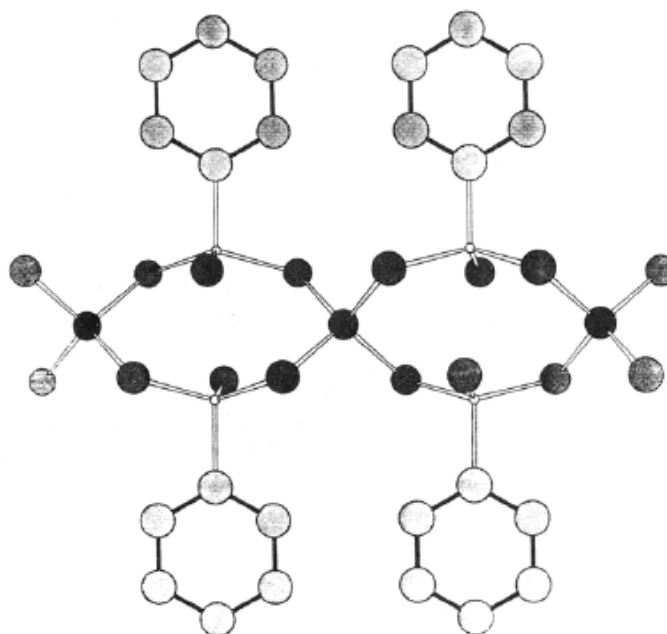


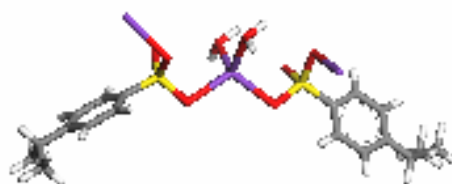
Figure 4.21 Possible structure for ZnSPS. Symbols as in Fig.4.14 (Grady and Cooper, 1994).

To gain more understanding about the local structure in K-SPS and K-SPEEK, four possible atomistic models of 4-fold oxygens in K-ionomers were simulated (Fig.4.22(a)-(d)). The K-O distance of the first coordination shell was set to 2.67 and 2.69 Å, for K-SPS and K-SPEEK, respectively according to the results from the fitting by $K_2S_2O_6$. Atomic coordinates of these models were extracted and used as the input files for FEFF program to generate FEFF scattering paths. These simulated FEFF paths are again fitted with the experimental data and then they are compared to see which one should be the best structural model to represent the local structure of K-ionomers. Fig.4.23(a)-(d) show the comparison of K- and R-space EXAFS between FEFF simulation of the model from Fig.4.22(a)-(d) and K-SPS. Fig.4.24(a)-(d) show comparison of K- and R-space EXAFS between FEFF simulation of the model from

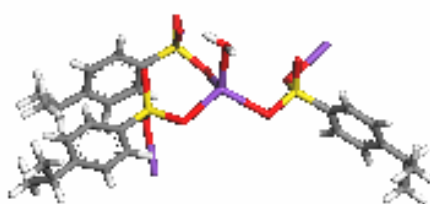
Fig.4.22(a)-(d) and K-SPEEK. Lists of atomic coordinates used to generate FEFF paths for model 4.22(a)-4.22(d) are in Table A.7-10 of appendix.

Considering both K-and R-space, the best-fit for K-SPS structure should be the dashed lines in Fig.4.23(a). For K-SPEEK, The model that provides EXAFS features closest to the experiment is the model in Fig.4.22(a). Based on these comparisons, four oxygens in first coordination shell of K-SPS and K-SPEEK ionomers are three from sulfonate groups and one from water molecules. This model is reasonable if the aggregate has a finite size which needs water to pack at the aggregate boundaries where the repeat structure terminates. However, the aggregate structures of K-ionomers will be considered again in the MD simulation part.

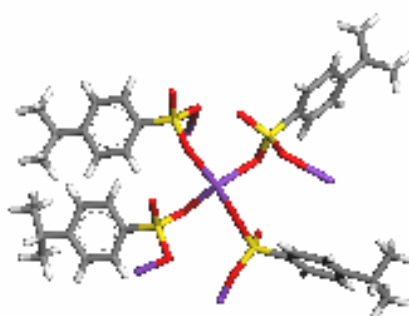
(a)



(b)



(c)



(d)

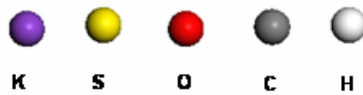
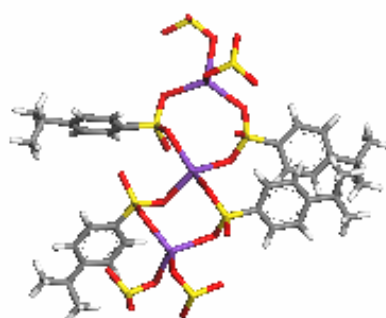


Figure 4.22 Structures of 4-fold oxygen atom used to generate EXAFS peaks in Fig.4.22 and 4.23 (a) two water molecule with two sulfonate groups, two sulfonate group which has one oxygen coordinated to a potassium atom has a different potassium atom for the other coordinating oxygen atom. (b) one water molecule with three sulfonate groups, two sulfonate group which has one oxygen coordinated to a potassium atom has a different potassium atom for the other coordinating oxygen atom. (c) four sulfonate groups, each sulfonate group which has one oxygen coordinated to a potassium atom has a different potassium atom for the other coordinating oxygen atom. (d) four sulfonate groups, two sulfonate groups share two potassium atoms.

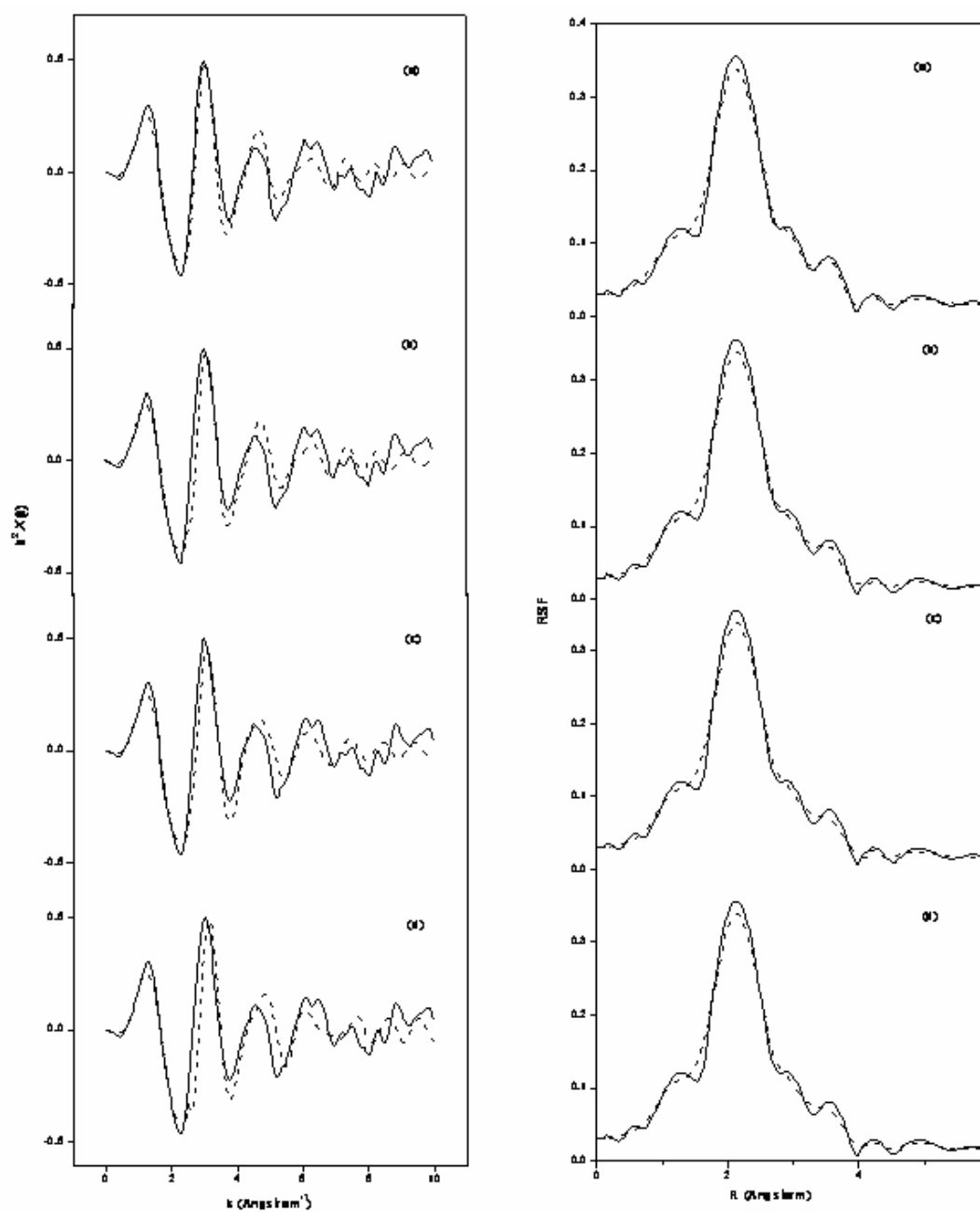


Figure 4.23 Comparison of $k^2\chi$ and radial structure function between K-SPS and the proposed 4-fold oxygen models. The solid line representing the experimental data (same for all the plots) and the dashed line representing the FEFF6 simulation.

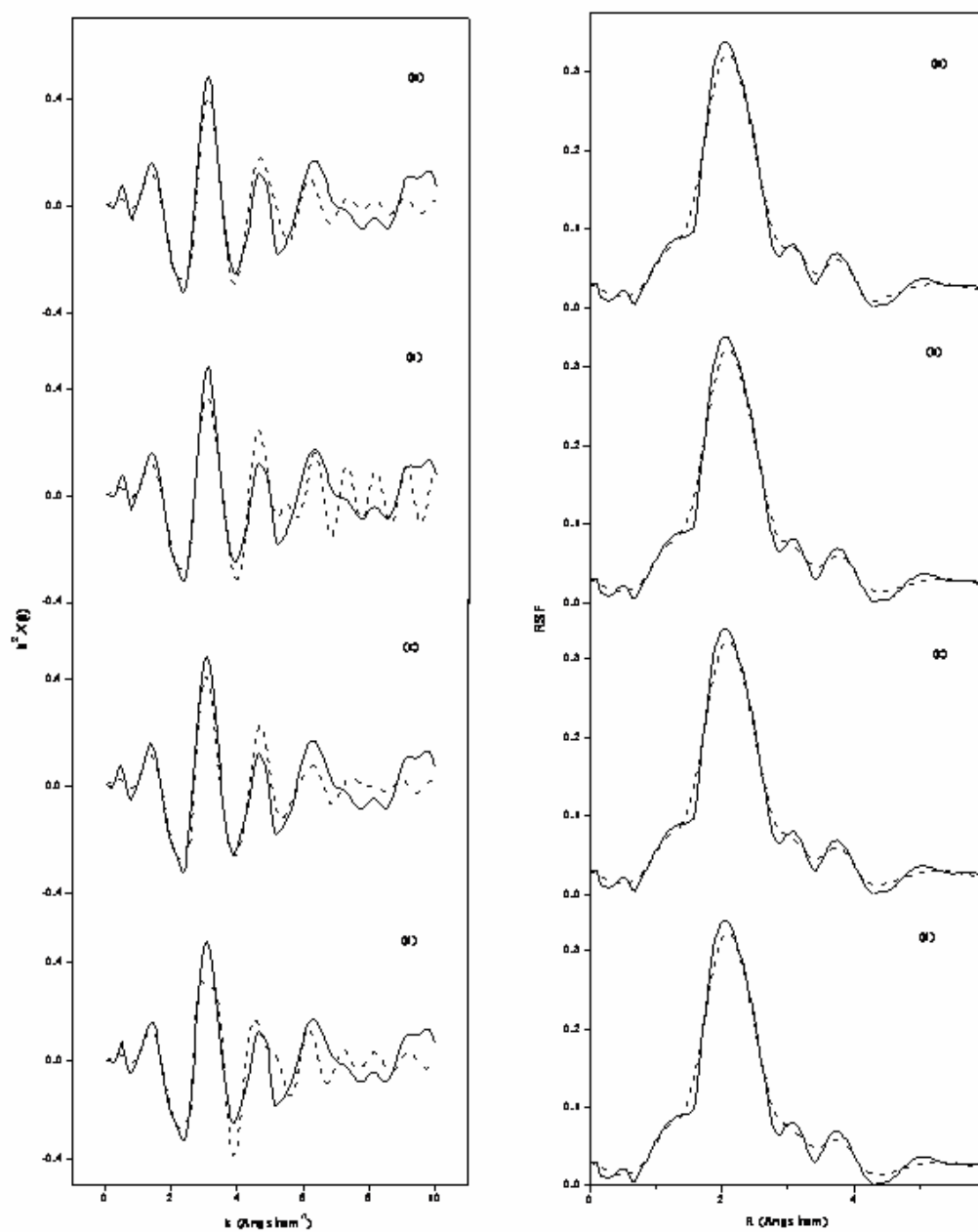


Figure 4.24 Comparison of $k^2\chi$ and radial structure function between K-SPEEK and the proposed 4-fold oxygen models. The solid line representing the experimental data (same for all the plots) and the dashed line representing the FEFF6 simulation.

4.2 Computational Part

4.2.1 Molecular dynamic simulations of Polystyrene and Poly (ether-ether-ketone)

4.2.1.1 Radial distribution function

Pair distribution functions, $g(r)$, for three different pairs of elements (CC, CH and HH) in bulk PS and PEEK were shown in Fig.4.25-30 which include only pairs that depend on the conformation of polymer chain.

For C-C atomic pair distribution in PS, the first and second sharp peak around 2.5 and 3.8 Å were from $C_{\text{aromatic}}-C_{\text{aromatic}}$ and $C_{\text{aromatic}}-C_{\text{aliphatic}}$ intra-correlation, respectively. For C-H atomic pair distribution in PS, they were three dominant peaks around 2, 3.6 and 4 Å which mainly contributed from the intra-correlations between $H_{\text{aliphatic}}-C_{\text{aliphatic}}$, $C_{\text{aliphatic}}-H_{\text{aliphatic}}$ and $H_{\text{aromatic}}-C_{\text{aromatic}}$, respectively. In H-H atomic pair distribution, the prominent peak around 2.3 Å belongs to $H_{\text{aromatic}}-H_{\text{aromatic}}$ inter and intra-action. As it has been shown, the most noticeable characteristic of these distributions is the absence of any apparent intermolecular correlation in all but the H-H pair distribution function. The $H_{\text{aliphatic}}-H_{\text{aromatic}}$ (Fig.C.5) and $H_{\text{aromatic}}-H_{\text{aromatic}}$ (Fig. C.6) distributions have definite intermolecular features, the contribution being predominantly intermolecular for the $H_{\text{aromatic}}-H_{\text{aromatic}}$ distribution. This might indicate that packing is determined mainly by interactions of aromatic moieties.

In PEEK chain, the two prominent peaks around 2.5 and 3 Å for C-C atomic pair distribution were belong to $C_{\text{aromatic}}-C_{\text{aromatic}}$ intra-correlations. For C-H atomic pair distribution, $H_{\text{aromatic}}-C_{\text{aromatic}}$ intra-interaction provides the main sharp peak around 2.1 Å. The second and third peaks around 3.3 and 3.8 Å were contributed from inter and intra-interactions between $H_{\text{aromatic}}-C_{\text{aromatic}}$. The main intermolecular

interaction was revealed in H-H atomic pair distribution, where $H_{\text{aromatic}}-H_{\text{aromatic}}$ inter-correlation become the main contribution (all three dominant peaks were from $H_{\text{aromatic}}-H_{\text{aromatic}}$ interaction). $H_{\text{aromatic}}-H_{\text{aromatic}}$ inter-correlation (Fig.C.12), however, is not the main interaction regulating the chain packing in PEEK polymer. It was contribution from carbonyl group that provides the main intermolecular interaction to the chain, as shown in Fig.C.15 and C.17. This lead to the conclusion that the carbonyl groups determine packing efficiency in PEEK chain. This result agrees well with Molecular Mechanic of PEEK on which the DPE molecule appears to be more mobile than the DPK molecule in the case of gear rotations.

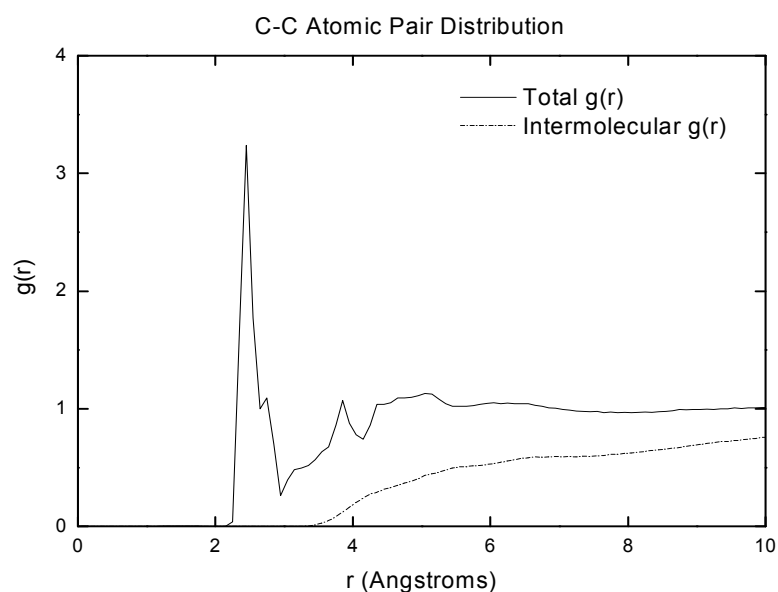


Figure 4.25 Elemental pair distribution function for all carbon atoms in PS.

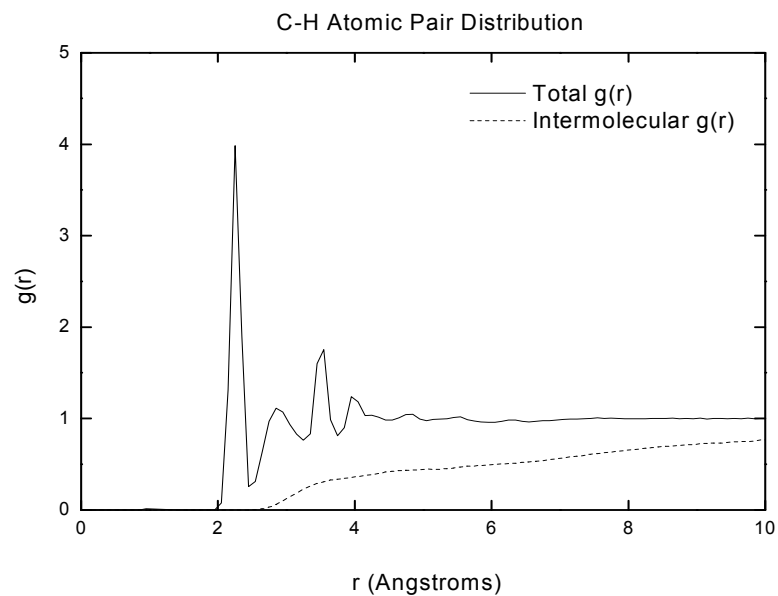


Figure 4.26 Elemental pair distribution function for all carbon atoms with all hydrogen atoms in PS.

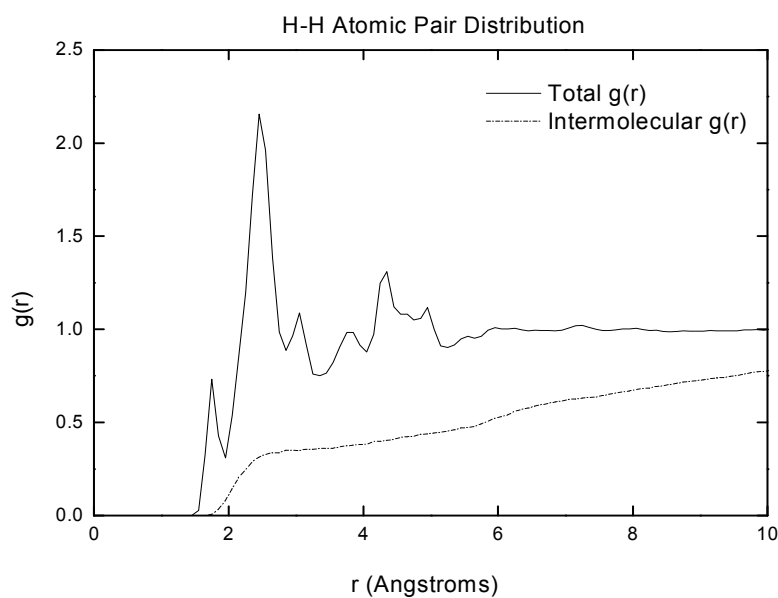


Figure 4.27 Elemental pair distribution function for all hydrogen atoms in PS.

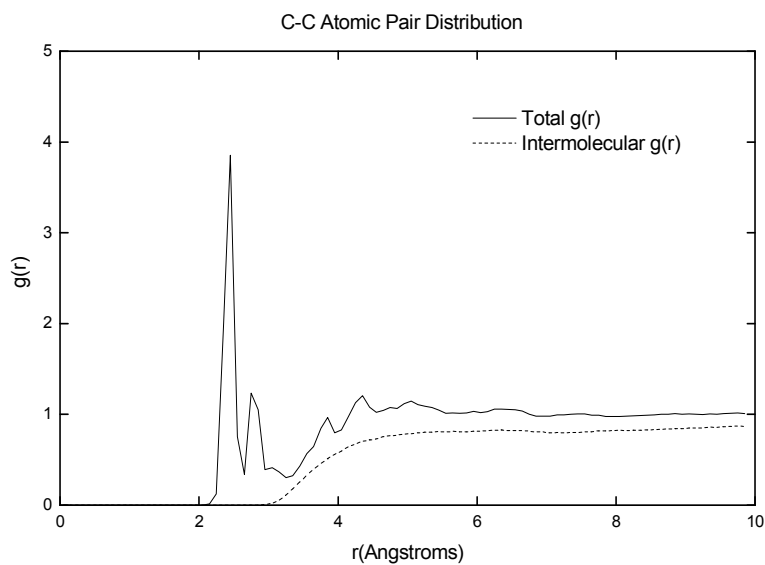


Figure 4.28 Elemental pair distribution function for all carbon atoms in PEEK.

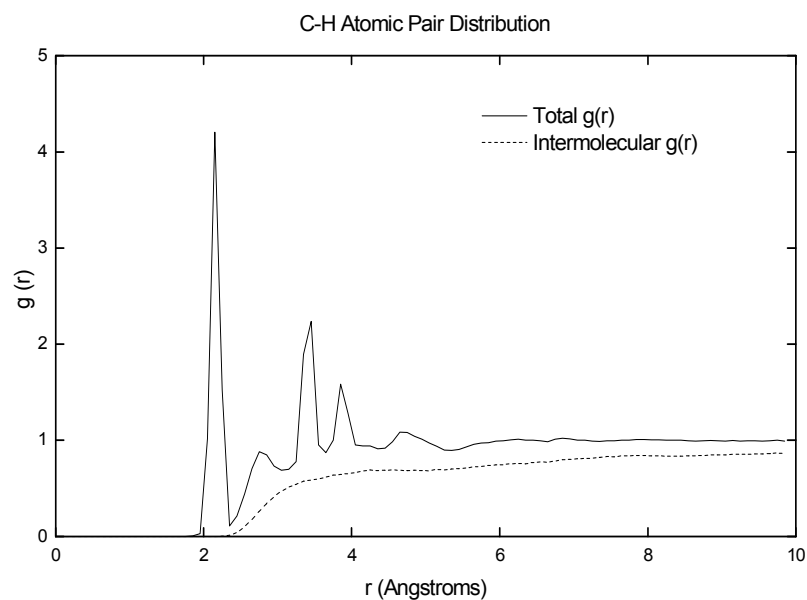


Figure 4.29 Elemental pair distribution function for all carbon atoms with all hydrogen atoms in PEEK.

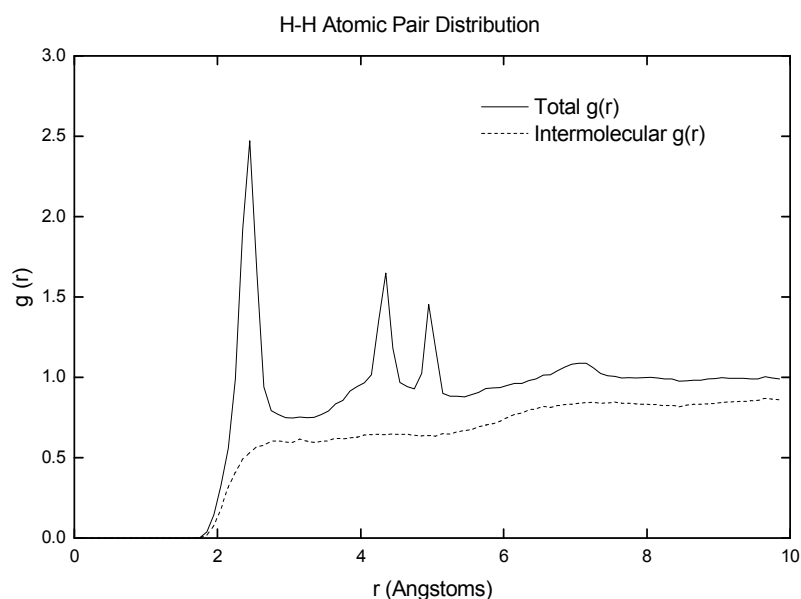


Figure 4.30 Elemental pair distribution function for all hydrogen atoms in PEEK.

4.2.1.2 Neutron and X-ray structure factor

From the elemental pair-distribution functions, it is straightforward to extract scattering patterns. The direct comparison of theoretical against experimental scattering results constitutes a useful check for the structural predictions of the model.

The neutron elastic structure factor $S(Q)$ for PS was calculated as a function of the scattering vector magnitude [$Q = (4\pi/\lambda) \cdot \sin\theta$]. The structure factor is calculated from the elemental radial pair-distribution function. The calculated spectrum shown in Fig.4.33 exhibits three peaks at $Q = 0.41, 1.25$ and 3.10 \AA^{-1} . These locations fit the experimentally observed peaks that occur at $Q = 0.60, 1.33$ and 3.00 \AA^{-1} (Scharp, Gabrys and Peiffer, 1990; Iradi, Alvarez, Colmenero and Arbe, 2004) very well. Experimentally, the second peak is the major one while the first is only a shoulder.

The difference at lowest Q is due to the relevant distant close to half of the periodic box.

One of the most interesting features of polystyrene is the so-called “polymerization peak” in its wide angle X-ray structure factor (Schubach, Nagy and Heise, 1981). The X-ray scattering pattern of atactic polystyrene (*a*-PS) reveals a diffuse halo (polymerization peak) at around $Q = 0.75 \text{ \AA}^{-1}$ in addition to higher Q feature at around 1.4 \AA^{-1} associated with the amorphous halo observed in polymer melts, glass, and rubber. The amorphous peak in *a*-PS arises primarily from phenyl-phenyl correlations while the polymerization is due to intermolecular correlations of backbone atoms. We conclude that the diffraction results indicate reasonable agreement between the computed and actual structure.

Scattering factors of PEEK structures were also calculated and shown in Fig. 4.34. Using the same method, scattering factor derived from the elemental radial pair-distribution function of Neutron structure factor was found at $Q = 1.34 \text{ \AA}^{-1}$ and 3.11 \AA^{-1} . No results were found for the neutron structure factor of PEEK in literature. For X-ray scattering, the structure factors were calculated to be 1.32 , 3.06 and 5.50 \AA^{-1} . These locations were slightly different from the experimentally observed peaks that occur at $Q = 1.00$ and 4.0 \AA^{-1} (Verma, Velikov, Kandert and Iarand, 1996; Jenkins, Haya and Terrill, 2003). Although the exact positions for each peak is different, all features found in experimental X-ray scattering can be captured in our simulated results. This difference may be come from the main chain rigidity of PEEK. Fortunately, other calculated properties of PEEK model were reasonable. Therefore, the current models of PEEK were used in this thesis.

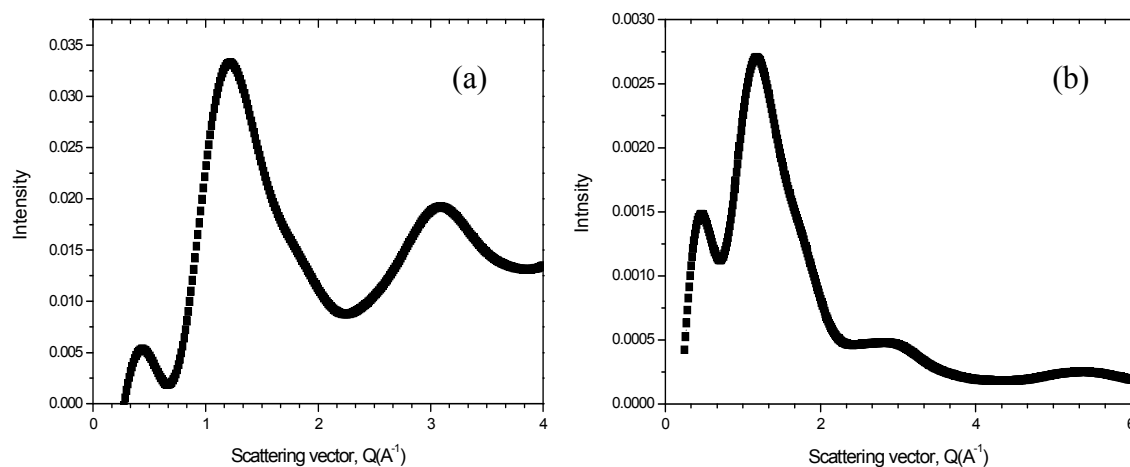


Figure 4.31 (a) Neutron scattering factor and (b) X-ray scattering intensity for PS.

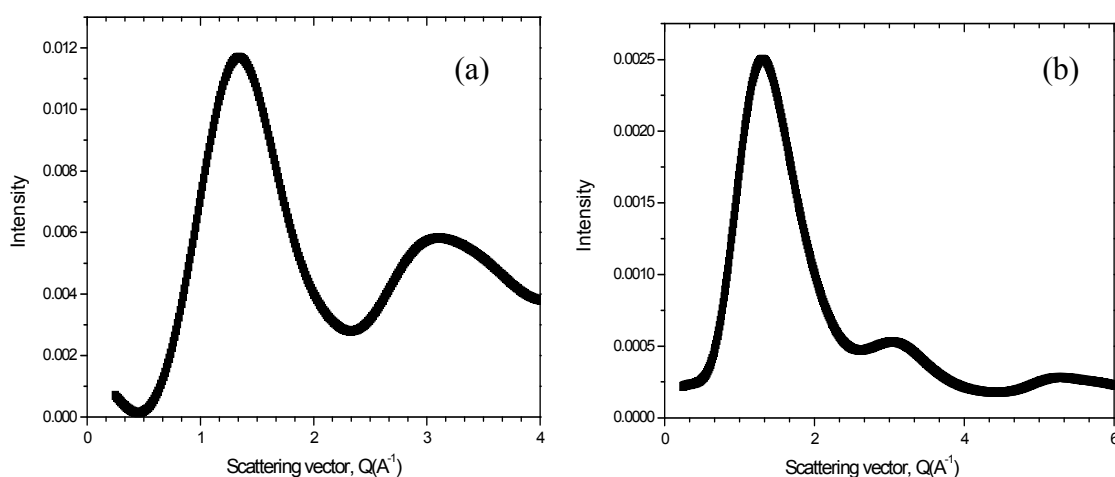


Figure 4.32 (a) Neutron scattering factor and (b) X-ray scattering intensity for PEEK.

4.2.1.3 Cohesive energy and solubility parameters

The cohesive energy density is the amount of energy needed to completely remove unit volume of molecules from their neighbours to infinite separation (an ideal gas), which is equal to the heat of vaporisation divided by molar volume. In this calculation, the cohesive energy, U_{coh} , is the energy associated with

the intermolecular interactions only and can be estimated by taking the difference between the total energy of the microstructure, U_{tot} , and that of the isolated parent chain, U_{par} . In order to determine the parent-chain energy, the cube edge length was simply set to very large value so that the chain was fully enclosed in the box and did not interact with its images. Hildebrand's solubility parameter, δ , is the square root of the cohesive energy density, as following

$$\delta = \left(\frac{E_{coh}}{V} \right)^{1/2} = \left(\frac{U_{par} - U_{tot}}{V} \right)^{1/2} \quad (4.3)$$

with V being the volume of the microstructure. The average Hildebrand solubility parameter for PS and PEEK were listed in Table 4.4

The reported experimental values for *a*-PS were between 8.12 and 9.88 cal^{1/2}/cm^{3/2} (Brandrup and Immergus, 1989), in agreement with the estimated results. No report is found for the solubility of PEEK in literature, so the data from SPEEK is presented in comparison. The calculated value of solubility parameter of PEEK is smaller than that of sulfonated PEEK. This result is reasonable due to the absent of sulfonate polar group in PEEK which give less interaction needed to separate molecules from each other.

4.2.1.4 Surface energy

The contribution of the internal energy to the surface energy, γ , is calculated using the relation

$$\gamma = \frac{E_{film} - E_{bulk}}{A} \quad (4.4)$$

where E_{bulk} is the energy of the amorphous bulk, E_{film} is the energy of the thin film and A is the area per free surface of the film having two free surfaces. Table 4.5 lists the simulated values of surface energy of PS and PEEK. The most dominant contribution to the formation of the free surface of the film comes from the Van der Waals dispersion energy. The value of A is determined by the dimensions of the periodic box. The calculation gives $\gamma = 36.3 \text{ erg.cm}^{-2}$ for PS which is slightly smaller than the experimental result 40.7 erg.cm^{-2} (Shimizu and Demarquette, 2000). The same method gives 38.5 erg.cm^{-2} for PEEK, which is slightly smaller than the experimental result of about 42.1 erg.cm^{-2} (Brandrup and Immergut, 1975). The simulation results presented here are able to predict successfully the experimentally derived surface energy of PS and PEEK.

Table 4.4 Hildebrand solubility parameter of the simulated bulk polymer (the indicated limit is the standard deviation).

Polymer	Hildebrand solubility parameter	
	Sim. ($\text{cal}^{1/2}/\text{cm}^{3/2}$)	Exp. ($\text{cal}^{1/2}/\text{cm}^{3/2}$)
PS	7.72 ± 0.10	8.12-9.88
PEEK	8.25 ± 0.10	12.10^a

(a) Data for SPEEK, Wu, Ma, Li and Chen, 2006.

Table 4.5 The contribution of the potential energy to the surface energy

Polymer	Potential energy (kcal/mol)		Difference of potential energy (kcal/mol)	Box size (Å) $x = y$	Surface energy (erg/cm ²)	
	Thin film	Bulk			Sim.	Exp.
PS	734.73	685.36	49.36	20.30	36.37	40.72 ^a
PEEK	2053.04	2003.41	49.63	19.76	38.52	42.10 ^b

(a) Shimizu, R. N. and Demarquette (2000).

(b) Brandrup, J. and Immergut (1975).

4.2.1.5 Diffusion of water molecules in polymer matrix

The diffusion of small molecules in polymer matrix is described as similar to a random walk process on a long time scale, which obeys Einstein's law as follows

$$D = \frac{1}{6N} \lim_{t \rightarrow \infty} \frac{d}{dt} \sum_{i=1}^N \langle [R, i(t) - R, i(0)]^2 \rangle \quad (4.5)$$

The sum term on the right-hand side of Eq 4.5 over N is called the mean-square displacement (MSD). N is the number of diffusing water molecules, t is time, and $R, i(t)$ is the position vector of a water molecule i at time event t . Average MSD curve as a function of time for each diffuser is calculated. It is essential to notice that Eq 4.5 is only valid when the Einstein diffusive regime is reached. This means that the motion of the diffusing particle follows a random walk; in other words, its motion is not correlated with its motion at any previous time. To test the region in which Eq 4.5 is valid, $\log(\text{MSD})$ against $\log(t)$ was plotted in this case. The slope of the curve is 1.0 ± 0.03 , when the Einstein diffusion is reached:

$$\frac{\Delta \log MSD}{\Delta \log t} = 1 \quad (4.6)$$

From the mean-square displacement of the water molecule as a function of time interval (Fig.4.35 and 4.36), the estimated diffusion coefficient of water in PS at 27°C is $0.28 \times 10^{-4} \text{ cm}^2/\text{s}$ which is close to the experimental value of $0.14 \times 10^{-4} \text{ cm}^2/\text{s}$ and the previous simulation report of $0.52 \times 10^{-6} \text{ cm}^2/\text{s}$ (Kucukpinar and Doruker, 2003). The diffusion coefficients of water molecules in PEEK at 30°C were estimated to be $0.99 \times 10^{-9} \text{ cm}^2/\text{s}$ which indicates that this result falls within the expected range (Tocci, Belluccio, Russo and Drioli, 2002).

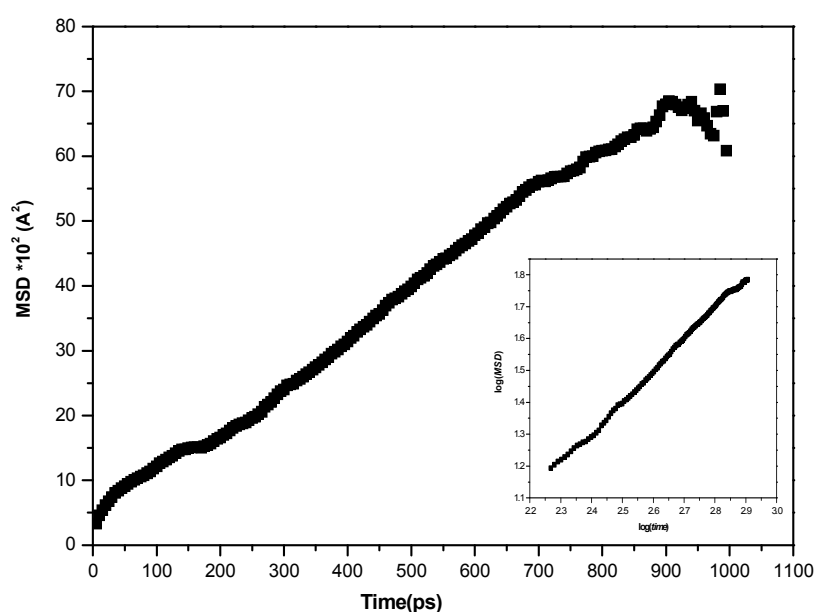


Figure 4.33 Mean-square displacement of H₂O as a function of time in PS at 27°C, the inserted figure is plot between log *MSD* and time.

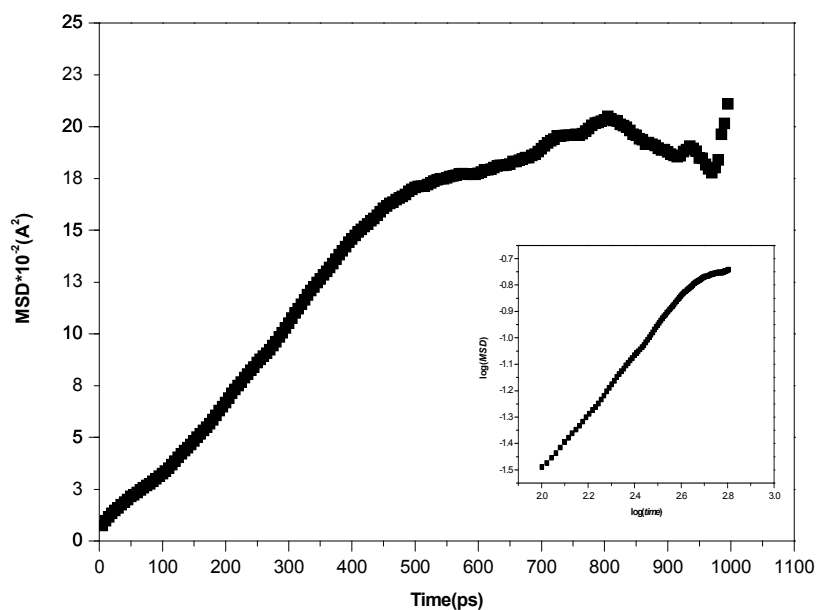


Figure 4.34 Mean-square displacement of H₂O as a function of time in PEEK at 30°C, the inserted figure is plot between log *MSD* and time.

4.2.2 MD simulations of benchmark models of sulfonated ionomers

The aim of this work is to present the structural results derived from experimental and theoretical methods and from a combination of them. Particular attention was devoted to the experimental determination of the first coordination shell of cation doped ionomers. The EXAFS analysis for cation doped SPS and SPEEK ionomers explore the detection limit of the techniques adopting the usual experimental tools whereas the structural results obtained from the MD simulations of the benchmark models of sulfonated ionomers provide the theoretical view. The radial distribution functions (RDF) and the running coordination number (CN) derived from MD simulations are both the most important keys that will be used to discuss the aggregation aspects obtained from EXAFS experiments.

Molecular dynamics simulations of the systems composed of an estimated amount of molecular species obtained from thermogravimetric analysis (TGA) (listed in Table 4.4) were performed. The compositions of these benchmark models fall in the same range as sulfonated ionomer membrane under an ambient humidity condition, according to TGA data. The correlation between radial distribution functions (RDF) and the coordination number (CN) obtained by an integration of the first peak in the RDF up to its first minimum as follows:

$$n_{x-z}(r) = 4\pi \frac{N_z}{\langle V \rangle} \int_0^r g_{x-z}(r) r^2 ds \quad (4.7)$$

For Eq 4.5, $n_{x-z}(r)$ is the number of x particles coordinated to particle the z within a radius r, $\langle V \rangle$ is the average cell volume, N_z is the total number of particles z in the system, and $g_{x-z}(r)$ is the radial distribution function between x and z.

Table 4.6 Description of the benchmark models of sulfonated ionomers. All MD simulations were performed at 227°C under NVT condition.

Ionomers	Number of particles				wt% of water	Density (g/cm ³)
	Sulfonate Fragment	H ₂ O	H ₃ O ⁺	Cation		
Ca-ionomer	26	72	24	1	6.83	1.08
K-ionomer	26	73	25	1	8.60	1.04

Note: All the cells were firstly subjected to 0.1 ns NPT simulation to find an appropriate density.

4.2.2.1 MD simulation of Ca-ionomer benchmark model

According to TGA results, the H₂O/SO₃H mole ratio in Ca-SPS sample was about 2.60. This ratio is not related directly to the local structure of Ca-ionomer due to some water molecules may be located at the film surface which do not respond to the aggregate structure. Water molecules that include in the crosslink structure should be located in the crystalline phase of ionomer film. These water should evaporate at the temperature higher than 100°C. Nevertheless, it is unable to separate two kinds of water from the TGA line because there was no data for the exact temperature to remove these waters from the crystalline phase of ionomer.

Fig. 4.35-40 show the RDFs between pair atoms of Ca-O (H₂O), Ca-S (SO₃H), Ca-O (-SO_{#1}), Ca-O (SO_{#2}), Ca-O (SO_{#2}), Ca-O (SO_{#3}) and Ca-O (H₃O⁺), respectively. The solid line represents RDF of pair atom while the dash line represents the integration peak of the area under RDF. The oxygen environment around Ca ions obtained from these RDFs was presented in Table 4.7.

The first coordination shell around Ca ions consists of around 9 oxygen atoms at the bond distance of 2.25-2.35 Å from their center of mass. Eight oxygen atoms were 8 atoms from the sulfonate groups. The remaining 1 atom was belonged to the surrounded water molecule. It was evident that the first coordination shell distances between Ca--O obtained from MD simulation agree very well with EXAFS result (2.35 Å). The difference of the coordination number between MD simulation and EXAFS (6 O atoms) might be because adding only one Ca cation allow all three oxygen atom of sulfonate group to attach alternately. This can be confirmed by RDF peaks in Fig.4.37 - 4.39 where the distance between Ca and three oxygens from the same sulfonate group are almost equal. These results different from the model proposed in

EXAFS results which suggest that it should have only one oxygen from each sulfonate group to join the first coordination shell while one of the remaining oxygens shares one adjacent calcium atom with other sulfonate group. The artifact occurred in this MD simulation might be solved by adding more cations to link with the sulfonate group. In this way, there would be only one oxygen from sulfonate group that was the closest one to the cation while other oxygen atoms from the same sulfonate group were drawn away by the nearest calcium ion. However, it is not yet possible to determine how many calcium ions needed to put in the simulation box to gain the phenomena similar to the real aggregation. Moreover, adding more cations mean it is needed to add more other particles to conform with TGA results. Unfortunately, this would spend much more time and computational resource to investigate this problem.

Given all the results above, thus, it was convinced that the best model to represent the number of sulfonate groups in the first coordination shell was the sulfur atom of sulfonate group. The RDF in Fig.4.36 reveals that there were about 3 sulfonate groups around the calcium ion. Thus, it was suggested by the MD simulation that Ca-ionomer contain 1 water molecule and 3 sulfonate groups in the first coordination shell. Although the coordination number obtained from MD simulation was still different from the EXAFS fitting, it was apparent from the simulation that the oxygen atoms linking to Ca ion were mainly from sulfonated groups. This result was consistent with the model discussed in EXAFS part. Fig.4.41 shows some snapshots extracted from MD trajectory frames. It shows the aggregate environment around calcium ions which clearly includes the first coordination shell of sulfonate groups and water molecules.

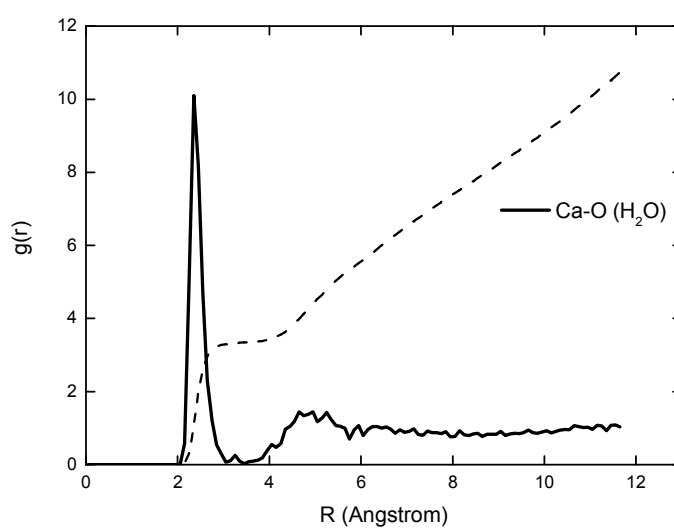


Figure 4.35 Simulated Ca-O (H_2O) RDF of Ca-ionomer.

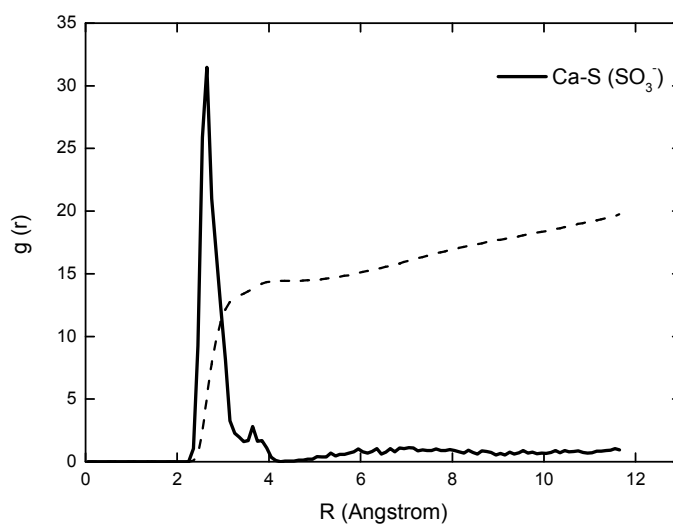


Figure 4.36 Simulated Ca-S ($-SO_3^-$) RDF of Ca-ionomer.

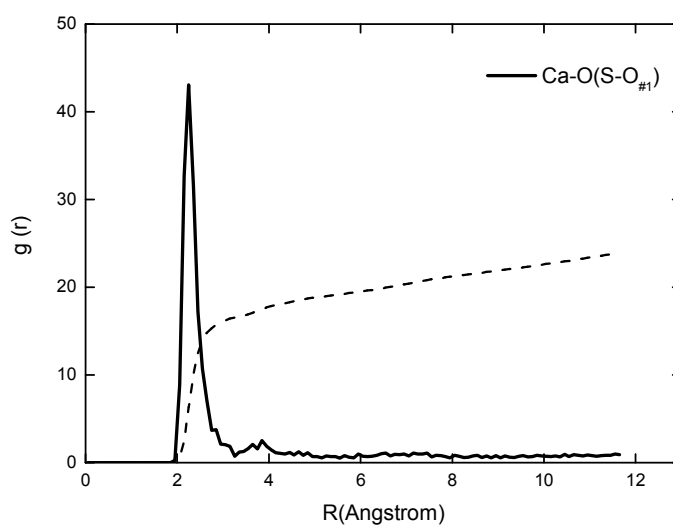


Figure 4.37 Simulated Ca-O (-S-O_{#1}) RDF of Ca-ionomer.

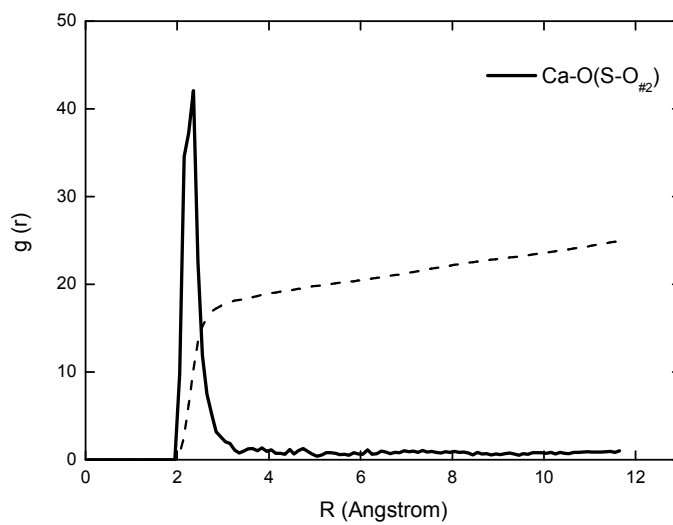


Figure 4.38 Simulated Ca-O (-S-O_{#2}) RDF of Ca-ionomer.

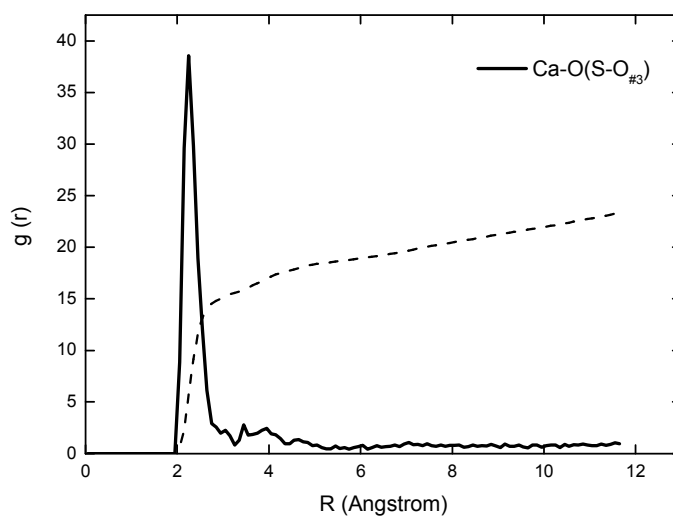


Figure 4.39 Simulated Ca-O (-S-O_{#3}) RDF of Ca-ionomer.

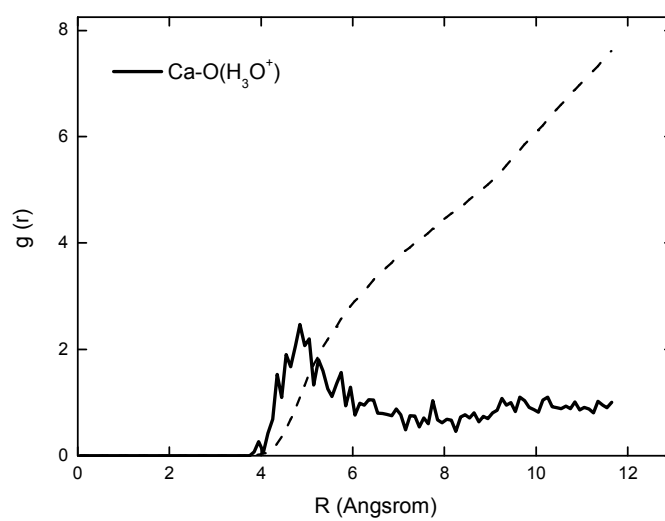


Figure 4.40 Simulated Ca-O (H₃O⁺) RDF of Ca-SPS ionomer.

Table 4.7 Parameters characterizing the first peak of the RDF from MD simulation of Ca-ionomer.

Pair atom	R(Å)	CN
Ca-O (H ₂ O)	2.35	1.07
Ca-O (-S-O _{#1})	2.25	2.78
Ca-O (-S-O _{#2})	2.35	2.68
Ca-O (-S-O _{#3})	2.25	2.78
Ca-S (-SO ₃ ⁻)	2.75	2.53
Ca-O (H ₃ O ⁺)	4.85	2.14

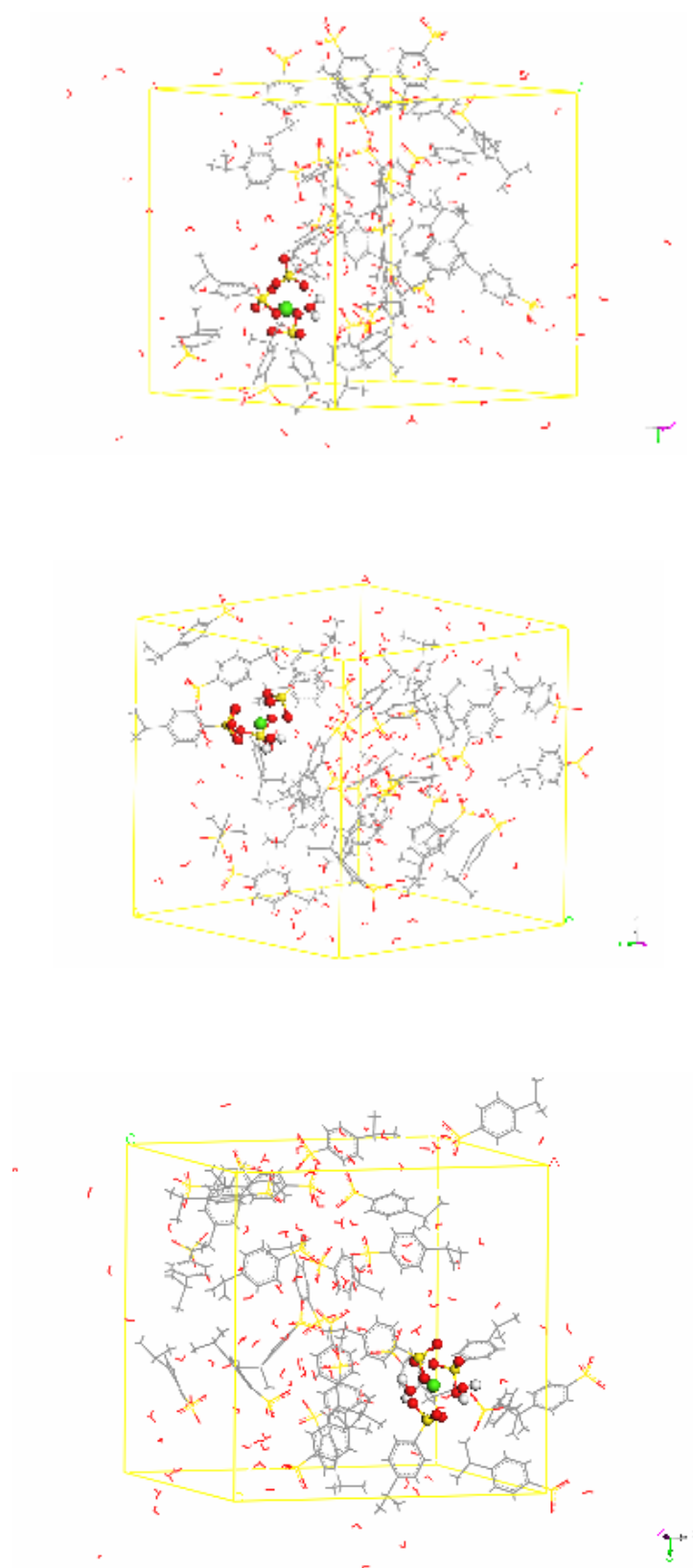


Figure 4.41 Typical snapshots of a Ca-ionomer from MD simulation.

4.2.2.2 MD simulation of the K-ionomer benchmark model

According to TGA results, the H₂O/SO₃H mole ratio in K-ionomers was about 2.75. Fig.4.42 - 4.47 show the RDFs between pair atoms of K-O (H₂O), K-S (SO₃H) K--O (-SO_{#1}), K-O (SO_{#2}), K-O (SO_{#2}), K-O (SO_{#3}) and K-O (H₃O⁺), respectively. The solid line represents RDF of pair atom while the dash line represents the integration peak of the area under RDF. The oxygen environment around K atoms obtained from these RDFs presented in Table 4.8.

The first coordination shell distances between Ca-O obtained from MD simulation (2.55-2.65 Å) fall in the same range of EXAFS result (2.68 Å). The first coordination shell of K atoms consists of 7 O atoms in average at the bond distance of 2.55-2.65 Å. Six of oxygen atoms were from sulfonate groups. The remaining 1 oxygen was from water molecule. The difference number of oxygen atom in the first shell between MD simulation (6 atoms) and experimental EXAFS (4 atoms) might be similar reasons described in the case of Ca-ionomer system. However, by considering S atom from the sulfonate group, 3 sulfonate groups were found in the first coordination shell of K. MD simulation suggests that four oxygen atoms from sulfonate groups were presented in the first coordination shell of K-ionomer. Of these 4 oxygen atoms, one of them was from the water molecule while the remaining oxygen atoms should belong to sulfonate anions. These results agree very well with the 4-fold oxygen model proposed in the EXAFS experimental part of K-ionomer. Although the 2H₂O--K--2SO₃⁻ model was proposed as the best model, the K and R-space features of the predicted spectra were not much different from the 1H₂O--K--3SO₃⁻ model. Therefore, as suggested by MD simulation, the 1H₂O--K--2SO₃⁻ might be the best model to describe the aggregate structure of K-SPS and K-SPEEK

ionomers. Fig.4.48 shows some snapshots extracted from MD trajectory frames. It shows the aggregate environment around calcium ions which clearly includes the first coordination shell of three sulfonate groups and one water molecules.

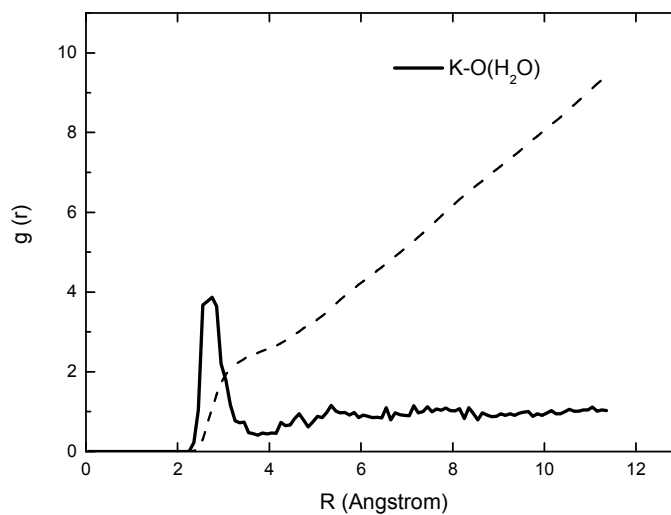


Figure 4.42 Simulated K-O (H_2O) RDF of K-ionomer.

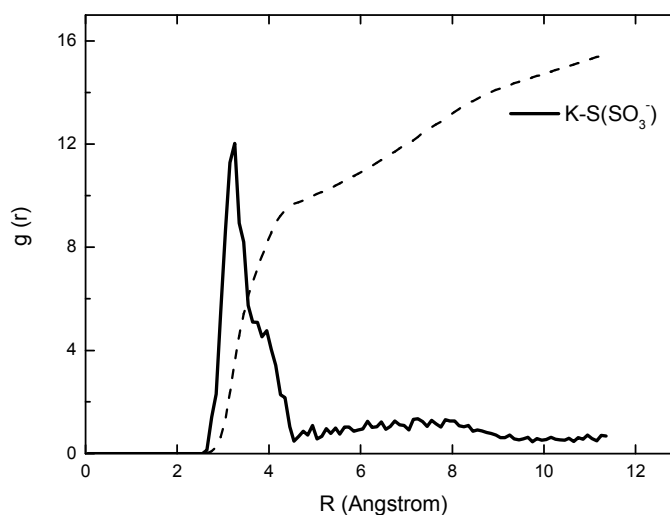


Figure 4.43 Simulated Ca-S ($-\text{SO}_3^-$) RDF of K-ionomer.

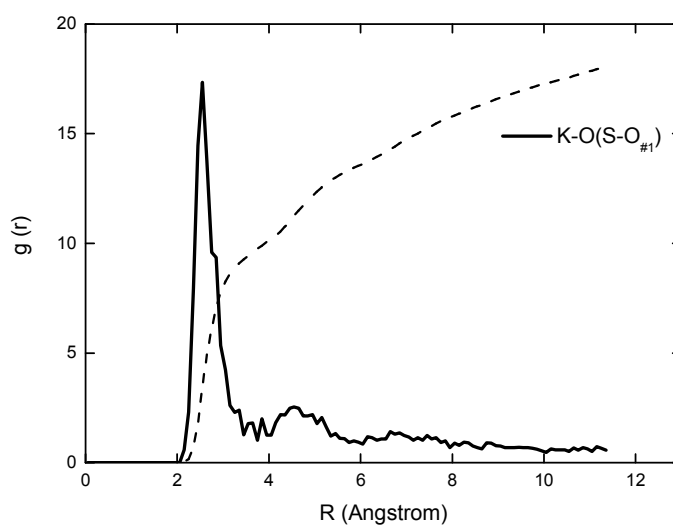


Figure 4.44 Simulated Ca-O (-S-O_{#1}) RDF of K-ionomer.

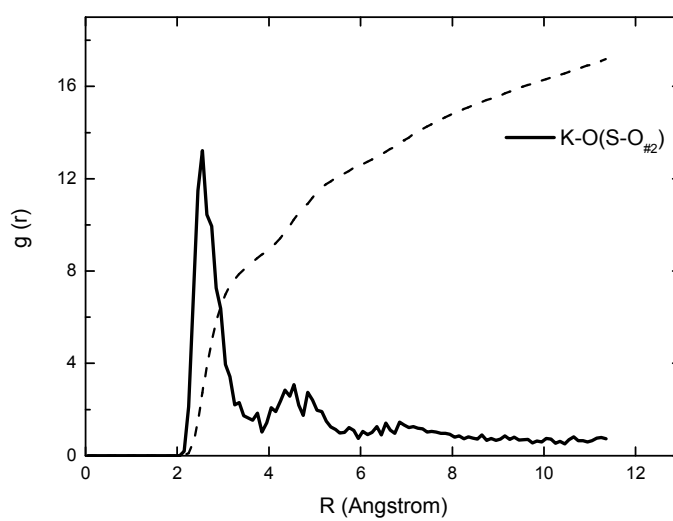


Figure 4.45 Simulated Ca-O (-S-O_{#2}) RDF of K-ionomer.

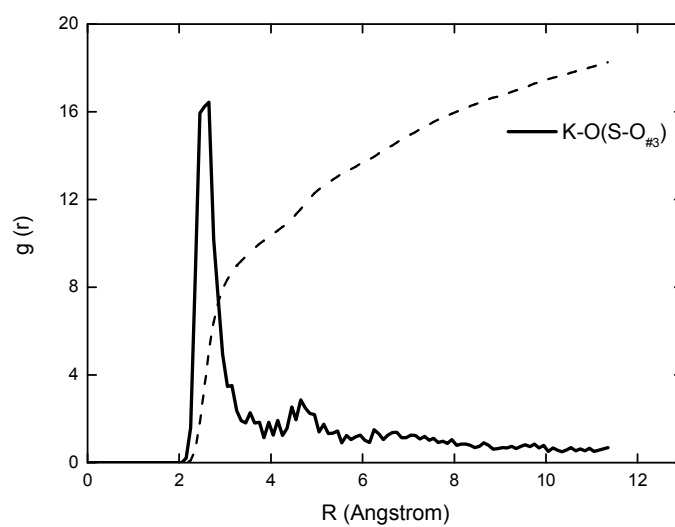


Figure 4.46 Simulated Ca-O (-S-O_{#3}) RDF of K-ionomer.

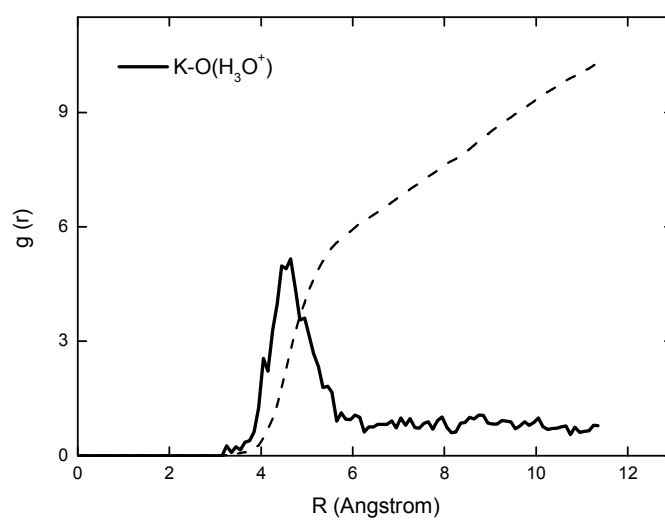


Figure 4.47 Simulated Ca-O (H₃O⁺) RDF of K-SPS ionomer.

Table 4.8 Parameters characterizing the first peak of the RDF from MD simulation of K-ionomer.

Pair atom	R(Å)	CN
K-(H ₂ O)	2.65	1.42
K-O(-S-O _{#1})	2.55	1.68
K-O (-S-O _{#2})	2.55	1.66
K -O (-S-O _{#3})	2.55	1.59
K -S(-SO ₃ ⁻)	3.25	2.98
K - (H ₃ O ⁺)	4.55	2.56

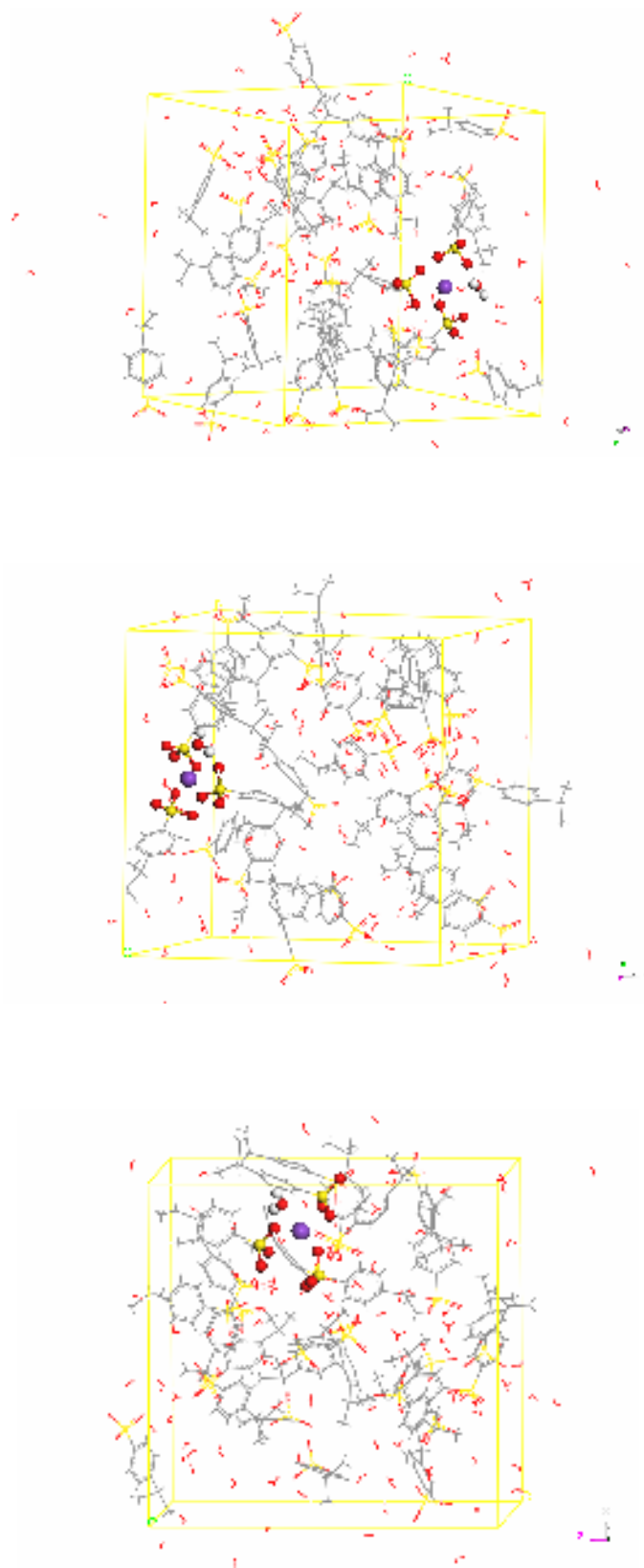


Figure 4.48 Typical snapshots of K-ionomer from MD simulation.

4.2.2.3 Diffusion coefficient of H_3O^+ and H_2O in the benchmark

models of sulfonated ionomers

In the review of ionic conductivity of cation doped ionomers, the ionic conductivity of the H-form membranes was considerably higher than that of the other cationic-form membranes (Saito, Hayamizu and Okada, 2004). It was suggested that the proton in the membranes transports by the hopping mechanism and other cations *i.e.* Li^+ and Na^+ ions by the vehicle mechanism. Hopping mechanism of proton has the hydrophilic donors *i.e.* water molecules and sulfonate groups to be the carriers. Thus it means that the mobility of the proton and carriers are the major factors to regulate the ionic conductivity. In this benchmark simulation we consider the situation where the H-form membranes were completely exchanged by K^+ and Ca^{2+} ions. Then, free hydroxonium ions (proton) were added to study their mobility comparing to ones in the parent membrane. This would correspond to the real fuel cells where free proton was feed from anode through the polymer membrane. To provide the charge neutrality, free added hydroxonium were neutralized by the same amount of hydroxyl ions (OH^-). The compositions of three benchmark models were presented in Table 4.9.

The mean square displacement of water and proton (in this case, hydroxonium ion) for the H, K and Ca-form of sulfonated membranes were calculated and shown in Fig.4.49-4.50. Diffusion coefficients (D) of water and hydronium ion in sulfonated membranes can be calculated as described previously in the section 4.2.1.5. The calculated diffusions coefficients of H_2O and H_3O^+ were summarized in Table 4.9.

Table 4.9 Description of the benchmark models of sulfonated ionomers. All MD simulations were performed at 127°C under NVT condition.

Membrane	Number of molecule					Density* (g/cm ³)
	Cation	Sulfonate fragment	Free H ₃ O ⁺	OH ⁻	H ₂ O	
H-form	26 H ₃ O ⁺	26	10	10	74	1.02
K-form	13K ⁺ + 13 H ₃ O ⁺	26	10	10	74	1.01
Ca-form	13Ca ²⁺	26	10	10	74	0.98

* All the cells were firstly subjected in 0.1 ns NPT simulation to obtain an appropriate density.

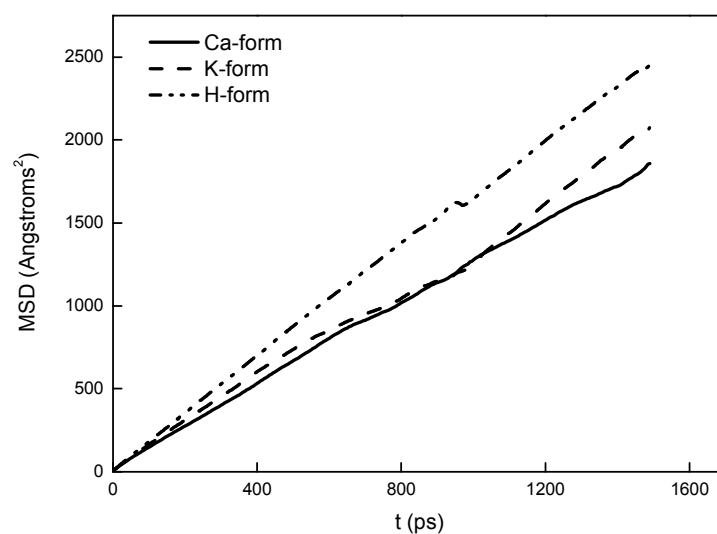


Figure 4.49 Mean square displacements of water molecules in H, K⁺ and Ca²⁺-from membranes at 127°C.

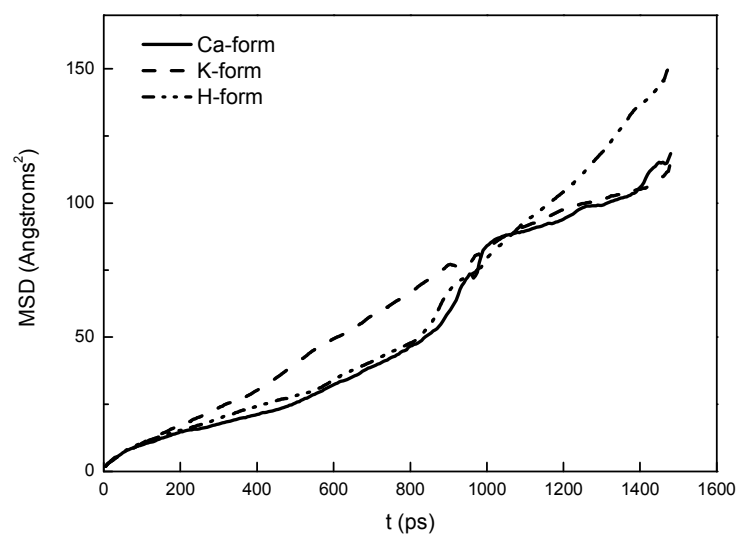


Figure 4.50 Mean square displacements of hydronium ions in H, K⁺ and Ca²⁺-form membranes at 127°C.

Table 4.10 Diffusion coefficients of atomic species in the benchmark NVT simulation at 127°C for 1.5 ns.

Membrane	D ($\times 10^{-1}$ Å ² /ps)	
	H ₂ O	H ₃ O ⁺
H-form	2.04	0.29
K-form	1.97	0.08
Ca-form	1.87	0.06

The magnitude of diffusion coefficients can be directly related to the ionic conductivity in ionomers. The simulations showed that $D_{\text{H}_2\text{O}}$ in the H-form at 400 K was higher than those in K and Ca-form membranes, respectively. The ionic conductivity of the membranes was mainly reflected by the proton transport through the intermediary of water. Clearly, $D_{\text{H}_3\text{O}^+}$ in ionomers after 1.0 ns has the same trend

with $D_{\text{H}_2\text{O}}$ which the highest $D_{\text{H}_3\text{O}^+}$ was found in the H-form followed by K and Ca-form, respectively. From these results, the cation species and their hydrophilic property are quite important for the mobility of water and hydronium ion. It might be inferred from the MSD lines that all membranes reached to an equilibrium after 1.0 ns and the sulfonate anions in cation doped systems become aggregated. In this study, the ionic aggregation in Ca-form was expected to reduce the hydronium permeability of the membrane. The crosslinks themselves may also decrease methanol diffusivity because of attraction between the penetrant and the ionic clusters. As in the benchmark simulation, the mobilities of the water and hydronium in Ca and K-form were slightly lower than those in H-form. When the diffusion of proton was considered, it would be the sulfonate fragments that play a dominant role in the ionic conduction by forming the aggregate domain to block proton diffusion. Thus, the more the expansion of sulfonate cluster regions, the slower the proton can be diffused. Fig.4.51 shows the RDFs between S ($-\text{SO}_3^-$) groups for all three membranes. By considering the distance and coordination number, it was clearly seen that the aggregation of sulfonate groups in Ca-form tends to be higher than that in K-form and H-form membrane, respectively. The aggregation of sulfonate groups should be induced by the doped cations due to the natural opposite charge type. As would be expected, the divalent Ca^{2+} ions play more inductive effect than monovalent K^+ and H_3O^+ , respectively. This can be confirmed by the RDFs between cation and sulfonate group shown in Fig.4.52. In addition, these inductive effects agree very well with EXAFS results where the first coordination shell in Ca-ionomers is composed of 4 sulfonate groups while there are only 2-3 anions in K-ionomers.

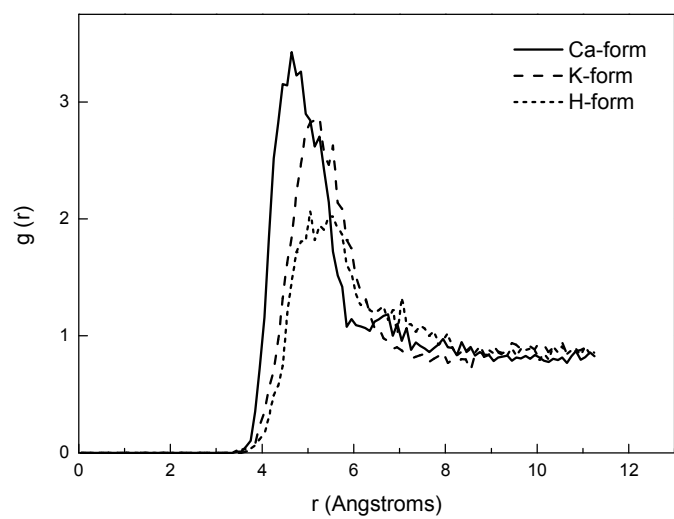


Figure 4.51 Comparison of the cumulative RDF between sulfonate fragments over a 1.5 ns NVT simulation at 127°C.

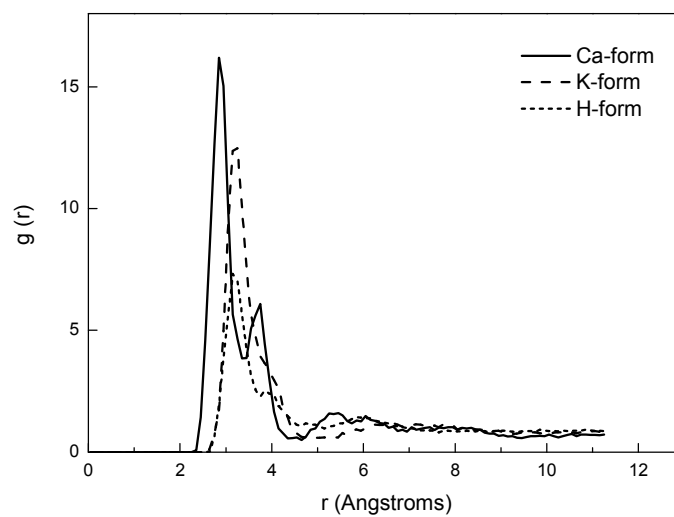


Figure 4.52 Comparison of the cumulative cation-sulfonate RDF over a 1.5 ns NVT simulation at 127°C.

CHAPTER V

CONCLUSION

In this thesis, the local atomistic structure of sulfonated polystyrene (SPS) and sulfonated poly (ether-ether-ketone) (SPEEK) ionomers were investigated mainly by EXAFS and molecular modeling techniques. 25.0 mol % sulfonate substitution level of SPEEK was obtained by sulfonation reaction of PEEK and concentrated sulfuric acid at room temperature for 120 hr. The H-form of 3.4 mol % SPS and the prepared 25.0 mol % SPEEK were fully neutralized by calcium and potassium ions via ion exchange process. Both Ca and K-ionomers were then probed by EXAFS to determine the local coordination structure about the cation. The first solvation shell in Ca-SPS consisted of six oxygen atoms, while Ca-SPEEK was coordinated by five oxygen atoms. The best-fit structures for both Ca-SPS and Ca-SPEEK contain four sulfonate groups surrounding calcium ion with the remaining two and one water of hydration, respectively. For the systems of monovalent cation, the best-fit structure for K-SPS and K-SPEEK was tetrahedrally rather than octahedrally coordinated. FEFF simulations indicated that potassium atoms in K-SPS and K-SPEEK were surrounded by two water molecules and two sulfonate anions. Amorphous model of PS and PEEK were then simulated via MD simulation technique. The predictions of neutron and X-ray structure factor, solubility parameters, surface energy and diffusion of water molecules were in good agreement with the experimental observation

implying that the generated models and force field-based MD calculation for PS and PEEK can be represent the real materials. Atomistic models of sulfonated ionomers with an estimated amount of molecular species obtained from TGA were then performed via MD simulation. It was evident from the RDFs of MD simulation that the first coordination shell distance between Ca-O and K-O agreed very well with the EXAFS fits. Coordination number obtained by an integration of the RDF peak revealed one water and three anions in the first coordination shell of cation in both Ca and K-ionomer. Although the numbers of water and sulfonate anion obtained form EXAFS and simulations are different. Both experimental and simulation techniques suggested that water molecule must be present in order to satisfy the coordination needs of the metal cation at the aggregate boundaries where the repeat structure terminates. According to the previous works, the ionic-crosslink occurred after the ionomers were neutralized by calcium and potassium should improve mechanical properties of SPS and SPEEK ionomers. Moreover, MD simulations suggested that the diffusion rate of proton through the matrix of Ca and K-form at 127°C is comparable to the one found in H-form ionomer at the same temperature. Finally, SPS and SPEEK ionomer neutralized with cations, especially divalent *i.e.* Ca^{2+} ion, should be a better candidate than monovalent *i.e.* K^+ for the membrane of PEMFC applications

REFERENCES

- Abd El-Rehim, H. A. (2005). Swelling of radiation crosslinked acrylamide-based microgels and their potential applications. **Radiat. Phys. Chem.** 74: 111-117.
- Acosta, J. L., Garcia-Fierro, J.L., Linares, A. and Canovas, M.J. (2000). Characterization of polymer systems based on sulfonated poly(2,6-dimethyl-1,4- phenylene oxide). **Polym. Int.** 49: 1534-1538.
- Allen, M. P. and Tildesley, D. J. (1987). **Computer simulation of liquids**. Oxford: Oxford University Press.
- Alupei, I., Popa, M., Hamcerencu, M. and Abadie, M. (2002). Superabsorbent hydrogels based on xanthan and poly(vinyl alcohol). The study of the swelling properties. **Eur. Polym. J.** 38: 2313-2320.
- Arico, A.S., Creti, P., Antonucci, P.C. and Antonucci, V. (1998). Comparison of ethanol and methanol oxidation in a liquid-feed solid polymer electrolyte fuel cell at high temperature. **Electrochem. Solid State Lett.** 1: 66.
- Atorngitjawat, P. and Runt, J. (2007). Dynamics of Sulfonated Polystyrene Ionomers Using Broadband Dielectric Spectroscopy. **Macromolecules.** 40: 991- 996.
- Bellinger, M.A., Sauer, J.A. and Hara, M. (1994). Deformation and tensile fracture behavior of sulfonated polystyrene ionomers: effects of counterion and excess neutralizing agent. **Polymer.** 35: 5478-5482.

- Bender, G. (1999). **Fuel cell application of poly-ether-ether-keto: electrochemical reaction kinetics and dielectric constant**. M. Sc. Dissertation, University of Stuttgart, German.
- Bauer, B., *et al.* (2000). Electrochemical characterisation of sulfonated Polyetherketone membranes. **J. New Mater. Electrochem. Syst.** 3: 93.
- Borodin, O., Bell, R. L., Li, Y., Bedrov, D. and Smith, G. D. (2001). Polarizable and nonpolarizable potentials for K^+ cation in water. **Chem. Phys. Lett.** 336: 292-302.
- Bonnet, B., Jones, D.J., Roziere, J., Tchicaya, L., Alberti, G., Casciola, M., Massinelli, L., Bauer, B., Peraio, A. and Ramunni, E. (2000). Hybrid organic-inorganic membranes for a medium temperature fuel cell. **J. New Mater. Electrochem. Syst.** 3: 87-92.
- Bozkurt, A., Ise, M., Kreuer, K.D., Meyer, W.H. and Wegner, G. (1999). Proton-conducting polymer electrolytes based on phosphoric acid. **Solid State Ionics.** 125: 225-233.
- Brandrup, J. and Immergut, E. H. (1975). **Polymer handbook**. 2nd ed., New York: Wiley-InterScience.
- Brandrup, J. and Immergut, E. H. (1989). **Polymer handbook**. 3rd ed., New York: Wiley-InterScience.
- Canovas, M.J., Sobrados, I., Sanzb, J., Acosta, J.L. and Linares, A. (2006). Proton mobility in hydrated sulfonated polystyrene: NMR and impedance studies. **J. Membr. Sci.** 280: 461-469.
- Capek, I. (2004). Dispersions of polymer ionomers: I. **Adv. Colloid Interface Sci.** 112: 1-29.

- Carretta, N., Tricoli, V. and Picchioni, F. (2000). Ionomeric membranes based on partially sulfonated poly(styrene): synthesis, proton conduction and methanol permeation. **J. Membr. Sci.** 166: 189-197.
- Charbonnier, P. F. and Loiseleur R.F.H. (1978). Structure crystalline of methanesulfonate dihydrate : $\text{Cd}(\text{CH}_3\text{SO}_3)_2 \cdot 2\text{H}_2\text{O}$. **Acta Cryst.** B34: 1504-1506.
- Chen, J., Asano, M., Yamaki, T. and Yoshida, M. (2005). Preparation of sulfonated crosslinked PTFE-graft-poly(alkyl vinyl ether) membranes for polymer electrolyte membrane fuel cells by radiation processing. **J. Membr. Sci.** 256: 38-45.
- Chen, W., Xin, Q., Suna, G., Yang, S., Zhou, Z., Mao, Q. and Sun, P. (2007). Effects of dissolved iron and chromium on the performance of direct methanol fuel cell. **Electrochim. Acta.** 52: 7115.
- Costamagna, P. and Srinivasan, S. (2001). Quantum jumps in the PEMFC science and technology from the 1960s to the year 2000, Part I. fundamental scientific aspects. **J. Power Sources.** 102: 242-252.
- Cui, W., Kerres, J. and Eigenberger, G. (1998). Development and characterization of ion-exchange polymer blend membranes. **Separ. Purif. Technol.** 14: 145-154.
- Dang, L. X. and Chang, T.-M. (1997). Molecular dynamics study of water clusters, liquid, and liquid-vapor interface of water with many-body potentials. **J. Chem. Phys.** 106: 8149-8159.
- Dang, L. X., Schenter, G. K., Glezakou, V-A John and Fulton, L. (2006). Molecular Simulation Analysis and X-ray Absorption Measurement of Ca^{2+} , K^+ and Cl^- Ions in Solution. **J. Phys. Chem. B.** 110: 23644.

- D'Angelo, P., Di Nola, A., Filipponi, A., Pavel, N. V. and Roccatano, D. (1994). An extended x-ray absorption fine structure study of aqueous solutions by employing molecular dynamics simulations. **J. Chem. Phys.** 100: 985-994.
- D' Cicco, A. D, Minicucci, M., Filipponi, A. (1997). New Advances in the Study of Local Structure of Molten Binary Salts. **Phys. Rev. Lett.** 78: 460-463.
- D' Cicco, A. D., Rosolen, M. J., Marassi, R., Tossici, R., Filipponi, A. and Rybicki, J. (1996). Short-range order in solid and liquid KBr probed by EXAFS. **J. Phys. : Condens. Matter.** 8: 10779.
- Desmarteau, D., et al. (2000). "Perfluorinated ionomers containing the sulfonimide function: promising membrane and electrocatalyst materials for high temperature PEM fuel cells", **11st annual meeting of the North American Membrane Society.**
- Ding, Y-P. S. (1986). **A study of the structure and properties of ion-containing polymers.** Ph.D. Dissertation, University of Wisconsin, USA.
- Ding, Y-P. S., Hubbard, S. R., Hodgson, K. O., Register, R. A. and Cooper, S. L. (1988). Anomalous small-angle x-ray scattering from a sulfonated polystyrene ionomer. **Macromolecules.** 21: 1698-1703.
- Ding, Y-P. S., Register, R. A., Yang, C. Z. and Cooper, S. L. (1989). Synthesis and characterization of sulphonated polyurethane ionomers based on toluene diisocyanate. **Polymer.** 30: 1204-1212.
- Ding, Y-P. S., Register, R. A., Yang, C. Z. and Cooper, S. L. (1989). Effect of cation local structure on the physical properties of sulphonated polyurethane ionomers based on toluene diisocyanate. **Polymer.** 30: 1221-1226.

- Ding, Y-P. S., Yarusso, D. J., Pan, H. K. and Cooper, S. L. (1984). Extended x-ray absorption fine structure: Studies of zinc-neutralized sulfonated polystyrene ionomers. **J. Appl. Phys.** 56: 2396-2403.
- Dippel, Th., Kreuer, K.D., Lassègues, J.C. and Rodriguez, D. (1993). Proton conductivity in fused phosphoric acid: a $^1\text{H}/^{31}\text{P}$ PPFG-NMR and QNS-study. **Solid State Ionics.** 61: 41-46.
- Doyle, M., Lewittes, M. E., Roelofs, M. G., Perusich, S. A. and Lowrey, R. E. (2001). Relationship between ionic conductivity of perfluorinated ionomeric membranes and nonaqueous solvent properties. **J. Membr. Sci.** 184: 257-273.
- Dreyfus, B. (1985). Model for the clustering of multiplets in ionomers. **Macromolecules.** 18: 284-192.
- Eisenberg, A., Hird, B. and Moore, R. B. (1990). A new multiplet-cluster model for the morphology of random ionomers. **Macromolecules.** 23: 4098-4107.
- Eisenberg, A. and Kim, J.-S. (1998). **Introduction to ionomers.** New York: Wiley-Interscience.
- Eisenberg, A., King, M. (1977). **Ion-containing polymers, physical properties and structure.** New York: Academic Press.
- Elliott, J.A., Hanna, S., Elliott, A. M. S. and Cooley, G. E. (1999). Atomistic simulation and molecular dynamics of model systems for perfluorinated ionomer membranes. **Phys. Chem. Chem. Phys.** 1 : 4855-4863.
- Farrell, K. V. and Grady, B. P. (2000). Effect of temperature on aggregate local structure in a zinc-neutralized carboxylate ionomer. **Macromolecules.** 33: 7122-7126.

- Farrell, K. V. and Grady, B. P. (2001). EXAFS spectroscopy studies of cation local environment in sodium-neutralized ethylene copolymer ionomers. **Macromolecules**. 34: 7108-7112.
- Filipponi, A. and Cicco D, (1995). Short-range order in crystalline, amorphous, liquid, and supercooled germanium probed by x-ray absorption spectroscopy. **Phys. Rev. B**. 51: 12322.
- Forsman, W. C., MacKnight, W. J. and Higgins, J. S. (1984). Aggregation of ion pairs in sodium poly(styrenesulfonate) ionomers: theory and experiment. **Macromolecules**. 17: 490-494.
- Galland, D., Belakhovsky, M., Medrignac, F., Pinéri, M., Vlaic, G. and Jérôme, R. (1986). Microstructure of copper(II) α,ω -dicarboxylato polybutadiene. **Polymer**. 27: 883-888.
- Gasa, J. V., Weiss, R.A. and Shaw, M. T. (2007). Ionic crosslinking of ionomer polymer electrolyte membranes using barium cations. **J. Membr. Sci.** 304: 173-180.
- Gebel, G. (2000). Structural evolution of water swollen perfluorosulfonated ionomers from dry membrane to solution. **Polymer**. 41: 5829-5838 .
- Gil, M., Ji, X. L., Li, X. F., Na, H., Hampsey, J. E. and Lu, Y.F. (2004). Direct synthesis of sulfonated aromatic poly(ether ether ketone) proton exchange membranes for fuel cell applications. **J. Membr. Sci.** 234: 75-81.
- Grady, B. P. (2000). Relative size of ionic aggregates determined by X-ray absorption spectroscopy. **Polymer**. 41: 2325-2328.

- Grady, B. P. and Cooper, S. L. (1994). Extended X-ray Absorption Fine-Structure Studies of the Internal Aggregate Structure in Lightly Sulfonated Polystyrene. 1. Determination of the Coordination Environment about the Cation. **Macromolecules**. 27: 6627-6634.
- Grady, B. P., Floyd, J. A., Genetti, W. B., Vanhoorne, P. and Register, R. A. (1999). X-ray absorption spectroscopy studies of zinc-neutralized ethylene-methacrylic acid ionomers. **Polymer**. 40: 283-288.
- Grady, B. P. and Moore, R. B. (1996). EXAFS Studies of Various Sulfonated and Carboxylated Cadmium Ionomers. **Macromolecules**. 29: 1685-1690.
- Guo, Q., Pintauro, P., Tang, H. and O'Connor, S. (1999). Sulfonated and crosslinked polyphosphazene-based proton-exchange membranes. **J. Membr. Sci.** 154: 175-181.
- Hamerton, I., Heald C. R. and Howlin, B.J. (1996). Molecular simulation of the comparative flexibility of bridging linkages in poly(aryl ether sulfone)s and poly(aryl ether ketone)s from a study of isolated oligomers. **Macromol. Theory Simul.** 5: 305-320.
- Hara, M., Eisenberg, A., Storey, R. F. and Kennedy, J. P. (1986). In 'Coulombic Interactions in Macromolecular Systems' (Eds A.Eisenberg and F. E. Bailey) **ACS Symp. Ser.** 302
- Hoffmann, M. M., Darab, J. G., Palmer, B. J. and Fulton, J. L. (1999). A Transition in the Ni²⁺ Complex Structure from Six- to Four-Coordinate upon Formation of Ion Pair Species in Supercritical Water: An X-ray Absorption Fine Structure, Near-Infrared, and Molecular Dynamics Study. **J. Phys. Chem.** 103: 8471-8482.

- Hsu, W.Y. and Gierke, T.D., (1982). Elastic theory for ionic clustering in perfluorinated ionomers. **Macromolecules**. 15: 101-105.
- Ianniello, R., Schmidt, V.M., Stimming, U., Stumper, J. and Wallan, A. (1994). CO adsorption and oxidation on Pt-Ru alloys -dependence on substrate composition. **Electrochim. Acta**. 39: 1863.
- Inzelt, G., Pineri, M. Schulze, J.W. and Vorotyntsev, M.A. (2000). Electron and proton conducting polymers: recent developments and prospects. **Electrochim. Acta**. 45: 2403.
- Iradia, I., Alvarez, F., Colmenero, J. and Arbe, A. (2004). Structure factors in polystyrene: a neutron scattering and MD-simulation study. **Physica B**. 350: 881.
- Ise, M. (2000). **Polymer elektrolyt membranen: untersuchungen zur mikrostruktur und zu den transporeigenschaften für protonen und wasser**. Ph.D. Dissertation, University of Stuttgart, German.
- Ise, M., Kreuer, K.D. and Maier, J. (1999). Electroosmotic drag in polymer electrolyte membranes: an electrophoretic NMR study. **Solid State Ionics**. 125: 213-223.
- Ishioka, T., Shimizu, M., Watanabe, I., Kawauchi, S. and Harada, M. (2000). Infrared and XAFS Study on Internal Structural Change of Ion Aggregate in a Zinc Salt of Poly(ethylene-co-methacrylic acid) Ionomer on Water Absorption. **Macromolecules**. 33: 2722-2727.

- Jalilehvand, F., Spangberg, D., Patric, L-R. Hermansson, K., Ingmar Persson, I. and Sandstrom M. (2001). Hydration of the Calcium Ion. An EXAFS, Large-Angle X-ray Scattering, and Molecular Dynamics Simulation Study. **J. Am. Chem. Soc.** 123: 431-441.
- Janik, I., Kasprzak, E., Al-Zier, A. and Rosiak, J.M. (2003). Radiation crosslinking and scission parameters for poly(vinyl methyl ether) in aqueous solution. **Nucl. Instrum. Methods Phys. Res. B.** 208: 374.
- Jar, P-Y. B. and Wu, Y. S. (1997). Effect of counter-ions on swelling and shrinkage of polyacrylamidebased ionic gels. **Polymer.** 38: 2557-2560.
- Jenkinsa, M.J., Haya, J.N. and Terrill, N.J. (2003). Structure evolution in melt crystallised PEEK. **Polymer.** 44: 6781-6787.
- Jerome, R., Vlais, G. and Williams, C. E. (1983). EXAFS evidence for local order in the ionic aggregates of halato-telechelic polymers. **J. Physique Lett.** 44: 717-723.
- Jin, X., Bishop, M.T., Ellis, T.S. and Karasz, F. (1985). A sulphonated poly(aryl ether ketone). **Br. Polym. J.** 17: 4-10.
- Karlsson, L.E. and Jannasch, P. (2005). Polysulfone ionomers for proton conducting fuel cell membranes. 2. Sulfophenylated polysulfones and polyphenylsulfones. **Electrochim. Acta.** 50: 1939.
- Kerres, J., Cui, W. and Junginger, M. (1998). Development and characterization of crosslinked ionomer membranes based upon sulfinated and sulfonated PSU crosslinked PSU blend membranes by alkylation of sulfinate groups with dihalogenoalkanes. **J. Membr. Sci.** 139: 227-241.

- Kerres, J., Ullrich, A., Meier, F. and Häring, T. (1999). Synthesis and characterization of novel acid–base polymer blends for application in membrane fuel cells, **Solid State Ionics**. 125: 243-249.
- Kim, S.H. and Kim, J.S. (2003). Effects of low matrix glass transition temperature on the cluster formation of ionomers having two ion pairs per ionic repeat units. **Macromolecules**. 36: 1870-1875.
- Kobayashi, T., Rikukawa, M., Sanui, K. and Ogata, N. (1998). Proton-conducting polymers derived from poly (ether-ether-ketone) and poly (4-phenoxybenzoyl-1,4-phenylene). **Solid State Ionics**. 106: 219-225.
- Koter, S., Piotrowski, P. and Kerres, J. (1999). Comparative investigations of ion-exchange membranes. **J. Membr. Sci.** 153: 83-90.
- Kreuer, K.D. (1996). Proton conductivity: materials and applications. **Chem. Mater.** 8: 610.
- Kreuer, K.D. (2001). On the development of proton conducting polymer membranes for hydrogen and methanol fuel cells. **J. Membr. Sci.** 185: 29-39.
- Kreuer, K.D., Rabenau, A. and Wepper, W. (1982). Vehicle mechanism. A new model for interpretation of the conductivity of fast proton conductors. **Angew. Chem. Int. Ed. Engl.** 21: 208.
- Kucera, F. and Jancar, J. (1998). Homogeneous and heterogeneous sulfonation of polymers: a review. **Polym. Eng. Sci.** 38: 783-792.
- Kucukpinar, E. and Doruker, P. (2003). Molecular simulations of small gas diffusion and solubility in copolymers of styrene. **Polymer**. 44: 3607-3620.
- Kyu, S. C., Maier, G., Andreaus, B. and Scherer, G. G. (2004). Block copolymer ionomers for ion conductive membranes. **J. Membr. Sci.** 245: 147-161.

- Larminie, J. and Dicks, A. (2000). **Fuel Cell System Explained**. West Sussex: Wiley-InterScience.
- Lassegues, J.C. (1992). **Mixed inorganic–organic systems: the acid/polymer blends, in: Ph. Colomban (Ed.), proton conductors: solids, membranes and gels — materials and devices**. Cambridge: Cambridge University Press.
- Lebrun, L., Blanco, J.F. and M'etayer, M. (2005). Preparation of ion-exchange membranes using pullulan as polymer matrix. **Carbohydr. Polym.** 61: 1.
- Li, L., Zhang, J. and Wang, Y. (2003). Sulfonated poly (ether-ether-ketone) membranes for direct methanol fuel cell. **J. Membr. Sci.** 226: 159-167.
- Lu, X. Y., Steckle, W. P. and Weiss, R. A. (1993). Ionic aggregation in a block copolymer ionomers. **Macromolecules.** 26: 5876-5884.
- Ludvigsson, M., Lindgren J. and Tegenfeldt. J. (2000). FTIR study of water in cast Nafion films. **Electrochim. Acta.** 45: 2267.
- Marcus, Y. (1988). Ion radii in aqueous solution. **Chem. Rev.** 88: 1475-1498.
- Mathew, K.T., Kumar, S. B., Lonappan, A., Jacob, J., Samuel, J., Xavier, T. and Kurian, T. (2002). Dielectric properties of ionomers at microwave frequencies. **Mater. Lett.** 56: 248-251.
- Meagher, A., Coey, J. M. D., Belakhovsky, M., Pineri, M., Jerome, R., Vlais, G., Williams, C. and Dang, N. V. (1986). Microstructure of iron(III) α,ω -dicarboxylatopolybutadiene. **Polymer.** 27: 979-985.
- Nagarale, R.K., Gohil, G.S. and Shahi, V. K. (2006). Sulfonated poly (ether-ether-ketone)/polyaniline composite. **J. Membr. Sci.** 280: 389-396.

- Newville, M., Livins, P., Yacoby, Y., Rehr, J. J. and Stern, E. A. (1993). Near-edge x-ray-absorption fine structure of Pb: A comparison of theory and experiment. **Phys. Rev. B.** 47: 14126-14131.
- Newville, M., Ravel, B., Haskel, D., Rehr, J. J., Stern, E. A. and Yacoby, Y. (1995). Analysis of multiple-scattering XAFS data using theoretical standards. **Physica.** 209: 154.
- Nolte, R., Ledjeff, K., Bauer, M. and Mulhaupt, R. (1993). Partially sulfonated poly(arylene ether sulfone) - A versatile proton conducting membrane material for modern energy conversion technologies. **J. Membr. Sci.** 83: 211-220.
- Noshay, A. and Robenson, L.M. (1976). Sulfonated polysulfone, **J. Appl. Polym. Sci.** 20: 1885.
- Okada, T., Arimura, N., Satou, H., Yuasa, M. and Kikuchi, T. (2005). Membrane transport characteristics of binary cation systems with Li^+ and alkali metal cations in perfluorosulfonated ionomer. **Electrochim. Acta.** 50: 3569.
- Okada, T., Ayato, Y., Yuasa, M. and Sekine, I. (1999). The Effect of Impurity Cations on the Transport Characteristics of Perfluorosulfonated Ionomer Membranes. **J. Phys. Chem. B.** 103: 3315.
- Paddison, St. J., Bender, G., Kreuer, K.D., Nicoloso, N. and Zawodzinski, T. (2000). The microwave region of the dielectric spectrum of hydrated NAFION and other sulfonated membranes. **J. New Mater. Electrochem. Syst.** 3: 293.
- Pan, H. K., Yarusso, D. J., Knapp, G. S., Pinrri, M., Meagher, A., Coey, J. M. D. and Cooper, S. L. (1983). EXAFS and Mössbauer studies of iron neutralized Nafion ionomers. **J. Chem. Phys.** 79: 4736-4745.

- Pan, H. K., Knapp, G. S. and Cooper, S. L. (1984). EXAFS and XANES studies of Zn^{2+} and Rb^+ neutralized perfluorinated ionomers. **Colloid Polym. Sci.** 262: 734-746.
- Pan, H. K., Meagher, A., Pineri, M., Knapp, G. S. and Cooper, S. L. (1985). EXAFS studies of Fe^{3+} neutralized Nafion: Interpretation of the second peak in the radial structure function. **J. Chem. Phys.** 82: 1529-1538.
- Praptowidodo, V.S. (2005). Influence of swelling on water transport through PVA based membrane. **J. Mol. Struct.** 739: 207.
- Radoslaw, A., Wach, R.A., Mitomo, H., Nagasawa, N. and Yoshii, F. (2003). Radiation crosslinking of carboxymethyl cellulose of various degree of substitution at high concentration in aqueous solutions of natural pH. **Phys. Chem.** 68: 771.
- Rehr, J. J., Zabinsky, S. I. and Albers, R. C. (1992). High-order multiple-scattering calculations of x-ray-absorption fine structure. **Phys. Rev. Lett.** 69: 3397-3400.
- Register, R. A., Foucart, M., Jerome, R., Ding, Y. S. and Cooper, S. L. (1988). Corrections: Structure-Property Relationships in Elastomeric Carboxy-Telechelic Polyisoprene Ionomers Neutralized with Divalent Cations. **Macromolecules.** 21: 2652-2652.
- Rikukawa, M. and Sanui, K. (2000). Proton-conducting polymer electrolyte membranes based on hydrocarbon polymer. **Prog. Polym. Sci.** 25: 1463-1502.

- Robertson, G. P., Mikhailenko, S. D., Wang, K., Xing, P., Guiver, M. D. and Kaliaguine, S. (2003). Casting solvent interactions with sulfonated poly(ether ether ketone) during proton exchange membrane fabrication. **J. Membr. Sci.** 219: 113-121.
- Roccatano, D., Berendsen, H. J. C. and D'Angelo, P. (1998). Assessment of the validity of intermolecular potential models used in molecular dynamics simulations by extended x-ray absorption fine structure spectroscopy: A case study of Sr^{2+} in methanol solution. **J. Chem. Phys.** 108: 9487.
- Savadogo, O. (1998). Emerging membranes for electrochemical systems: (I) solid polymer electrolyte membranes for fuel cell systems. **J. New Electrochem. Syst.** 1: 47.
- Savas, H. and Güven, O. (2002). Gelation, swelling and water vapor permeability behavior of radiation synthesized poly(ethylene oxide) hydrogels. **Radiat. Phys. Chem.** 64: 35.
- Saito, M., Arimura, N., Hayamizu, K. and Okada, T. (2004). Mechanisms of Ion and Water Transport in Perfluorosulfonated Ionomer Membranes for Fuel Cells. **J. Phys. Chem. B.** 108: 16064.
- Saito, M., Hayamizu, K. and Okada, T. (2005). Temperature Dependence of Ion and Water Transport in Perfluorinated Ionomer Membranes for Fuel Cells. **J. Phys. Chem. B.** 109: 3112.
- Sakamoto, K., MacKnight, W. J. and Porter, R. S. (1970). Dynamic and steady-shear melt rheology of and ethylene-methacrylic acid copolymer and its salts. **J. Polym. Sci. A-2: Polym. Phys.** 8: 277-287.

- Sannino, A. and Nicolais, L. (2005). Concurrent effect of microporosity and chemical structure on the equilibrium sorption properties of cellulose-based hydrogels. **Polymer**. 46: 4676-4685.
- Schneider, N.S. and Rivin, D. (2006). Solvent transport in hydrocarbon and perfluorocarbon ionomers. **Polymer**. 47: 3119-3131.
- Schubach, H. R., Nagy, E. and Heise, B. (1981). Short range order of amorphous polymers derived by WAXS. **Colloid. Polym. Sci.** 259: 789-796.
- Serpico, J. M., Ehrenberg, S. G., Fontanella, J. J., Jiao, X., Perahia, D., McGrady, K. A., Sanders, E. H., Kellogg, G. E. and Wnek, G. E. (2002). Transport and structural studies of sulfonated styrene-ethylene copolymer membranes. **Macromolecules**. 35: 5916-5921.
- Shimizu, R. N. and Demarquette N. R. (2000). Evaluation of surface energy of solid polymers using different models. **J. Appl. Polym. Sci.** 76: 1831-1845.
- Shin, J., Chang, B., Kim, J., Lee, S. and Suh, D. (2005). Sulfonated polystyrene/PTFE composite membranes. **J. Membr. Sci.** 251: 247-254.
- Siroma, Z., Ioroi, T., Fujiwara, N. and Yasuda, K. (2002) Proton conductivity along interface in thin cast film of Nafion. **Electrochem. Commun.** 4: 143.
- Smita, B. B. and Montgomery, T. S. (2007). Magnetic ion-exchange nanoparticles and their application in proton exchange membranes. **J. Membr. Sci.** 303: 64-71.
- Smitha, B., Sridhar, S. and Khan, A.A. (2003). Synthesis and characterization of proton conducting polymer membranes for fuel cells. **J. Membr. Sci.** 225: 63-76.

- Stern, E. A., Sayers, D. E. and Lytle, F. W. (1975). Extended x-ray-absorption fine-structure technique. III. Determination of physical parameters. **Phys. Rev. B.** 11: 4836
- Squires, E., Painter, P. and Howe, S. (1987). Cluster formation and chain extension in ionomers. **Macromolecules.** 20: 1740-1744.
- Suchocka-Galas, K. and Kowalonek J. (2006). The surface properties of ionomers based on styrene-co-acrylic acid copolymers. **Surf. Sci.** 600: 1134-1139.
- Sundmacher, K. and Scott, K. (1999). Direct methanol polymer electrolyte fuel cell: analysis of charge and mass transfer in the vapour–liquid–solid system. **Chem. Eng. Sci.** 54: 2927.
- Sung, Y. J., Chen, C. L. and Su, A. C. (1990). CNDO calculations for phenylene rotations in bisphenol A polycarbonate. **Macromolecules.** 23: 1941-1945.
- Teo, B. K. (1986). **EXAFS Basic Principles and Data Analysis.** New York: Springer-Verlag.
- Teo, B.-K. and Lee, P. A. (1979). Ab initio calculations of amplitude and phase functions for extended x-ray absorption fine structure spectroscopy. **J. Am. Chem. Soc.** 101: 2815-2832.
- Trotta, F., Drioli, E., Moraglio, G. and Poma, E.B. (1998). Sulfonation of polyetheretherketone by chlorosulfuric acid. **J. Appl. Polym. Sci.** 70: 477-482.
- Tocci, E., Bellacchio, E., Russo, N. and Drioli, E. (2002). Diffusion of gases in PEEKs membranes: molecular dynamics simulations. **J. Membr. Sci.** 206: 389-398.

- Verma R. K., Velikov, V., Kandert R. G. and Iarand H. (1996). SAXS studies of lamellar level morphological changes during crystallization and melting in PEEK. **Polymer**. 37: 5357-5365.
- Vielstich, W. and Ives, D. J. G. (1970). **Fuel cells; Modern processes for the electrochemical production of energy**. London: Wiley-InterScience.
- Visser, S. A and Cooper, S. L. (1991). Comparison of the physical properties of carboxylated and sulfonated model polyurethane ionomers. **Macromolecules**. 24: 2576-2583.
- Wainright, J. S., Wang, J.-T., Savinell, R. F., Litt, M., Moaddel, H. and Rogers, C. (1994). Acid doped polybenzimidazole, a new polymer electrolyte. **Proc. Electrochem. Soc.** 94: 255.
- Wang, J. T., Wasmus, S. and Savinell, R.F. (1996). Real-time mass spectrometric study of the methanol cross-over in a direct methanol fuel cell. **J. Electrochem. Soc.** 143: 1225.
- Wang, Y., Kawano, Y., Aubuchon, S. R. and Palmer, R. A. (2003). TGA and time-dependent FTIR study of dehydrating Nafion-Na membrane. **Macromolecules**. 36: 1138-1146.
- Weiss, R.A., Ashish, S., Willis, C.L. and Pottick, L.A. (1991). Block copolymer ionomers: 1. Synthesis and physical properties of sulphonated poly(styreneethylene/ butylene-styrene). **Polymer**. 32: 1867-1874.
- Welty, A., Ooi, S. and Grady, B. P. (1999). Effect of water on internal aggregate structure in zinc-neutralized ionomers. **Macromolecules**. 32: 2989-2995.

- Wu, G. M., Lin, S. J. and Yang, C. C. (2006). Preparation and characterization of high ionic conducting alkaline non-woven membranes by sulfonation. **J. Membr. Sci.** 284: 120-127.
- Wu, H.-L., Ma, C.-C. M., Li, C.-H. and Chen, C.-Y. (2006). Swelling behavior and solubility parameter of sulfonated poly(ether ether ketone). **J. Polym. Sci., Part B: Polym. Phys.** 44: 3128-3134.
- Xing, P., Robertson, G.P., Guiver, M.D., Mikhailenko, S.D., Wang, K. and Kaliauine, S. (2004). Synthesis and characterization of sulfonated poly(ether ether ketone) for proton exchange membranes. **J. Membr. Sci.** 229: 95-106.
- Xue, S. and Yin, G. (2006). Methanol permeability in sulfonated poly (ether ether ketone) membranes: A comparison with Nafion membranes. **Eur. Polym. J.** 42: 776.
- Yang, B. and Manthiram, A. (2003). Sulfonated poly(ether ether ketone) membranes for direct methanol fuel cells. **Electrochem. Solid-State Lett.** 6: A229-A231.
- Yang, J. C., Jablonsly, M. J. and Mays, J. W. (2002). NMR and FT-IR studies of sulphonated styrene-based homopolymers and copolymers. **Polymer.** 43: 5125-5132.
- Ye, G., Janzen, N. and Goward, G. R. (2006). Solid-State NMR Study of Two Classic Proton Conducting Polymers: Nafion and Sulfonated poly (ether-ether-ketone). **Macromolecules.** 39: 3283-3290.
- Zaidi, S. M. J., Mikailenko, S. D., Robertson, G. P., Guiver, M. D. and Kaliaguine, S. (2000). Proton conducting composite membranes from polyether ether ketone and heteropolyacids for fuel cell applications. **J. Membr. Sci.** 173: 17-34.

- Zhang, S., Dou, S., Colby, R. H. and Runt, J. (2005). Glass transition and ionic conduction in plasticized and doped ionomers. **J. Non-Crystalline Solids.** 351: 2825.
- Zhang, W., Dai, G. and Kerres, J. (1998). Synthesis of cross-linked poly(sulfone) ion exchange membranes. **Acta Polym. Sin.** 5: 608.
- Zoppi, R.A., Yoshida, I.V.P. and Nunes, S.P. (1998). Hybrids of perfluorosulfonic acid ionomer and silicon oxide by sol–gel reaction from solution: morphology and thermal analysis. **Polymer.** 39: 1309-1315.

APPENDICES

APPENDIX A

ATOMIC COORDINATES FOR CRYSTALS AND

MODELS USED TO INTERPRETE EXAFS DATA

Table A.1 Atomic coordinates for Calcium Oxide^a

X(Å)	Y(Å)	Z(Å)	Atom type
0.00000	0.00000	0.00000	Ca
2.40525	0.00000	0.00000	O
-2.40525	0.00000	0.00000	O
0.00000	2.40525	0.00000	O
0.00000	-2.40525	0.00000	O
0.00000	0.00000	2.40525	O
0.00000	0.00000	-2.40525	O
2.40525	2.40525	0.00000	Ca
-2.40525	2.40525	0.00000	Ca
2.40525	-2.40525	0.00000	Ca
-2.40525	-2.40525	0.00000	Ca
2.40525	0.00000	2.40525	Ca
-2.40525	0.00000	2.40525	Ca
0.00000	2.40525	2.40525	Ca
0.00000	-2.40525	2.40525	Ca
2.40525	0.00000	-2.40525	Ca
-2.40525	0.00000	-2.40525	Ca
0.00000	2.40525	-2.40525	Ca
0.00000	-2.40525	-2.40525	Ca

(a) wyckoff 1,III,88.

Available: <http://cars9.uchicago.edu/cgi-bin/atoms/atoms.cgi?file=CaO.inp>

Table A.2 Atomic coordinates for cadmium methanesulfonate dehydrate^b

X(Å)	Y(Å)	Z(Å)	Atom type
0.00000	0.00000	0.00000	Cd
1.46880	-0.51370	1.63940	O
-1.46880	0.51370	-1.63940	O
0.55720	-1.72270	-1.36890	O
-0.55720	1.72270	1.36890	O
-1.55410	-1.40100	0.94220	O
1.55410	1.40100	-0.94220	O
2.36940	-1.66550	1.70310	S
-2.36940	1.66550	-1.70310	S
-2.37320	-1.30310	2.14670	S
2.37320	1.30310	-2.14670	S
-3.18840	1.76330	-0.49860	O
3.18840	-1.76330	0.49860	O
1.30180	0.98370	-3.49800	C
-1.30180	-0.98370	3.49800	C
-3.27380	-0.15140	2.08310	O
3.27380	0.15140	-2.08310	O
1.68120	-2.89610	1.97280	O
-1.68120	2.89610	-1.97280	O
-1.68120	-3.20190	-1.97280	O
1.68120	3.20190	1.97280	O
4.18530	1.36040	0.92530	O
-4.18530	-1.36040	-0.92530	O
4.74250	-0.36230	-0.44370	Cd
-4.74250	0.36230	0.44370	Cd

(b) Charbonnier *et al.*, 1978.

Table A.3 Atomic coordinates for the model in Fig.4.15(a)

X(Å)	Y(Å)	Z(Å)	Atom type
-2.34793	-0.35581	0.89983	Ca
-5.01959	2.96361	-0.61411	O
-2.25541	0.32576	3.16801	O
-1.92894	4.43130	-0.98677	O
-1.22886	2.88414	-0.13291	S
-2.17497	1.34894	-0.73789	O
-1.42067	3.03002	1.75138	O
-4.69939	-0.06088	0.89462	O
2.39101	-1.88493	-0.71541	O
0.49638	-1.75042	-0.66940	S
-0.02348	-0.81559	0.90211	O
-0.11456	-0.79401	-2.19296	O
-3.93254	-5.34474	1.16335	O
-3.70572	-3.52085	1.64659	S
-5.41018	-2.70750	1.85158	O
-2.72043	-2.61696	0.29612	O
-4.01820	5.03446	-0.04385	Ca
-5.11437	-5.52927	-0.88294	Ca
-8.82033	6.29429	0.82661	O
-7.36512	5.74901	-0.04151	S
-5.99841	5.65886	1.09586	O
-7.67005	4.15031	-0.76146	O
-4.35009	6.81684	-1.56798	O
-0.42443	5.95044	0.69026	O
-1.62925	6.55865	1.85108	S
-2.94061	5.36898	2.03892	O

Table A.4 Atomic coordinates for the model in Fig.4.15(a) (cont.)

X(Å)	Y(Å)	Z(Å)	Atom type
-7.48658	-7.67540	1.04366	O
-8.09642	-6.04990	0.65040	S
-7.52025	-4.89048	1.87220	O
-7.48403	-5.56422	-0.94823	O
-2.24983	-7.39022	-4.57065	O
-3.32123	-7.3238	-3.15079	S
-4.74899	-8.34841	-3.43209	O
-3.83701	-5.64206	-2.87750	O
-5.10201	-7.89256	-0.69900	O
0.64531	2.81269	-0.58946	C
-0.25141	-3.52864	-0.66965	C
-2.74201	-3.42959	3.31600	C
1.41796	4.12169	-0.83816	C
2.92905	4.08164	-1.13299	C
3.67478	2.73453	-1.14946	C
2.91148	1.43035	-0.85412	C
1.40109	1.47345	-0.55890	C
-1.4739	-4.27973	3.51789	C
-0.66378	-4.15761	4.82177	C
-1.11135	-3.17223	5.9172	C
-2.36408	-2.30249	5.70471	C
-3.17443	-2.42535	4.40121	C
-0.49005	-4.26266	0.66386	C
-0.97612	-5.72356	0.66398	C
-1.19034	-6.46340	-0.66912	C
-0.92080	-5.74077	-2.00195	C

Table A.5 Atomic coordinates for the model in Fig.4.15(b)

X(Å)	Y(Å)	Z(Å)	Atom type
-2.49753	3.55374	3.46843	Ca
-5.51098	9.62014	6.28552	O
-4.29818	10.50183	5.32547	S
-4.45964	10.06719	3.60718	O
-2.66803	10.07575	5.89992	O
-3.41527	13.26219	5.17528	C
-2.74638	16.78482	7.39825	C
-1.73806	5.36274	2.13821	O
-4.06022	4.98084	4.53476	O
-4.21111	2.19439	2.55465	O
-0.84377	2.16367	2.49381	O
-1.51943	3.05911	5.56964	O
-2.67581	5.88912	0.71798	S
-1.6529	6.93377	-0.29689	O
-4.10207	6.80799	1.25821	O
-1.13757	1.37477	5.99691	S
-2.54337	0.33975	5.64776	O
-0.72256	1.27247	7.72514	O
-3.50414	6.12508	5.78103	S
-4.79957	6.40839	6.9673	O
-2.98155	7.65777	5.04406	O
-0.97045	1.67875	0.78671	S
-2.67368	1.76152	0.27757	O
0.01866	2.75768	-0.22654	O
-0.36636	-0.02028	0.62768	C

Table A.6 Atomic coordinates for the model in Fig.4.15(b) (cont.)

X(Å)	Y(Å)	Z(Å)	Atom type
1.29923	-4.31457	0.26282	C
1.15905	-5.06616	1.60021	C
0.48675	-5.04951	-0.81868	C
2.00999	-4.37836	2.68339	C
-4.84180	8.42096	8.21725	Ca
-8.85773	14.39652	10.44347	O
-7.82688	13.45654	12.35940	Ca
-9.36974	14.53801	13.79655	O
-8.64445	11.32722	13.00408	O
-6.07266	12.50852	11.07837	O
-6.14420	14.62334	13.55266	O
-10.36459	15.33014	10.61753	S
-9.94856	17.05312	10.77974	O
-11.23058	14.78122	12.07165	O
-11.49313	15.15104	9.21421	C
-11.41027	13.91756	8.29590	C
-12.39366	13.76976	7.11849	C
-13.43790	14.86874	6.84449	C
-6.21725	14.73022	15.32805	S
-7.66634	13.88258	15.92033	O
-6.28906	16.44125	15.81427	O
-9.31610	16.30547	14.01460	S
-10.71240	17.06497	13.21383	O
-7.80918	16.95383	13.32482	O
-6.39473	11.21504	9.89797	S

Table A.7 Atomic coordinates for the model in Fig.4.15(c)

X(Å)	Y(Å)	Z(Å)	Atom type
-1.10892	3.74138	4.95893	Ca
-2.78562	12.36523	8.43882	O
-3.01973	11.91458	10.75412	Ca
-4.86458	13.40036	10.81779	O
-4.42343	10.15363	11.49392	O
-1.25311	10.34133	10.93815	O
-1.74052	13.22396	12.25881	O
-4.15970	11.84222	7.43024	S
-4.35906	10.07349	7.43891	O
-3.88036	12.38361	5.75813	O
-8.95690	13.69725	11.95765	C
-2.31054	12.96759	13.92565	S
-3.17693	11.41490	14.00823	O
-3.39614	14.28727	14.42338	O
-0.88231	12.88345	15.03440	C
-0.52219	11.54929	15.71354	C
0.70315	11.46361	16.64157	C
1.57455	12.70938	16.88195	C
1.18689	14.05610	16.24253	C
2.78637	12.62431	17.82695	C
3.01650	13.98767	18.50220	C
-4.33050	15.09864	10.79641	S
-5.38944	16.05500	9.73298	O
-2.64825	15.20648	10.22401	O
-1.72006	8.81275	10.15438	S

Table A.8 Atomic coordinates for the model in Fig.4.15(c) (cont.)

X(Å)	Y(Å)	Z(Å)	Atom type
-3.38742	8.97848	9.55717	O
-0.69765	8.45455	8.74005	O
-2.52972	6.18798	11.09040	C
-2.31135	8.95805	7.01232	Ca
-0.72450	6.01300	4.39933	O
-2.70310	4.32246	6.61446	O
-2.75620	2.33429	3.99908	O
0.39063	3.15132	3.22118	O
0.25748	2.71438	6.60168	O
-2.25050	6.90269	4.15781	S
-2.05590	8.59633	4.68388	O
-3.61590	6.18686	5.04562	O
0.25410	0.94676	6.37298	S
-1.35700	0.43451	5.81609	O
0.60136	0.17275	7.93708	O
1.51586	0.38899	5.19818	C
-2.02430	5.63789	7.60370	S
-3.28650	6.88726	7.71690	O
-0.61360	6.38124	6.81609	O
2.75771	3.65150	11.87340	C
-0.35120	3.27673	1.60746	S
-2.10190	3.56822	1.74340	O
0.40610	4.59026	0.67493	O
-1.19790	11.01390	6.62967	O

Table A.9 Atomic coordinates for Potassium Dithionate^c

X(Å)	Y(Å)	Z(Å)	Atom type
0.00000	0.00000	0.00000	K
-0.35438	-0.67223	1.71720	S
-0.75936	0.02921	-1.71720	S
1.53079	-0.78560	2.16240	O
0.08504	1.71850	-2.16240	O
-1.78592	-1.57120	1.46280	O
-2.25366	-0.76105	-1.46280	O
-1.40322	2.08675	1.27200	O
1.10557	-2.25860	-1.27200	O
1.02052	2.65140	1.27200	O
2.80644	-0.44190	-1.27200	O
-3.18914	-1.84125	1.01760	S
-3.18914	-1.84125	-1.01760	S
2.48047	-1.84130	2.60760	S
-0.35438	3.06880	-2.60760	S
2.04105	-3.19150	2.16240	O
-1.74340	3.36335	-2.16240	O
2.67888	1.54665	3.18000	K
2.67888	1.54665	-3.18000	K

(c) American Mineralogist 16 (1931) 580-591.

Available: <http://cars9.uchicago.edu/cgi-bin/atoms/atoms.cgi?file=K2S2O6.inp>

Table A.10 Atomic coordinates for the model in Fig.4.22(a)

X(Å)	Y(Å)	Z(Å)	Atom type
0.96356	0.61939	0.89657	K
-0.54754	2.69269	1.63748	O
5.70794	3.11664	-0.27443	C
6.94610	2.29514	0.13116	C
8.30951	2.58042	-0.52442	C
8.43265	3.68013	-1.59430	C
7.18051	4.44723	-2.05697	C
5.81526	4.15851	-1.40395	C
3.99397	2.70928	0.51283	S
2.95955	4.29318	0.69203	O
3.03264	1.47138	-0.56089	O
4.30010	1.94094	2.22356	O
9.79167	3.94798	-2.26474	C
9.55908	4.47872	-3.69112	C
10.59394	2.63480	-2.31931	C
-3.75294	-4.34360	-2.37481	C
-4.60967	-5.31920	-1.54643	C
-2.83542	-3.33074	-1.66434	C
-1.67700	-1.98790	0.77376	S
-2.79021	-0.69558	1.61297	O
-0.50264	-1.14999	-0.46229	O
-0.63304	-2.85811	2.10217	O
1.92509	-0.58263	3.07875	O
4.25163	6.10078	2.39634	K
-4.41578	0.63431	-0.23941	K

Table A.11 Atomic coordinates for the model in Fig.4.22(b)

X(Å)	Y(Å)	Z(Å)	Atom type
1.88616	-1.94403	0.33279	K
1.00197	-8.81205	-2.81075	C
-0.33865	-9.56897	-2.77607	C
1.10837	-7.40591	-2.19214	C
-0.00927	-4.97790	-0.80463	S
-1.19175	-3.85520	-1.77578	O
-0.46773	-5.04907	1.03731	O
-0.46224	-10.94750	-3.44952	C
-1.87672	-11.08821	-4.04088	C
-0.22643	-12.05295	-2.40388	C
-0.29877	-3.72742	-4.42651	K
1.72955	-4.24425	-1.01405	O
5.57562	2.11692	-0.40283	C
4.05820	1.15068	0.29590	S
2.48418	2.20453	0.14577	O
3.85440	-0.45968	-0.69273	O
4.36593	0.74806	2.12708	O
-3.07527	-2.57819	-1.13038	C
-1.66206	-1.61794	1.36447	S
-2.87207	-0.45759	2.26460	O
-0.42896	-0.61458	0.32280	O
-0.67478	-2.56745	2.68277	O
2.45428	-2.48983	2.88399	O
2.73804	4.52099	1.69906	K
-4.22045	1.39243	0.65051	K

Table A.12 Atomic coordinates for the model in Fig.4.22(c)

X(Å)	Y(Å)	Z(Å)	Atom type
1.00796	0.91107	0.38865	K
-2.97723	4.30579	0.08689	C
-1.09675	3.89408	-0.05138	S
-0.87577	2.86420	-1.63411	O
-0.05366	5.47809	-0.19643	O
-0.49122	2.86263	1.42561	O
-7.47666	5.31025	0.35284	C
3.90587	3.07676	0.13874	S
3.08402	4.76738	0.41203	O
2.89723	2.05958	-1.10857	O
3.92861	2.14480	1.79520	O
-3.91178	-4.21705	-2.31520	C
-1.48383	-1.76941	0.49405	S
-2.49189	-0.66873	1.67018	O
-0.66939	-0.73556	-0.87764	O
-0.09567	-2.61561	1.47860	O
5.62779	-0.42927	1.25776	C
3.16844	-2.09012	1.84891	S
2.37717	-3.00288	0.37866	O
2.21530	-0.50409	2.30409	O
3.05449	-3.19399	3.39312	O
-0.13812	7.06463	2.11111	K
4.08734	5.95235	2.74323	K
3.29293	-2.21313	-2.15053	K
-4.79153	0.32946	0.42338	K

Table A.13 Atomic coordinates for the model in Fig.4.22(d)

X(Å)	Y(Å)	Z(Å)	Atom type
1.24799	0.99488	0.14620	K
-6.15531	3.42458	0.32484	C
-5.60849	3.22727	-1.10070	C
-1.22195	3.58117	-0.50218	S
-0.67067	2.49624	-1.96094	O
-0.91717	5.40837	-0.91645	O
-0.25602	3.01600	1.03131	O
4.06606	3.33754	-0.68440	S
3.65648	5.06954	-1.35398	O
3.05479	1.98328	-1.55237	O
3.74743	3.25209	1.18661	O
10.48704	2.38753	-1.51560	C
-4.48090	-2.53885	-0.19501	C
-1.87337	-1.06764	0.06619	S
-2.79479	0.54234	0.47903	O
-0.42060	-0.67839	-1.09618	O
-1.26303	-1.86713	1.67920	O
5.82011	0.21202	1.53459	C
3.58274	-1.71006	1.53657	S
2.81296	-2.67406	0.09060	O
2.44044	-0.31526	2.14327	O
3.88663	-2.87753	3.00516	O
1.57644	6.43541	-0.24736	K
0.48872	-3.79369	1.09201	K
1.67220	9.10173	-1.09542	O

Table A.14 Atomic coordinates for the model in Fig.4.22(d) (cont.)

X(Å)	Y(Å)	Z(Å)	Atom type
1.90680	6.37391	2.53181	O
-0.52537	-5.38014	-0.98117	O
1.02347	-5.39502	3.32502	O
2.20991	-6.63645	2.85671	S
3.47863	7.10817	2.92877	S
0.31209	9.99278	-0.37240	S
-1.98638	-6.23065	-0.42316	S
3.49896	8.79109	2.34845	O
4.77138	6.18853	2.12138	O
-1.21998	9.27765	-0.92858	O
0.41074	9.87696	1.40092	O
-1.55444	-7.30998	0.92510	O
-3.19387	-5.04583	0.13040	O
1.53820	-7.61973	1.53329	O
3.70395	-5.84268	2.30217	O

APPENDIX B

GERNERAL PROPERTIES OF PS AND PEEK

Polystyrene^a	
Density	1050 kg/m ³
Specific Gravity	1.05
Electrical conductivity (σ)	10 ⁻¹⁶ S/m
Thermal conductivity (κ)	0.08 W/(m·K)
Young's modulus (E)	3000-3600 MPa
Tensile strength (σ_t)	46-60 MPa
Elongation at break	3-4%
Glass temperature	95°C
Melting point	240°C
Heat transfer coefficient (λ)	0.17 W/(m.K)
Linear expansion coefficient (α)	8 10 ⁻⁵ /K
Water absorption (ASTM)	0.03-0.1

(a) International Labour Organisation chemical safety card for polystyrene
Available: <http://en.wikipedia.org/wiki/Polystyrene>

Poly(ether ether ketone)^b	
Density	1300 kg/m ³
Young's modulus (E)	3700 MPa
Tensile strength (σ_t)	90 MPa
Elongation at break	50%
Glass temperature	130-150°C and 260-290°C
Melting point	~350°C
Heat transfer coefficient (λ)	0.25 W/m.K
Linear expansion coefficient (α)	1.7 10 ⁻⁵ /K
Water absorption (ASTM)	- 0.1%

(b) A.K. van der Vegt & L.E. Govaert, Polymeren, van keten tot kunstof, ISBN 90-407-2388-5.

Available: <http://en.wikipedia.org/wiki/PEEK>

APPENDIX C

**PAIR DISTRIBUTION FUNCTIONS, $g(r)$, FOR THREE
DIFFERENT PAIRS OF ELEMENTS (CC, CH and HH) IN
BULK PS AND PEEK**

Detailed Pair Distribution Functions of Polystyrene: the ten detailed pair distribution functions for the four atom types $C_{\text{aliphatic}}$, C_{aromatic} , $H_{\text{aliphatic}}$ and H_{aromatic} are depicted in this section.

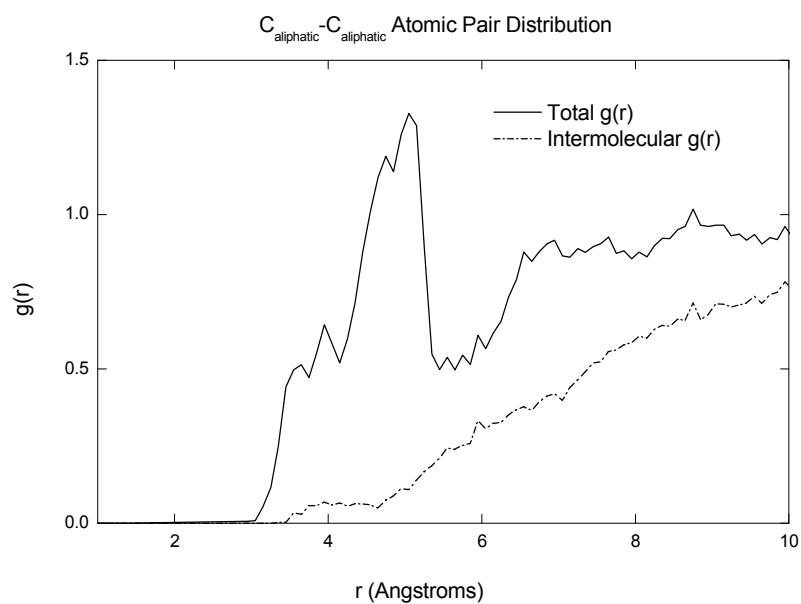


Figure C.1 Pair distribution functions for the aliphatic carbons.

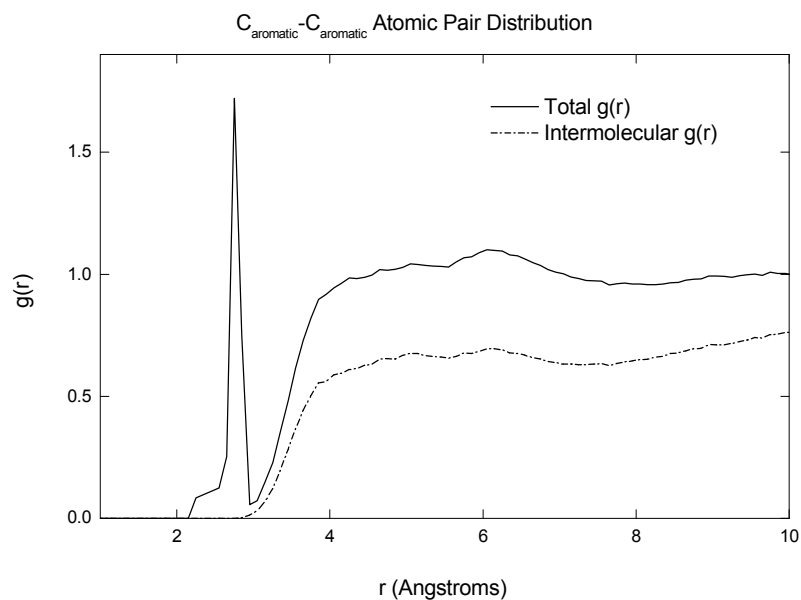


Figure C.2 Pair distribution functions for the aromatic carbons.

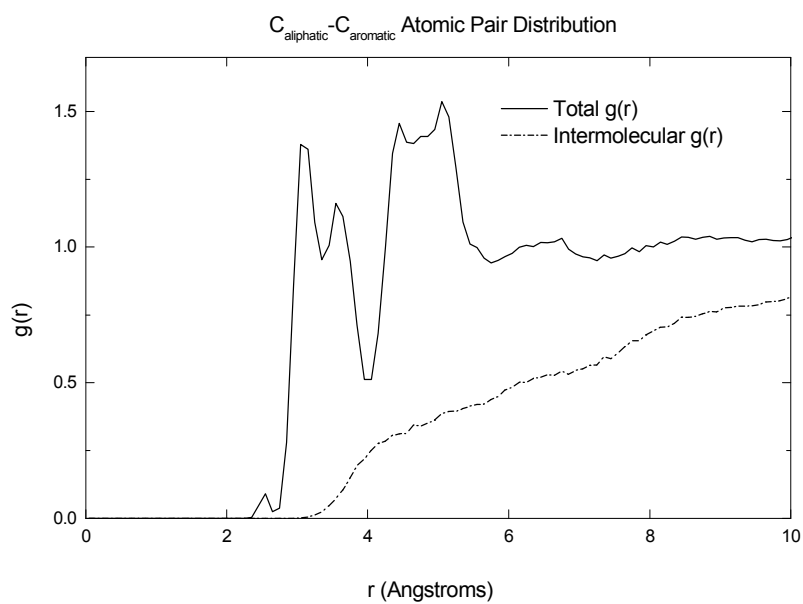


Figure C.3 Pair distribution functions for the aliphatic carbons with aromatic carbons.

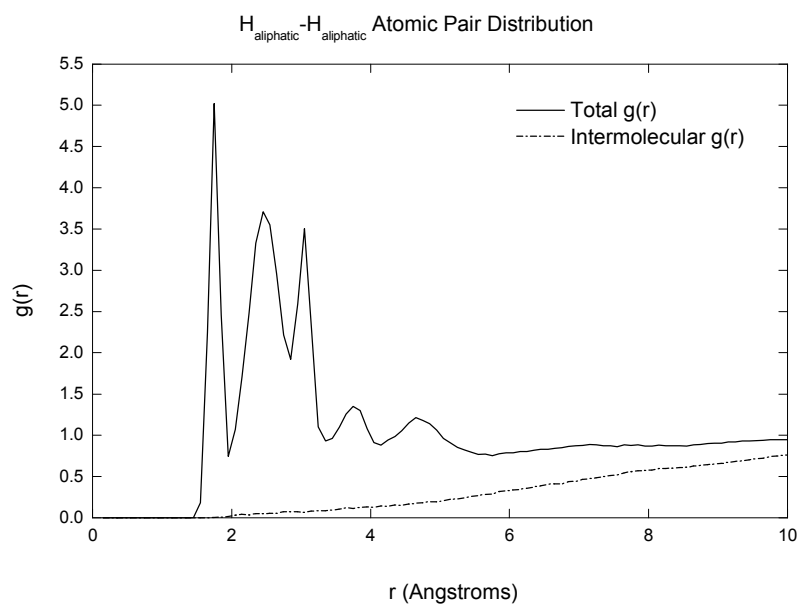


Figure C.4 Pair distribution functions for the aliphatic hydrogens.

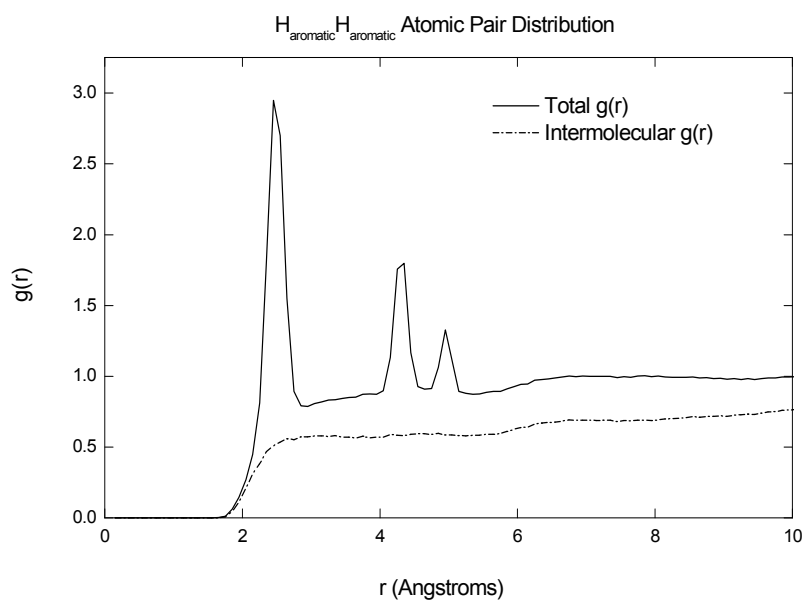


Figure C.5 Pair distribution functions for the aromatic hydrogens.

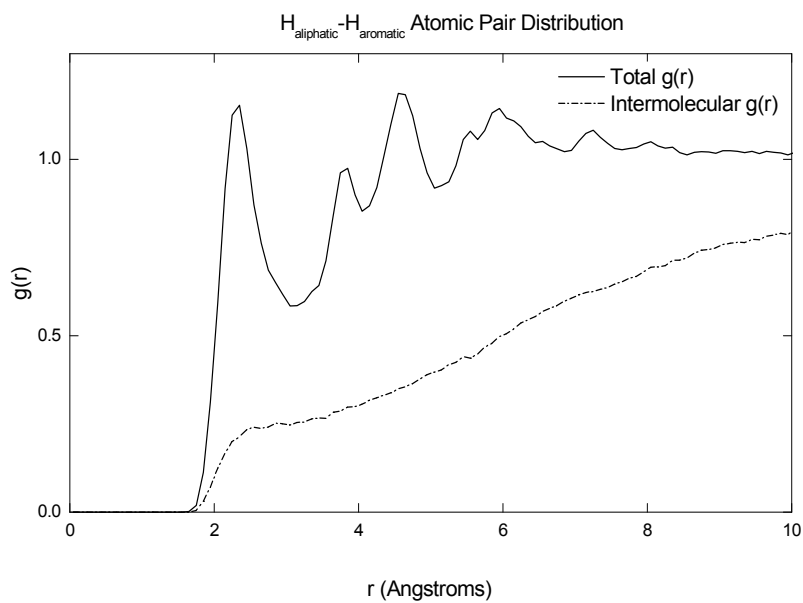


Figure C.6 Pair distribution functions for the aliphatic hydrogens with aromatic hydrogens.

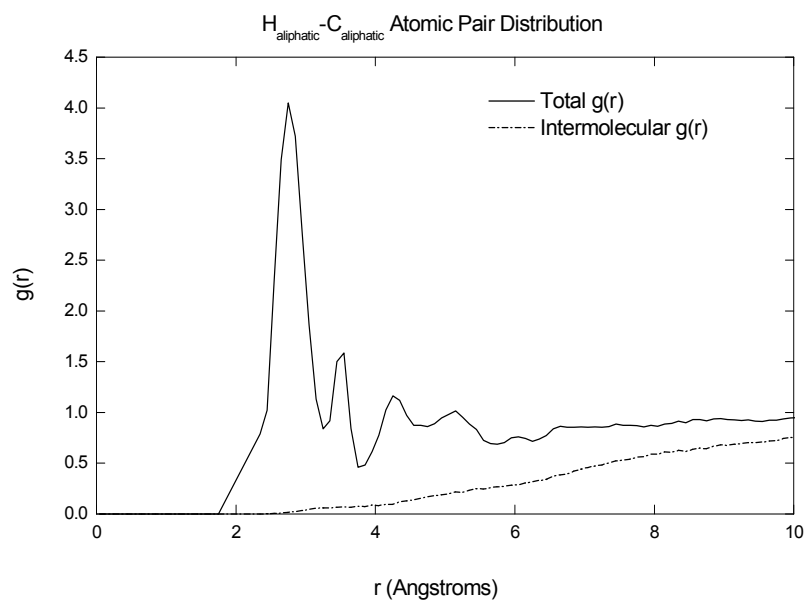


Figure C.7 Pair distribution functions for the aliphatic hydrogens with aliphatic carbons.

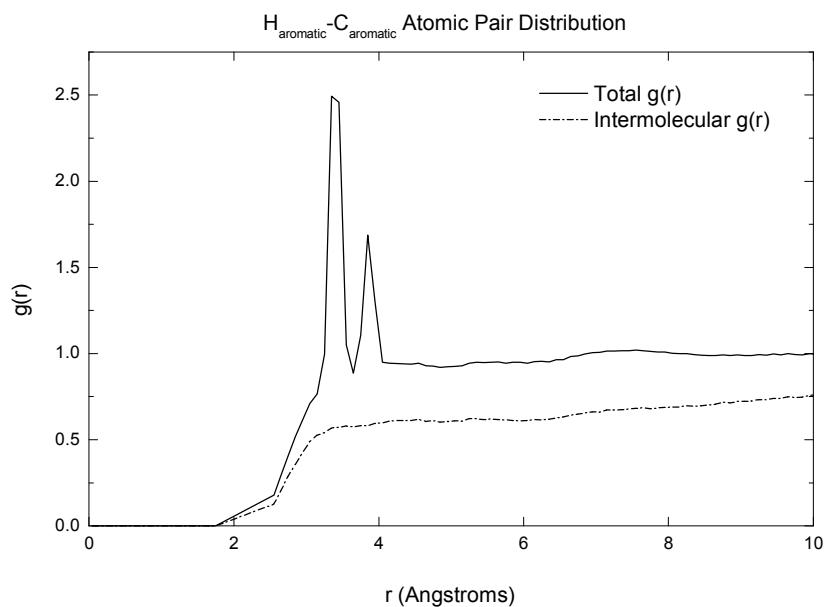


Figure C.8 Pair distribution functions for the aromatic hydrogens with aromatic carbons.

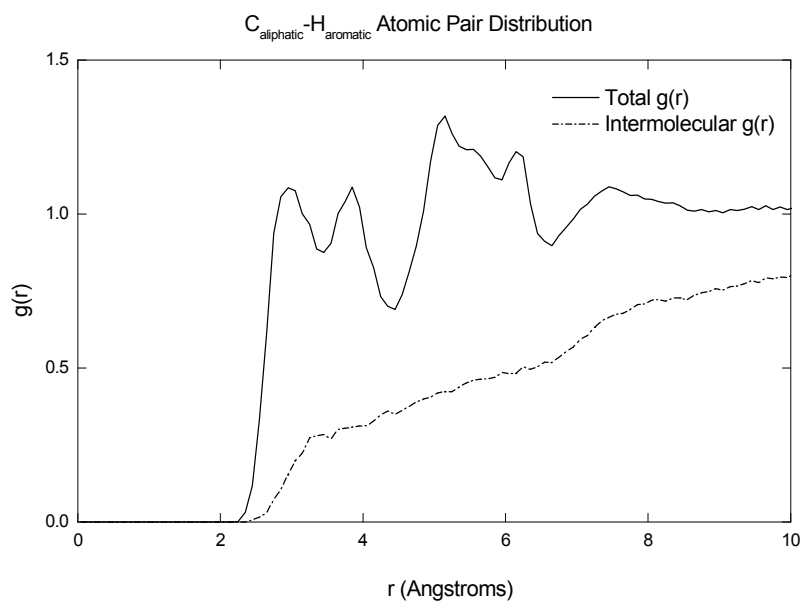


Figure C.9 Pair distribution functions for the aliphatic carbons with aromatic hydrogens.

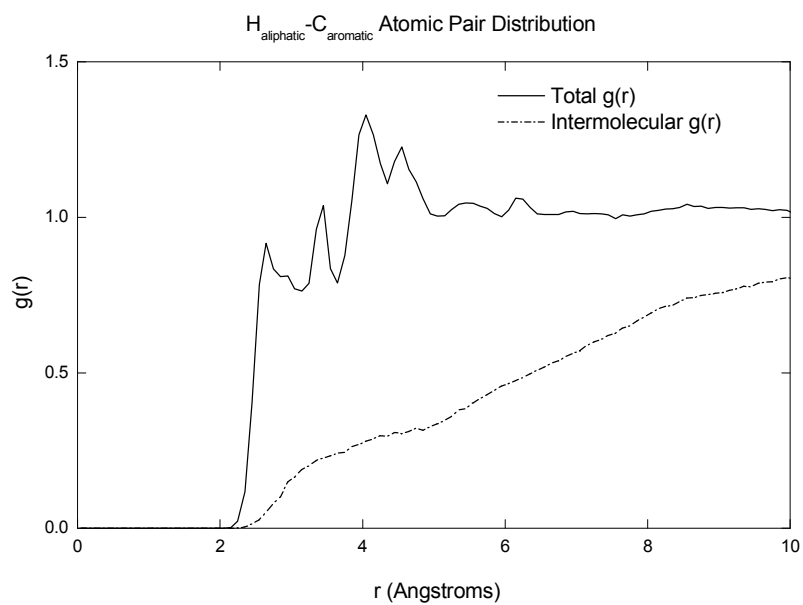


Figure C.10 Pair distribution functions for the aliphatic hydrogens with aromatic carbons.

Detailed Pair Distribution Functions of poly (ether-ether-ketone): the seven detailed pair distribution functions for the four atom types C_{aromatic} , H_{aromatic} , O_{ether} and O_{ketone} are depicted in this section.

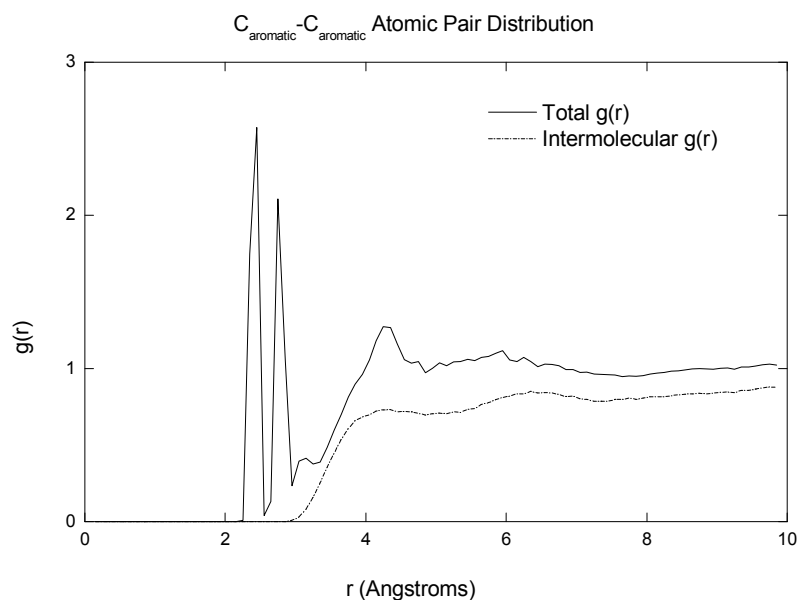


Figure C.11 Pair distribution functions for the aromatic carbons.

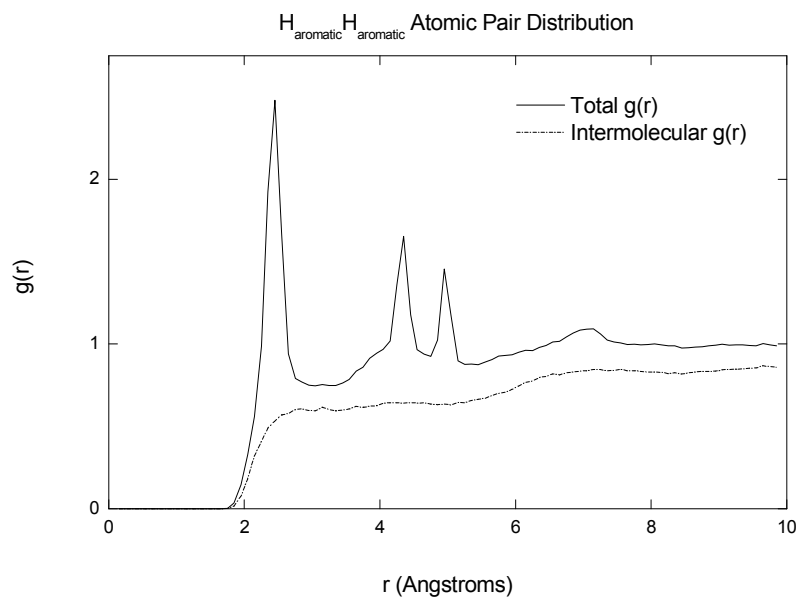


Figure C.12 Pair distribution functions for the aromatic hydrogens.

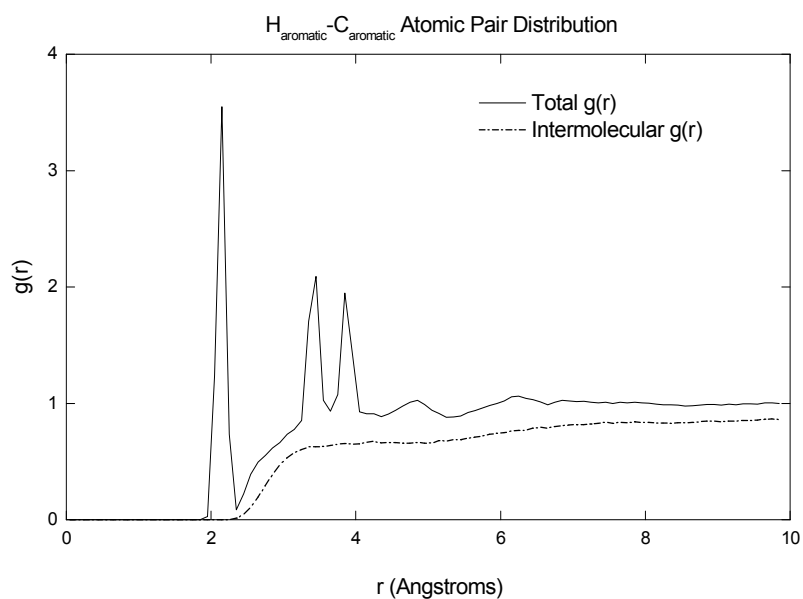


Figure C.13 Pair distribution functions for the aromatic hydrogens with aromatic carbons.

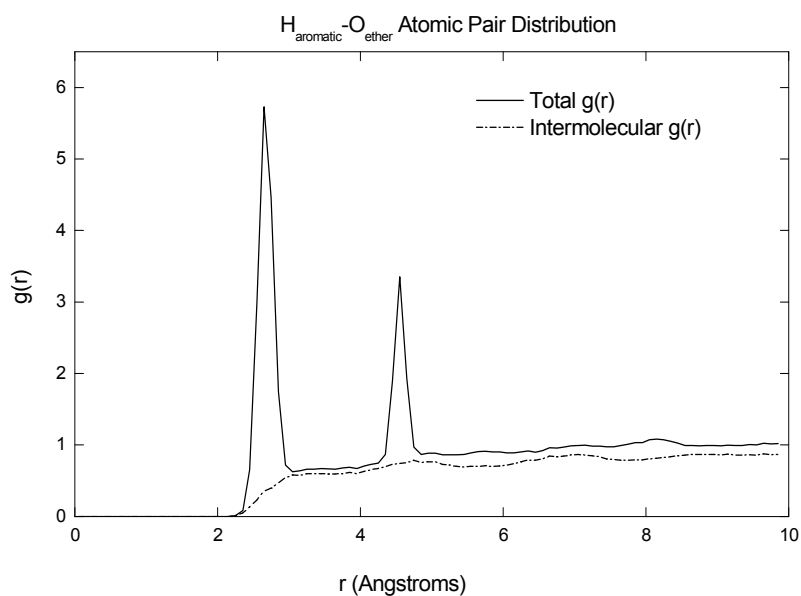


Figure C.14 Pair distribution functions for the aromatic hydrogens with oxygens of ether groups.

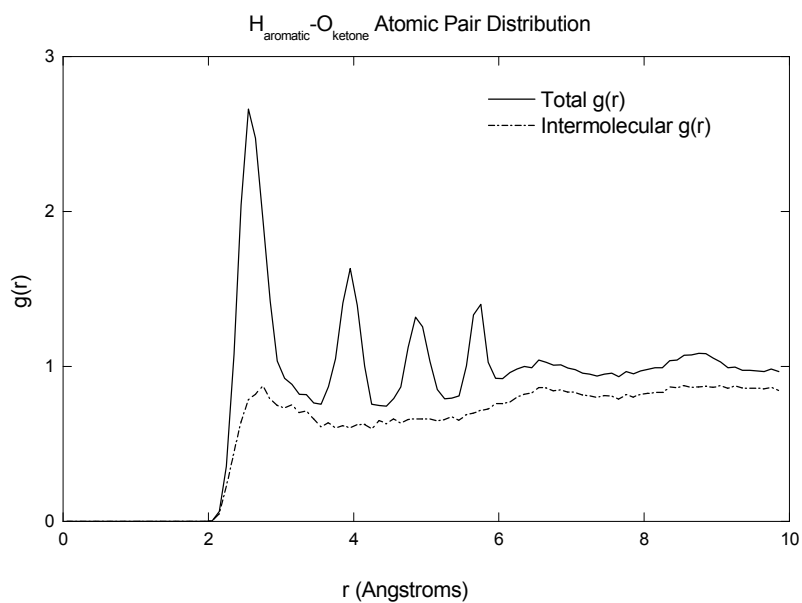


Figure C.15 Pair distribution functions for the aromatic hydrogens with oxygens of ketone groups.

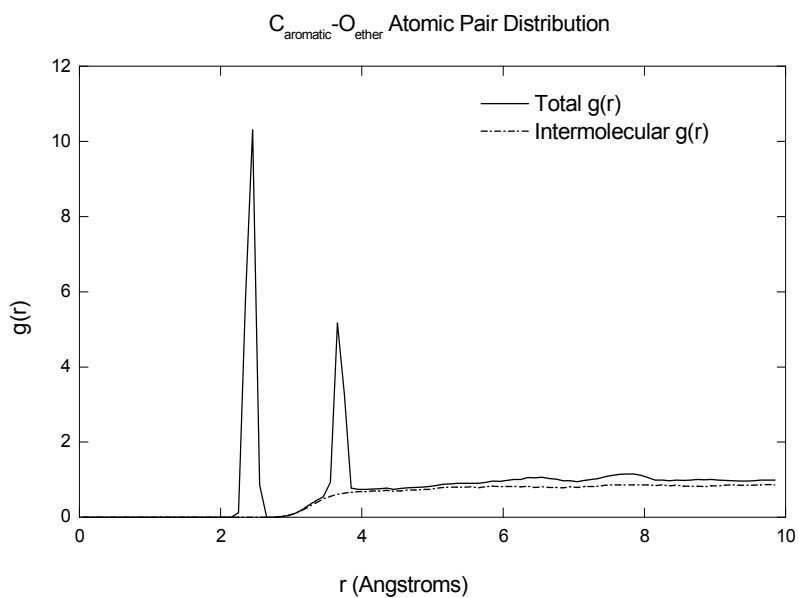


Figure C.16 Pair distribution functions for the aromatic carbons with oxygens of ether groups.

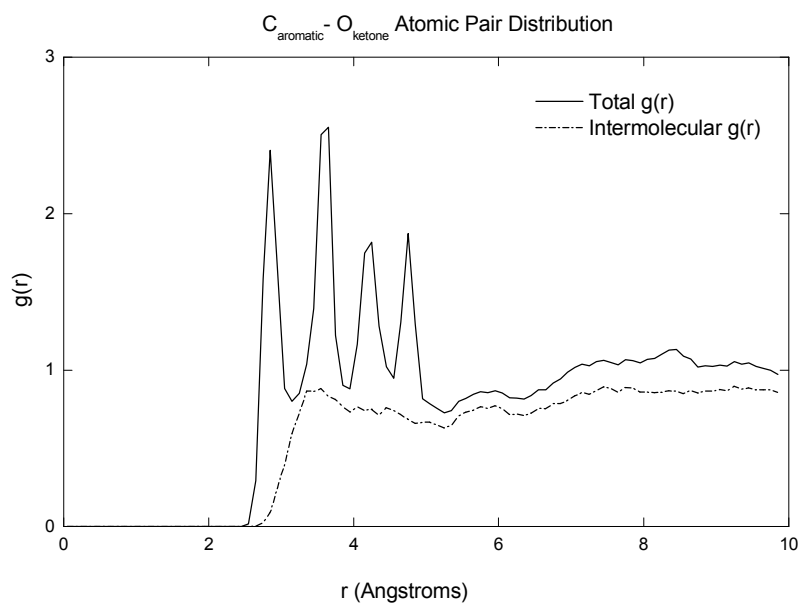


Figure C.17 Pair distribution functions for the aromatic carbons with oxygens of ketone groups.

APPENDIX D
PAPER PRESENTATIONS

1. Molecular Modeling of Proton Exchange Membrane Fuel Cells based on Sulfonated Poly(Ether Ether Ketone), Asian Workshop on Polymer Processing 2006 (AWPP 2006), December 6-8, 2006, Rama Gardens Hotel, Bangkok, Thailand.
2. Atomistic Simulation of the Structure of Amorphous Polystyrene, 32 nd Congress on Science and Technology of Thailand, October 10-12, 2006, Queen Sirikit National Convention Center, Bangkok, Thailand.
3. Molecular Dynamics studies of Poly (ether ether ketone) and Polystyrene, 33 rd Congress on Science and Technology of Thailand, October 18-20, 2007, Walailuk University, Nakhonsrithummarat, Thailand.

MOLECULAR MODELING OF PROTON EXCHANGE MEMBRANE FUEL CELL BASED ON SULFONATED POLY(ETHER ETHER KETONE)

Kongvit Prasitnok^{1,2}, Wantana Klysubun³, Visit Vao-soongnern^{1,2*}

Laboratory of Computational and Applied Polymer Science (LCAPS)¹, School of Chemistry², Institute of Science, Suranaree University of Technology, National Synchrotron Research Center³, Nakhon Ratchasima, Thailand 30000, visit@sut.ac.th

Abstract Membranes cast from partially sulfonated poly(etheretherketone) (SPEEK) have been studied as polymer electrolytes for direct methanol fuel cells (DMFCs). The proton exchange membrane fuel cell (PEMFC), which transfers protons from anode to cathode and acts as a barrier to avoid the crossover of fuel, is a key part of PEMFCs. In order to understand the mechanism of proton transport in PEM, it is necessary to know the role played by the sulfonate groups on PEEK backbone conformation which is related the feasibility of these functional groups to form microphase-separated clusters. In this respect, molecular mechanics and semi-empirical quantum chemistry calculations (AM1 and PM3) with full geometry optimization on diphenyl ether (DPE) and diphenyl ketone (DPK), a model compound of poly(oxy-1,4-phenyleneoxy-1,4-phenylenecarbonyl-1,4-phenylene) or PEEK, and the sulfonated DPE and DPK were carried out to determine molecular geometries and conformational energies and then to compute the unperturbed chain dimensions of PEEK and SPEEK. From the analysis of the relative energy maps, it is shown that the most probable route for a molecule to move is through gear rotations. The DPE molecule is also found to move more easily than the DPK molecule. Sulfonation of DPE and DPK causes significant changes in backbone conformation.

Introduction Polymers based on oxy-1,4-phenylene and carbonyl-1,4-phenylene repeating units (poly aryl ether ketone) are now found to be widely used as thermoplastic matrices for advanced composites. One of the most well known polymer of the series is the semi-crystalline poly(ether-ether-ketone) (PEEK) which is characterized by a good impact behavior and a high solvent resistance conjugated with high values for the glass transition temperature (144°C) and for the melting point (335°C). A lot of work dealing with the subglass relaxations of PEEK and with the conformations of its repeating units has been done in the past few years.

Semi-empirical and *ab initio* calculations have been conducted on molecular conformations of diphenyl ether (DPE) and diphenyl ketone (DPK). Semi-empirical molecular-orbital calculations by CNDO (Complete Neglect of Differential Overlap) of molecular units of PEEK (DPE, DPK and the repeating unit EEK) showed that the activation energies associated with isolated crankshaft motions are consistent with the dielectric results of Starkweather and Avakian where the activation energy was ca. 10 kcal.mol⁻¹ in PEEK. It was also demonstrated that the ether-ether phenylene ring has a high probability to lie in the PEEK backbone plane, contrary to the ether-ketone phenylene ring which is more likely to be perpendicular to it.

A conformational analysis of DPE and DPK by means of CNDO/2 has been recently published. The computations were first run disregarding electronic interactions and steric effects, then introducing them in the calculations using a modified CNDO/2. The absolute minimum energy conformers were shown to have torsional angles (ϕ_1, ϕ_2)=(30°, 150°) for DPE and (ϕ_1, ϕ_2) = (70°, 110°) for DPK, the mobility of DPE being greater than that of DPK. Considering the polymer chains of some poly(ether ketone), the DPE molecular units were then expected to be more mobile than the DPK ones in regions of local motions and for equivalent steric effects. We report here our calculation on DPE and DPK molecules for both native and sulfonated forms. The experimental activation energies are compared with those given by relative potential energy maps constructed by the use of the MM+ method. The process is validated by a comparative study between calculated and experimental values of the dipole moment of the molecular units.

Materials and Methods

Diphenyl ether (DPE) and diphenyl ketone (DPK) were used as model compounds, being the molecular constituents of polymers such as PEEK. The molecular formula of PEEK is given in Fig. 1, together with a schematic view of DPE and DPK showing the rotational angles of the phenyl rings. Each phenyl can rotate to angles ϕ_1 and ϕ_2 . Rotational motions of the phenylene rings of the molecular units DPE and DPK in PEEK have been investigated by means of molecular mechanics, which can be used to treat molecules that are too large to be handled in quantum chemistry methods. On the basis of the crystallographic information above and results of the semi-empirical molecular orbital calculations, bond angles and bond lengths in PEEK were assigned as those given in Table 1. HyperChem software was used for the total energy calculation of DPE and DPK. In these calculations, the rotational angles of phenylene rings were varied in 10° increments whereas values of bond lengths and bond angles were assumed not to vary with the rotation of aromatic rings. The relative energy map may be constructed after the identification of the absolute energy minimum.

Energy maps The rotational angles ϕ_1 and ϕ_2 have been varied in the range 0° to 360° by steps of 10° . In the case of DPE, the minimum absolute energy is obtained for the conformation defined by the rotational angles (30° , 150°) and their symmetrical equivalents, in reasonable agreement with the experimentally observed alternative inclination angle of ca. 40° from the plane of the zigzagging PEEK backbone. The aromatic rings resist coplanarity (where the absolute energy maximum appears). This may be attributable to the repulsion between ortho hydrogens on different rings. In the case of DPK, the minimum absolute energy is obtained for the conformation defined by the rotational angles (70° , 110°) and its symmetrical equivalents, quite different from the reported inclination angle of 40° in crystalline PEEK. The tendency for the two rings to avoid the coplanar conformation is similar to the case of DPE. These results are also significantly different from the ones recently reported which are (90° , 90°) for the ether linkage and (30° , 30°) for the ketone linkage. These linkages were however studied as part of the monomer of the considered polymer (PEIS or PEIK), where the presence of the methyl moieties has a strong constraining effect on the ability of the phenyls to rotate, the motions being limited in very small zones. For these minimum absolute energies, conformation maps can be drawn showing the values of the relative energy for each conformer. Fig. 2 and 3 illustrate the conformations of DPE and DPK, respectively, where each iso-energetic line corresponds to 2 kcal/mol.

Molecular motions A great number of motions can be envisaged for the phenyl rings from each possible conformation. Among them, only the simultaneous and the alternated rotations will be considered. There are actually two types of simultaneous rotations: the first one consists of rotating the two aromatic rings in opposite directions by increasing or decreasing both rotational angles (gear rotation), whereas the second one makes the two rings rotate in the same direction by increasing one angle and decreasing the other (correlated rotation). The gear rotation, characterized by a straight line with a negative unity slope on the conformational maps, is considered by several authors as the easiest possible motion. Considering the molecule to lie first at its lowest energy position, such a type of rotation is illustrated by the motions following the negative (N) lines in Fig. 2 and 3 for DPE and DPK respectively. The values of the relative energies taken by the molecules in this way are presented in Fig. 4. On the same scheme, the correlated motions can be visualized on the energy maps when the molecule is moving from its low-energy position along a straight line with a positive unity slope corresponding to the positive (P) lines in Fig. 2 and 3. The related picture is shown in Fig. 5 for the two molecules. If we compare correlated motions with gear motions, it is clear from the figures that gear motions are most likely because of the lower energy barriers encountered. Moreover, the DPE molecule appears to be more mobile than the DPK molecule in the case of gear rotations. The alternated rotations consist in fixing one of the phenylene rings and allowing the other one to undergo a complete 360° rotation. This motion can be described by considering either a horizontal (H) or a

vertical (V) lines in the energy maps. Fig. 6 depicts the phenylene ring motion along H lines whereas Fig. 7 shows motions along V lines. These various rotations do not differ significantly from each other, the energy barriers being very high in all cases, although being lower than in the case of correlated rotations. From a general point of view, it is thought that an isolated molecule could follow the most favorable energetic path from its most stable conformation by modifying its conformation structure near an energetic barrier, following then a broken line on the energetic map. Such a route will allow the molecule to minimize its energetic jumps. From these results, it is also possible to suppose that the DPE unit will move more easily than the DPK unit in a polymer chain such as PEEK in the sub- T_g temperature region.

Sulfonated DPE1 and DPE2 In general, sulfonation onto the PEEK backbone causes more hinder on bond rotation. According to the Fig. 4-7, the energy barriers for all types of molecular motions (P, N, H and V lines) are higher at almost all values of rotational angle. Comparing DPE and sDPE, both the magnitude of energy barrier and location of the maximum are changed according to the interaction from bulk sulfonate group. For two sDPE model compounds where the location of sulfonate groups are at 1 and 2 position on the benzene ring, the results suggest that the energy barrier for molecular motion of sDPE2 is largely higher than that of sDPE1 for all kinds of motion.

Conclusions

Molecular Mechanic and semi-empirical quantum chemistry calculations on DPE and DPK molecules were done in this study. The calculations on these repeating units using MM+ force field and AM1, PM3 confirmed previous reports revealing that the DPE molecule has a higher mobility than the DPK one. This suggests that the motions of the DPK units can be the determining element in a polymer chain containing DPE and DPK, such as PEEK. The easiest routes for the motions of the phenylene rings are those followed by gear rotations. Sulfonation of PEEK as seen in the polymer membrane fuel cell causes more energetic barrier of backbone rotation.

Acknowledgement: This project was supported by National Synchrotron Research Center (2-2548/PS02).

Table 1: Structural parameters used in the calculation

Bond lengths (nm)		Bond angle (deg)	
C-C _{aromatic}	0.140	C-C-C _{aromatic}	120
C-H	0.108	H-C-C _{aromatic}	120
C=O	0.123	C-C-C _{carbonyl}	126
C-C _{nonaromatic}	0.142	O-C-C _{carbonyl}	117
C-O	0.142	C-O-C _{ether}	126

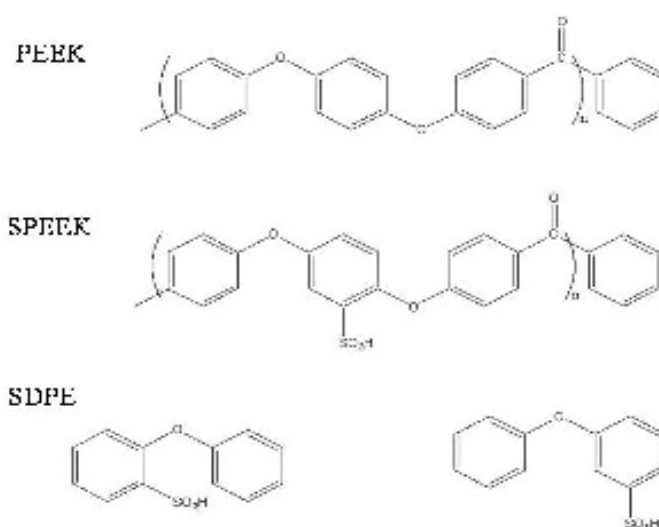


Fig. 1. Structures of the model compounds for PEEK, sPEEK, sDPE1 and sDPE2. The dihedral angle is defined as the angle between planes of the corresponding ring and the plane of the paper (molecular plane). DPK is similar to DPE structure by changing O for DPE to C=O for DPK.

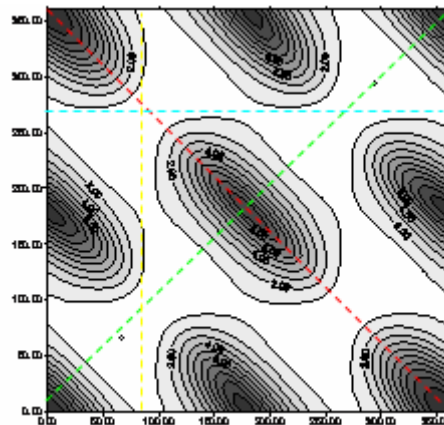


Fig. 2. Energy map and main motion routes for DPE (N-gear motion, P-correlated motion, V-alternated motion and H-alternated motion, where N, P, V and H are negative, positive, vertical and horizontal line, respectively).

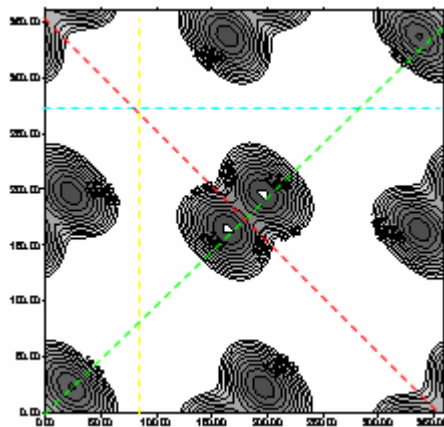


Fig. 3. Energy map and main motion routes for DPK (N-gear motion, P-correlated motion, V-alternated motion and H-alternated motion, where N, P, V and H are negative, positive, vertical and horizontal line, respectively).

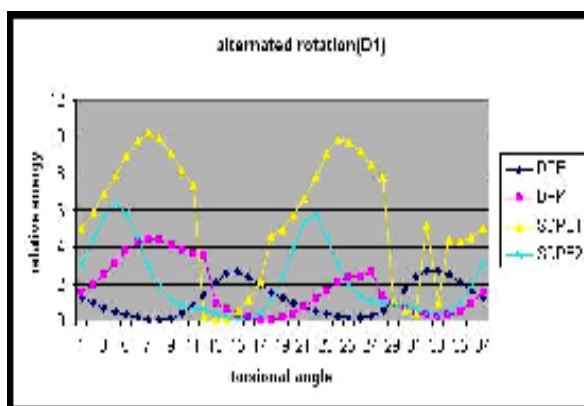


Fig. 4. Variation of the relative energy versus the torsional angle for DPE, DPK, sDPE1 and sDPE2 molecules following a correlated motion route (P line)

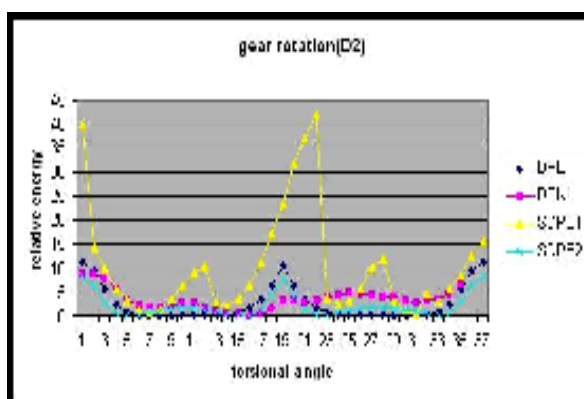


Fig. 5. Variation of the relative energy versus the torsional angle for DPE, DPK, sDPE1 and sDPE2 molecules following a gear motion route (N line).

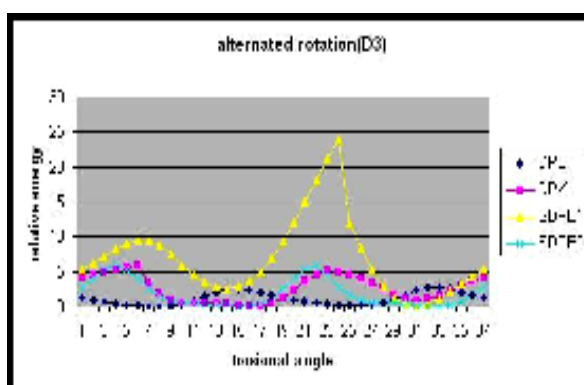


Fig. 6. Variation of the relative energy versus the torsional angle for DPE, DPK, sDPE1 and sDPE2 molecules following an alternated motion route (H line).

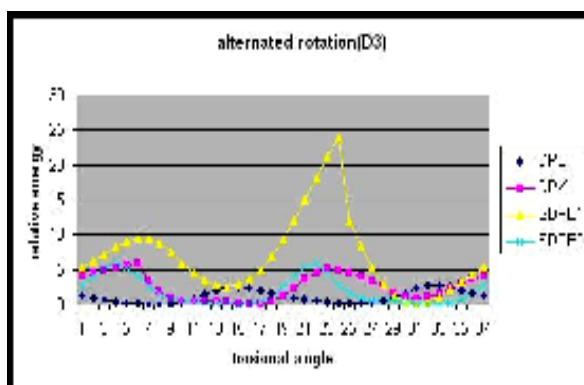


Fig. 7. Variation of the relative energy versus the torsional angle for DPE, DPK, sDPE1 and sDPE2 molecules following an alternated motion route (V line).

References

1. CHEN, C.L., CHANG, J.L., SU, A.C. *Macromolecules* **25**, p. 1941 (1992)
2. CHEN, C.L., LEE, C.L., CHEN, H.L., SHIH J.H. *Macromolecules* **27**, p. 7872 (1994)
3. HAMERTON, I., HEALD, C.R., HOWLIN, B.J. *Macromol Theory Simul* **5**, p. 305 (1996)

การจำลองระดับอะตอมสำหรับโครงสร้างของพอลิสไตรีนอสัณฐาน

ATOMISTIC SIMULATION OF THE STRUCTURE OF AMORPHOUS POLYSTYRENE

คงวิทย์ ประสิทธิ์นอก^{1,2}, ศุภกร รักใหม่^{3,4}, วันทนา คล้ายสุบรรณ⁴, วิศิษฐ์ แววสูงเนิน^{1,2*}
 Kongvit Prasitnok^{1,2}, Supagorn Rugmai^{3,4}, Wantana Klysubun⁴, Visit Vao-soongnern^{1,2*}

Laboratory of Computational and Applied Polymer Science (LCAPS)¹, School of Chemistry² and School of Physics³, Institute of Science, Suranaree University of Technology, National Synchrotron Research Center⁴, Nakhon Ratchasima, Thailand. E-mail: visit@sut.ac.th, Fax: 04-4224-185

บทคัดย่อ: ได้สร้างแบบจำลองสถิตระดับอะตอมสำหรับพอลิสไตรีนอสัณฐานขึ้นโดยใช้เทคนิคไฮบริดระหว่างโมเลกุลาร์แมคคาณิกส์/โมเลกุลาร์ไดนามิกส์ โดยโครงสร้างเริ่มต้นของพอลิเมอร์สร้างขึ้นจากการใช้เทคนิคมอนติ คาร์โลภายใต้เงื่อนไขขอบเขตเป็นคาบ ตามด้วยการลดพลังงานระบบลงเพื่อให้ได้โครงสร้างที่เสถียร การวิเคราะห์อย่างละเอียดพบว่าผลของการจัดตัวระหว่างโมเลกุลทำให้ได้โครงสร้างที่แตกต่างไปจากสภาวะพื้นของโมเลกุลเดี่ยว การกระจายของมุมบิดมีความหลากหลายที่แตกต่างไปจากลักษณะของโคเมอร์แสดงว่าเป็นผลที่เกิดจากแรงกระทำระหว่างโมเลกุล ระบบพอลิเมอร์ที่ได้จึงมีลักษณะเป็นอสัณฐาน โดยมีโครงสร้างแบบสุ่ม ค่าการทำนาย Hildebrand solubility parameter และ Neutron/X-Ray structure factor ได้ผลใกล้เคียงกับการทดลองมาก

Abstract: A static, atomistically detailed model of dense, glassy polystyrene was simulated using molecular mechanics/molecular dynamic hybrid method. Initial chain conformations which were generated using a Monte Carlo technique including periodic boundary conditions, were relaxed by potential energy minimization. Detailed analysis of the minimized structure indicated that intermolecular packing effects create a large variety of chain conformations different from the purely intramolecular ground states. The distribution of the torsion angles of the minimized structures did not show the expected behavior of the model compounds (dimer) indicating the intermolecular interaction dominate the local preferences. The systems are amorphous, exhibiting random coil behavior. The predict Hildebrand solubility parameter and Neutron/X-Ray structure factor are in reasonable agreement with the experimental values

Introduction: The experimental design and synthesis of new polymers for a particular application is a time consuming and expensive procedure. The properties of polymeric materials at the molecular level can be predicted to a reasonable degree of success, at the present time, using computer based molecular simulations. Atomistic modeling can give useful insights when applied to polymeric systems in their condensed phases without loss of the details of their chemical structure. Simulations of amorphous polymers are typically performed by several established methodologies, whereby atoms are subjected to Monte Carlo simulations (MC), energy minimizations (EM) and molecular dynamics (MD). Such simulation methods can be used to obtain equilibrium conformations of polymer chains which bring the polymers sufficiently close to their thermodynamically realistic states, depending on how the simulations are performed and the nature of the overall simulation strategy. The quality of the force field that is employed in such atomistic simulations is an important factor in determining the ability of the simulations to predict the particular properties of experimental interest. In this work, we illustrate the application of computer simulation technique to generate and equilibrate the amorphous model of polystyrene which is a common plastics used in daily life.

Methodology: The amorphous bulk of the polymer was modeled by periodic cubic microstructures. The first repeat unit was filled into the box by choosing place and orientation at random. Then, a random conformation of a polymer is built one residue at a time within the cell. A

conformation was accepted if the generated residue is free of strong steric clashes with all the previously generated ones. The generated structures were then equilibrated by performing energy minimization which were performed by both steepest descent and conjugated gradient methods. For molecular dynamics simulations, the standard Verlet algorithm was used to integrate Newton's law of motion with a time step of 0.001 ps. Each molecular dynamics run was started by assigning initial velocity for the atoms according to a Boltzmann distribution. NVT-MD was run for 2 ns after an equilibration stage. The last 1 ns was used for data analysis.

Results, Discussion, and Conclusion:

Rotational Isomeric State (RIS) Model: The conformational characteristics of PS were evaluated with a force field that includes flexible phenyl rings and a description of charge distribution in the chain by atomic partial charges. The most drastic effect was the elimination of the *meso-tt* state, but all states are affected and the resulting RIS model differs significantly from previous ones. The RIS model performs well in predicting values for the characteristic ratio and the vicinal NMR coupling of PS.

Chain dimensions and conformation:

The characteristic ratio and the radius of gyration for the minimized structure were found to ca. 9.7 and 15.1 Å, respectively. The dimension are about the same for the minimized structures as for the initial guess structure. From the distribution of torsion angles as displayed in Fig. 1, the population of the g^- state is not negligible, despite its intramolecular high energies. This effect may be a consequence of the steric interaction in the bulk due to intermolecular interactions. The overlap of the *t* and g^+ state is quite pronounced. The orientation of the phenyl ring groups are found perpendicular to the backbone.

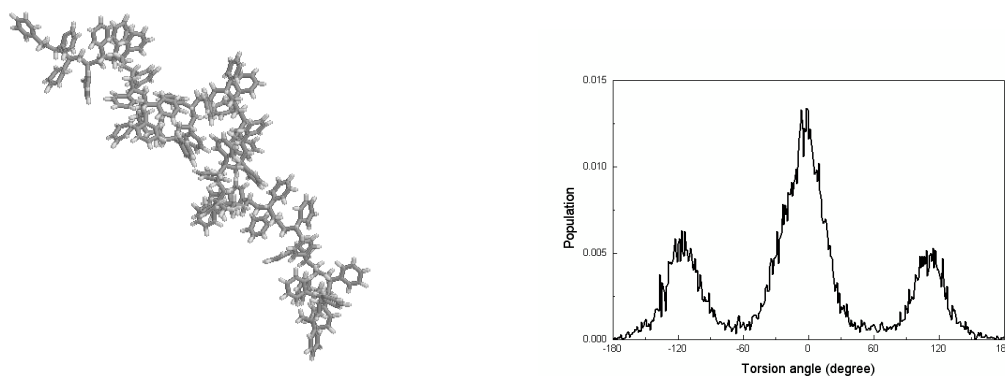


Figure 1 (a) Atomistic model of *a*-PS used in this work (b) Distribution of the skeletal torsion angles for the relaxed *a*-PS structures

Cohesive energy and solubility parameters: The cohesive energy is the energy associated with the intermolecular interactions only and can be estimated by taking the difference between the total energy of the microstructure and the energy of the parent chains. Hildebrand's solubility parameter is the square root of the cohesive energy density. The average Hildebrand's solubility parameter is $\delta = 7.72 \pm 0.10 \text{ cal}^{1/2}/\text{cm}^{3/2}$. The reported experimental values for *a*-PS are between 8.12 and 9.88 $\text{cal}^{1/2}/\text{cm}^{3/2}$, in agreement with the estimated results.

Radial distribution function and Neutron/X-Ray structure factor:

Radial distribution functions for three different pairs of elements (CC, CH and HH) were calculated. The most noticeable characteristic of these distributions is the absence of any apparent

intermolecular correlation in all but the H-H pair distribution function. The $H_{\text{aliphatic}}-H_{\text{aromatic}}$ and $H_{\text{aromatic}}-H_{\text{aromatic}}$ distributions have definite intermolecular features. This might indicate that packing is determined mainly by interactions of aromatic moieties. Next, the neutron elastic structure factor $S(Q)$ was calculated as a function of the scattering vector magnitude ($Q = 4\pi/\lambda\sin\theta$). The structure factor is calculated from the elemental radial pair-distribution function. The calculated spectrum exhibits three peaks at $Q = 0.41, 1.25$ and 3.10 \AA^{-1} . These locations fit the experimentally observed peaks that occur at $Q = 0.6, 1.33$ and 3.0 \AA^{-1} very well. Experimentally, the second peak is the major one while the first is only a shoulder. The difference at lowest Q is due to the relevant distant close to half of the periodic box.

One of the most interesting features of polystyrene is the so-called ‘‘polymerization peak’’ in its wide angle X-Ray structure factor. The X-Ray scattering pattern of atactic polystyrene (*a*-PS) reveals a diffuse halo (polymerization peak) at around $Q = 0.75 \text{ \AA}^{-1}$ in addition to a higher Q feature at around 1.4 \AA^{-1} associated with the amorphous halo observed in polymer melts, glass, and rubber. The amorphous peak in *a*-PS arises primarily from phenyl-phenyl correlations while the polymerization is due to intermolecular correlations of backbone atoms. We conclude that the diffraction results indicate reasonable agreement between computed and actual structure.

References:

- (1) Theodorou, D. and Suter, U. (1985) *Macromolecules* **18**, 1467
- (2) Ayyagari, C., Bedrov, D., and Smith, G. D. *Macromolecules* **33**, 6194

Acknowledgement: This work is supported by National Synchrotron Research Center (2-2548/PS02) and NSRC Graduate Student Fellowship.

Keywords: Polystyrene (PS), Molecular Simulation, X-Ray/Neutron Diffraction

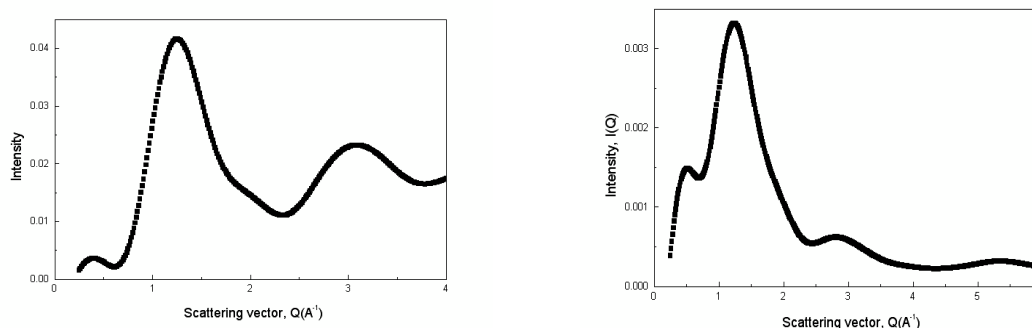


Figure 2 (a) Neutron scattering factor and (b) X-Ray scattering intensity for *a*-PS.

การศึกษาโดยเทคนิคโมเลกุลาร์ไดนามิกส์ของพอลิอีเทอร์-อีเทอร์-คีโตน และ พอลิสไตรีน

MOLECULAR DYNAMICS STUDIES OF POLYETHER-ETHER-KETONE AND POLYSTYRENE

คงวิทย์ ประสิทธิ์นอก^{1,2}, มนตรี เกตมาลา^{1,2}, วันทนา คล้ายสุบรรณ³, วิสิษฐ์ แวสูงเนิน^{1,2}

Kongvit Prasitnok^{1,2}, Montree Gatumala^{1,2}, Wantana Klysubun³, and Visit Vao-soongnern^{1,2}

¹Laboratory of Computational and Applied Polymer Science (LCAPS). ²School of Chemistry, Institute of Science, Suranaree University of Technology. ³National Synchrotron Research Center, Nakhon Ratchasima, 30000 Thailand. E-mail: visit@sut.ac.th

บทคัดย่อ: ได้ใช้เทคนิคโมเลกุลาร์ไดนามิกส์ศึกษาพอลิอีเทอร์-อีเทอร์-คีโตนและพอลิสไตรีนซึ่งเป็นแบบจำลองขั้นต้นของเซลล์เชื้อเพลิงชนิดฟิล์มพอลิเมอร์โดยได้คำนวณค่าสัมประสิทธิ์การแพร่ผ่านของโมเลกุลน้ำในเมมเบรนของพอลิอีเทอร์-อีเทอร์-คีโตนและ พอลิสไตรีนที่อุณหภูมิ 303 และ 410 เคลวิน ตามลำดับ โดยพบว่าค่าสัมประสิทธิ์การแพร่ผ่านที่ได้จากการจำลองแบบมีค่าสอดคล้องกับผลการทดลองนอกจากนี้ได้ทำนายพลังงานพื้นผิวของพอลิเมอร์ทั้งสองชนิดซึ่งพบว่าผลที่ได้

ใกล้เคียงกับผลการทดลอง

Abstract: Molecular dynamics (MD) simulations was used to study amorphous bulk and membrane as models of polymer fuel cell *i.e.* poly-ether-ether-ketone (PEEK) and polystyrene (PS). Diffusion coefficients of water in membrane of PEEK and PS were determined at two different temperatures (303 and 410 K, respectively). Diffusion coefficient from simulations were consistent with experimental values. For thin film simulation, the contribution of the internal energy to the surface energy of the film was estimated and the predicted surface energy is closed to the previous experimental reports.

Introduction: The experimental design and synthesis of new polymers for a particular application is a time consuming and expensive procedure. The properties of polymeric materials at the molecular level can be predicted to a reasonable degree of success, at the present time, using computer based molecular simulations. Atomistic modeling can give useful insights when applied to polymeric systems in their condensed phases without loss of the details of their chemical structure [1]. Molecular dynamics (MD) is the simulation method that can be used to obtain equilibrium conformations of polymer chains which bring the polymers sufficiently close to their thermodynamically realistic states, depending on how the simulations are performed and the nature of the overall simulation strategy. Previous studies have demonstrated the reliability of this method in the study of diffusion behavior of small molecules in chemically complex polymers with stiff polymer chains [2]. In this study, the diffusion of water molecule in poly(ether-ether-ketone) (PEEK) and polystyrene (PS) were estimated and compared with the previous reports. PEEK and PS are an interesting material well established as commercially important, high performance-engineering thermoplastic. Furthermore, we evidence that in the last decade considerable effort was made to produce modifications of the chemical nature of this class of polymers in order to obtain excellent physical properties and to build-up membrane useful for electro dialysis, gas dehumidification and fuel cell. Due to the occurrence of polymer surfaces is important in several areas of polymer science and technology such as coatings, adhesives and paints. We also calculated surface energy of these two polymers and compared results with experimental reports.

Methodology: Amorphous cells of PEEK and PS with water absorbed were generated and simulated using Materials Studio 4.1 with COMPASS force field, licensed from NANOTEC, Thailand. All MD simulations were performed under NVT conditions with the working

temperature $T = 30$ and 27 °C K for PEEK and PS, respectively. A time step $\delta = 1$ fs for the integration of the atomic motion equations was used. The van der Waals and Coulombic nonbonding interactions were calculated by the atom based and cell multipole method, respectively. The structure of both systems were first minimized with respect to all the internal coordinates by a conjugate gradient method until the maximum derivative was smaller than 0.1 kcal/(Å mol). Then, the system was submitted to an equilibration process consisting on a 200 ps long MD run. The data collecting stage consisted on MD runs of 1 ns. In both cases, the trajectories were saved each 5000 fs for subsequent analysis. For surface energy calculations, thin films of PEEK and PS were constructed by using the method of confine layer. The dimension of the periodic box along the z axis was increased by adding 100 Å to the old length, and the other two dimensions were left unchanged. The relaxation and the data collecting stage of the films were achieved in the same way of amorphous cells.

Results, Discussion and Conclusion: Table 1 represents the polymer systems used in an amorphous cell construction. The models for equilibrated amorphous bulk and thin film are shown in Fig. 1. The diffusion of small molecules in a polymer matrix is described as similar to a random

walk process on a long time scale, which obeys Einstein's law $D = \lim_{t \rightarrow \infty} \frac{1}{6t} \left\langle \sum_{i=1}^n r_i^2 \right\rangle$ Here D is the diffusion coefficient, t is the time over which D is estimated, r_i is the displacement of the diffusant molecule in a time interval, n is the total number of time intervals in time t, and $\left\langle \sum_{i=1}^n r_i^2 \right\rangle$ is the

mean-square displacement (MSD) of the diffusant. Fig. 2 depicts the MSD as a function of the simulation time t for the water molecule in PEEK and PS. A slope of $\log(\text{msd}(t)) \approx 1$, that is an indication that real Einstein diffusion is reached. From the mean-square displacement of the water molecule as a function of time interval, the diffusion coefficients of water molecules in PEEK at 30 °C are estimated to be 0.99×10^{-9} cm²/s which indicates that this result falls within the expected range [2]. The estimated diffusion coefficient of H₂O in PS at 27 °C is 0.28×10^{-4} cm²/s which is close to the experimental value of 0.14×10^{-4} cm²/s [3] and previous simulation report of 0.52×10^{-6} cm²/s [3].

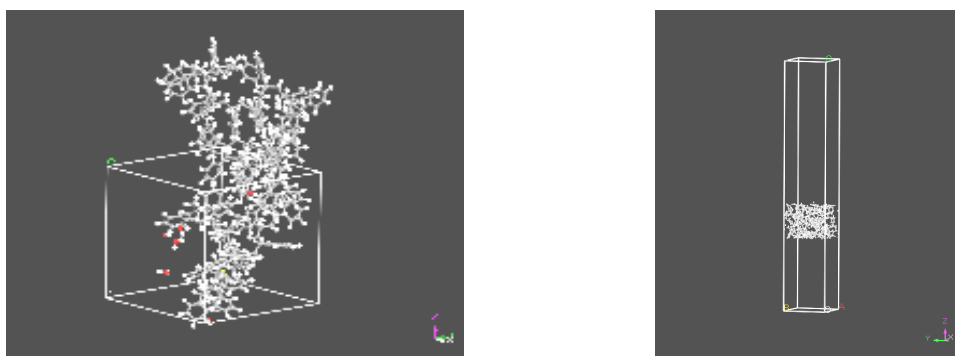
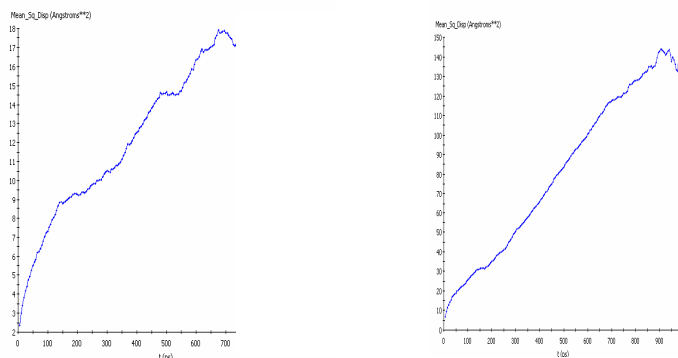


Figure 1 (a) periodic cell of PS with water absorbed and (b) thin film of PS used to calculate Surface energy.

Table 1 Description of the Different Simulated Cells

polymer	Chain length	Number of H ₂ O molecules	Temperature(K)	Box size(Å) x = y = z	Density (g/cm ³)
PEEK	20	5	303	19.76	1.260
PS	50	5	410	20.30	1.051

**Figure 2** Mean-square displacement of H₂O as a function of time in (a) PEEK at 30 °C and (b) PS at 27 °C.

Thin Film: The contribution of the internal energy to the surface energy, γ , was calculated using

the relation $\gamma = \frac{E_{film} - E_{bulk}}{A}$ where E_{bulk} is the energy of the amorphous bulk, E_{film} is the energy

of the thin film and A is the area per free surface of the film having two free surfaces. The most dominant contribution to the formation of the free surface of the film comes from the van der Waals dispersion energy. The value of A is determined by the dimensions of the periodic box. The calculation gives $\gamma = 38.5 \text{ erg} \cdot \text{cm}^{-2}$ for PEEK, which is slightly smaller than the experimental result of about $42.1 \text{ erg} \cdot \text{cm}^{-2}$ [5]. The same method obtained $36.3 \text{ erg} \cdot \text{cm}^{-2}$ for PS which is smaller than the experimental result for that material of $40.7 \text{ erg} \cdot \text{cm}^{-2}$ [5]. This shows that the simulation results presented here are able to predict successfully the experimentally derived surface energy of PEEK and PS.

References:

1. A.s. Ijantkar and U.Natarajan, *Polymer*, 2004, **45**, 1373-1381.
2. Elena Tocci, Emanuele Bellacchio, Nino Russo and Enrico Drioli, *Journal of Membrane Science*, 2002, **206**, 389-398.
3. Esra Kucukpinar and Pemra Doruker, *Polymer*, 2003, **44**, 3607-3620.
4. Jie Han and Richard H. Boyd, *Polymer*, 1996, **37**, 1797-1804.
5. Brandrup, J. and Immergut, E. H. (eds), *Polymer Handbook*, 1975, 2nd edn. Wiley Interscience, New York.

Keywords: Poly-ether-ether-ketone; Polystyrene; Molecular Dynamics; Film, Diffusion

Acknowledgement: This work is supported by National Synchrotron Research Center (GS-49-M01) and National Nanotechnology Center (NANOTEC) & Computational Nanotechnology Consortium (CNC), Thailand.

CURRICULUM VITAE

KHONGVIT PRASITNOK

Born: June 2, 1982, Nakhon Ratchasima

Citizenship: Thailand

Education:

2001-2004 B.Sc. Chemistry (First Class Honor), Ubon Rajathanee University, Thailand.

2005-2006 Grad. Dip. (Teaching Profession), Khon Khean University, Thailand.

Experience:

2007 Research observation in topic of Extended X-ray Absorption Fine Structure (EXAFS) studies of Polymer Electrolyte: Data processing and Fitting at National Taiwan University of Technology (NTUST), August-September, 2007. Taipei, Taiwan.

Presentation:

1. Atomistic Structure and Ionic Mobility of Sulfonated Polystyrene Ionomers by Molecular Simulation and X-Ray Absorption Spectroscopy, 33 rd- International Workshop for Far East Asian Young Rheologists (IWFEAYR-3), Shanghai Jiao Tong University, Shanghai, China.
2. Molecular Dynamics studies of Poly (ether ether ketone) and Polystyrene, 33 rd Congress on Science and Technology of Thailand, October 18-20, 2007, Walailuk University, Nakhonsrithummarat, Thailand.
3. Molecular Modeling of Proton Exchange Membrane Fuel Cells based on Sulfonated Poly(Ether Ether Ketone), Asian Workshop on Polymer Processing 2006 (AWPP 2006), December 6-8, 2006, Rama Gardens Hotel, Bangkok, Thailand.
4. Atomistic Simulation of the Structure of Amorphous Polystyrene, 32 nd Congress on Science and Technology of Thailand, October 10-12, 2006, Queen Sirikit National Convention Center, Bangkok, Thailand.